Application of the Hybrid Explicit/Implicit Finite-Difference Time-Domain Method (FDTD) for Electromagnetic Computations in Cold Magnetized Toroidal Plasma

Toepassing van de hybride expliciete/impliciete FDTD-methode voor elektromagnetische simulaties in een gemagnetiseerd koud toroïdaal plasma

Maryna Surkova

Promotoren: prof. dr. ir. D. De Zutter, ereprof. dr. ir. G. Van Oost
Proefschrift ingediend tot het behalen van de graad van
Doctor in de Ingenieurswetenschappen: Toegepaste Natuurkunde

Vakgroep Informatietechnologie
Voorzitter: prof. dr. ir. D. De Zutter

Vakgroep Toegepaste Fysica
Voorzitter: prof. dr. ir. C. Leys

Faculteit Ingenieurswetenschappen en Architectuur
Academiejaar 2015 - 2016

UNIVERSITEIT GENT

ISBN 978-90-8578-838-6
NUR 928
Wettelijk depot: D/2015/10.500/82

Application of the Hybrid Explicit/Implicit Finite-Difference Time-Domain Method (FDTD) for Electromagnetic Computations in Cold Magnetized Toroidal Plasma

Maryna Surkova

Dissertation submitted to obtain the academic degree of
Doctor of Applied Physics/ Plasma Physics and Nuclear Fusion

Research funded by a doctoral grant from the Research Foundation in Flanders (FWO).

Supervisor:
prof. dr. ir. D. De Zutter
Electromagnetic Group
Department of Information Technology
Faculty of Engineering and Architecture
Ghent University
St.-Pietersnieuwstraat 41
B-9000 Ghent, Belgium
http://emweb.intec.ugent.be

Supervisor:
ereprof. dr. ir. G. Van Oost
Plasma Physics and Nuclear Fusion
Vakgroep Toegepaste Fysica
Faculty of Engineering and Architecture
Ghent University
St.-Pietersnieuwstraat 41
B-9000 Ghent, Belgium
http://www.ugent.be/ea/appliedphysicsen/research/fusion

Members of the examining board:

prof. Hendrik Van Landeghem (chairman)	Ghent University, Belgium
prof. Jean-Marie Noterdaeme (secretary)	Ghent University, Belgium
prof. dr. ir. D. De Zutter (supervisor)	Ghent University, Belgium
ereprof. dr. ir. G. Van Oost (supervisor)	Ghent University, Belgium
dr. Dirk Van Eester (reading committee)	Koninklijke Militaire School, Belgium
prof. Stefaan Cottenier (reading committee)	Ghent University, Belgium
prof. dr. ir. D. De Zutter (reading committee)	Ghent University, Belgium
prof. Kristel Crombé	Ghent University, Belgium
prof. Ivan Pavlenko	V.N. Karazin Kharkiv National University, Kharkiv, Ukraine
dr. Wouter Tierens	IT-IS International Ltd., Stokesley, Middlesbrough, UK

Acknowledgments

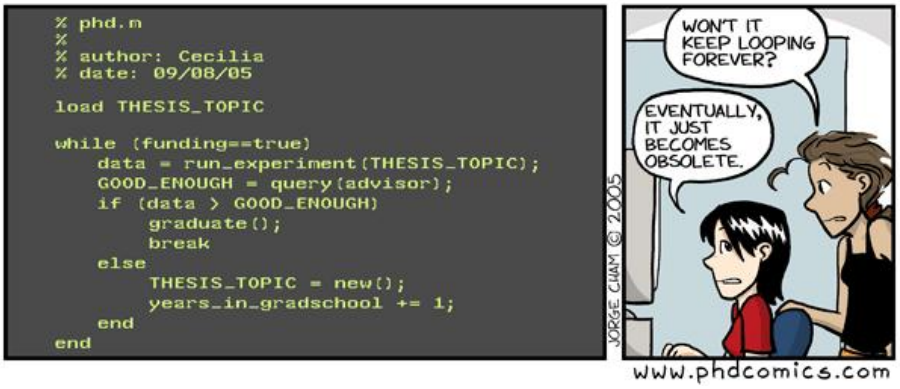

Once I've seen a saying that "a PhD should come with a government health warning". Well, when you are not along the PhD journey and you have many great people who kept encouraging and supporting you, 'a government health warning' could be kept aside. With this thank word I would like to take this opportunity to express my gratitude to some special people for their help and support during this thesis.

First of all I would like to give a special thanks to my promotors, prof. Daniël De Zutter and ereprof. Guido Van Oost for their expertise, support and patience. A special thanks goes to my colleague and constant dissertation advisor dr. Wouter Tierens who's feedback is priceless. Wouter, I really appreciate your help and support especially during 'het laatste loodje' of my thesis. I would like to express my gratitude to dr. Dirk Van Eester and prof. Ivan Pavlenko for their feedback, assistance and guidance. I would also like to express my sincere appreciation to prof. Hendrik Van Landeghem, prof. Stefaan Cottenier, prof. Kristel Crombé and prof. Jean-Marie Noterdaeme for serving as my dissertation committee members.

I owe special thanks to my boyfriend Erland whose talent and ability to lead me through the secrets of efficient programming, endless loving support, respect and incredible patience during my thesis made me go this far. I would like to thank my family and the family of Erland for their support, encouragement and for their limitless 'schaaltjes garnaalsla'. Papa, Dima, dedushka Misha, Inge, Tyra, Bomma, tante Leen, Paul, Katrien - hartelijk dank voor jullie aandacht en steun!

Finally I want to say thanks to all my dear friends for your understanding, interest and humor, for helping me to enjoy my life-beside-work. My Ukrainian friends-dear Ira, Vika, Yulja and another Ira- thank you very much for 'was-be-and will

be'-ing my friends. Dear Lenka, thank you for becoming one of my closest friends here in Belgium, and thank you for involving me in a hot yoga practise which has helped me to develop and to calm down at the same time. Dear Katja, thank you for your friendship, cold mind, sharp advice and patience with my driving. My incredible INTEC team: dearest Celina - thank you for becoming one of my first really close Belgian friends, thank you for all our marvelous shopping, cold-cake-cooking experience, our endless discussions and fun at all our badminton battles. Dear Mima, and Marina- thank you for all our pyjama parties and movie nights, for your immeasurable amount of cup-cakes. Marina, the ones with salty caramel are the best! Kolja- thank you for sharing your experience with me, for your philosophy and fun we had. I would like to thank our Indian friend Abhi whose humor is rib-tickling and who can comfort anyone with a kind word. Dear Elena, my chemist friend, thank you for your 'tiramisu-in-the-movies time' and private yoga classes. I would like to thank Bart for his 'GoBart' mood, incredible help and ability to be right in time. Another special thank goes to all salsa- Bruno, Guido, Eveline - and badminton- Danny, Peixia- people. Thank you all for your endless support, your constant attention and faith, and thank you for sharing your experience. Once again thank you all!

Gent, October 6
Maryna Surkova

Chance favors the prepared mind.

Luis Pasteur

Contents

Samenvatting

De FDTD-methode wordt heden ten dage intensief gebruikt voor het oplossen van de vergelijkingen van Maxwell voor een zeer gamma van toepassingen. De afkorting 'FDTD' staat voor 'Finite Difference Time Domein', dus 'eindige verschillen in het tijdsdomein'. De infinitesimale verschillen die opduiken in differentiaaloperatoren omzetten in kleine, eindige verschillen is een intuïtieve techniek om differentiaalvergelijkingen op te lossen. In de afgelopen 20 jaar werd veel aandacht besteed aan het modelleren van golven in allerlei media. Het succes dat de techniek kende maakte dat gaandeweg de complexiteit van de media waarin het golfgedrag bekeken werd kon opgedreven worden. Door de grote nood aan het doorgronden van golfverhittingsproblemen in experimentele fusiemachines werd FDTD onder andere ook toegepast op gemagnetiseerde plasma's. Verschillende 'smaken' van FDTD kwamen daarbij aan bod: recursieve convolutie, directe integratie, de Z-transformatiemethode, de transmissielijnmatrixtechniek, de opgedeelde-stap-methode, het volledig expliciet en volledig impliciet formuleren van de vergelijkingen, en tenslotte de hybride methoden. Volledig expliciete methodes zijn zeer intuïtief en makkelijk te implementeren maar vereisen het nemen van zeer kleine tijdstappen om stabiliteit te garanderen. Volledig impliciete methoden zijn daarentegen bewijsbaar stabiel maar vereisen complexere matrixmanipulaties. Gezien in dat licht lijken hybriede technieken een groot potentieel te hebben: ze zijn stabiel als aan de relatief weinig beperkende Courant-voorwaarde voldaan is, en ze vereisen bij elke tijdstap slechts het oplossen van een beperkt aantal vergelijkingen. Het onderwerp van deze doctoraatsthesis is de ontwikkeling van een globaal FDTD-model dat toelaat golven (en meer in het bijzonder golfkoppeling) te beschrijven in een koud, gemagnetiseerd plasma. Teneinde dat model te kunnen bouwen werd eerst een algoritme opgesteld en uitgebreid getest. Conform met de geometrie van een tokamak werd geopteerd de vergelijkingen te beschrijven in cylindercoördinaten, waar bij de radiale richting fungeert als de grote straal van de tokamak, en de polaire hoek toelaat de toroidale geometrie te beschrijven. De poloïdale periodiciteit werd voorlopig buiten beschouwing gelaten en vormt mogelijk het onderwerp van later werk. Het opgestelde model laat toe golfvoortplanting in toroïdale geometrie te bestuderen; de hoek tussen het magneetveld en de richting waarin de golf zich voortplant kan willekeurig gekozen worden.

Niet enkel in fusiemachines is de relevante geometrie torusvormig: fluxbuizen in de zonnecorona hebben dezelfde vorm. Het hier ontwikkelde model kan dus - zij het in een drastisch ander frequentiegebied en voor karakteristieke lengten die beduidend groter zijn dan die van een laboratoriumopstelling - toegepast worden om astrofysische plasma's te helpen begrijpen. De volledige dynamiek van plasmagolven vatten in een thesis is onbegonnen werk. Afbakenen van het doel was daarom noodzakelijk. De focus in deze thesis ligt op de golfdynamica terwijl golfinterferentie kunstmatig omzeild werd. Die interferentie is in belangrijke mate het gevolg van het feit dat golven in een tokamak weerkaatsen op de metalen wanden

die een Faraday-kooi vormen voor de elektromagnetische golven. Reflecties vermijden gebeurt door kunstmatige wijze demping in te voeren. Een hoofdstuk van de thesis wordt gewijd aan het ontwerpen van een dempingsschema dat enerzijds toelaat ongewenste weerkaatsingen te vermijden maar dat anderzijds de fase en amplitude van de golven in het gebied waar we de echte fysische oplossing willen kennen niet aantast.

Een van de specificiteiten van golven in fusiemachines is dat alnaargelang van het antenneontwerp verschillende soorten golven kunnen opgewekt worden in het plasma. Bovendien zorgt het feit dat het magneetveld en de dichtheid intrinsiek inhomogeen zijn er in een tokamak voor dat er zones in het plasma bestaan waar de verschillende golfsoorten met mekaar koppelen en dat er zones zijn waar de golven evanescent zijn. Met name tussen de antenne en het eigenlijke plasma ligt er een evanescentiezone. En vlak bij de plaats waar de golven hun energie overdragen aan het plasma is er een zone waar de beide types golfgedrag (koppeling en evanescentie) gezamenlijk optreden. Hoewel een voldoende gesofistikeerd model - buiten het bereik van deze thesis - nodig is om die energieoverdracht van golven naar geladen deeltjes te beschrijven, ligt het beschrijven van de golfkoppeling en de tunneling perfect binnen het toepassingsgebied van het hier beschreven werk.

In deze thesis is de beschrijving van de diëlectrische respons vervat in de koudplasma diëlectrische tensor (voor het stuk dat over de dispersie handelt), of de 'vloeistof'-plasmastroom (voor de eigenlijke FDTD-toepassing). Zulke beschrijving is voldoende accuraat om de belangrijkste aspecten van de golfdynamiek te vatten. Voor een meer volledige beschrijving moet echter overgegaan worden op een model dat het plasma niet als een vloeistof beschrijft maar als een distributie van deeltjes, elk met een eigen snelheid. In het frequentiedomein zijn er uitdrukkingen voor de diëlectrische respons voorhanden die rekening houden met zulke kinetische effecten. Binnen FDTD-domein is dat vooralsnog niet het geval. Een niet onbelangrijk aspect van een computerberekening is een criterium dat bepaalt wanneer de oplossing gevonden is. Zulke 'stopcriteria' zijn belangrijk om de berekening tijdig stop te zetten (het maken van grote aantallen kleine tijdstappen vereist veel computertijd) maar ook om ze niet voortijdig te beëindigen wanneer de oplossing onvoldoende geconvergeerd is. Een aantal golfkoppelingsvoorbeelden worden in deze thesis getoond.

Deze thesis bestaat uit 6 hoofdstukken. Hoofdstuk 1 geeft de nodige achtergrond over het gebruikte fysisch model dat een 'koud gemagnetiseerd plasma' beschrijft en een introductie tot Maxwells vergelijkingen samen met de stroomvergelijking. In hoofdstuk 2 komt de FDTD-techniek aan bod en worden een aantal eerder bereikte resultaten besproken teneinde de specifieke bijdrage van deze thesis beter te kunnen plaatsen. Hoofdstuk 3 is één van de zwaartepunten van deze thesis: hier wordt het ontwikkelde numeriek algoritme afgeleid en besproken. Een bespreking van de aangewende randvoorwaarden is gereserveerd voor een van de delen van het hoofdstuk 3, zie (3.4). In dit hoofdstuk ging ook speciale aandacht uit naar

het ontwikkelen van criteria die toelaten na te gaan of een stationaire toestand bereikt is. Een 'stop'-criterium dient hoofdzakelijk - en dit voor een systeem waarin de oplossing 'aangedreven' wordt en dus steeds tijdafhankelijk blijft - onderscheid te maken tussen een stationaire en een niet-stationaire toestand. De Poynting flux wordt gebruikt om na te gaan of convergentie bereikt is (zie (3.5)). De afleiding van de numerieke dispersie-uitdrukking die verbonden is met het numeriek FDTD algoritme is het onderwerp van hoofdstuk 4. In het hoofdstuk 4 is ook verklaard waarom het afgeleiden van de discrete dispersie relatie in een cylindrisch coördinaatstelsel niet vanzelfsprekend is en waarom deze analyse ook in een cartesiaans coördinaten stelsel kan worden uitgevoerd. Ook de stabiliteitsanalyse van een aantal speciale gevallen komt hier aan bod. Een bespreking van de nauwkeurigheid en de stabiliteit van het algoritme gebeurt in het hoofdstuk 5 samen met de numerieke validatie van de code. Simulatieresultaten van de golfkoppeling wordt bekeken in sectie (5.5). In hoofdstuk 6, tenslotte, worden de conclusies die in dit thesiswerk bereikt werden opgesomd. De alternatieve methode om de discrete dispersie relatie te bekomen is weergegeven in het addendum A.

Summary

The finite-difference time-domain method is widely used to obtain solutions of Maxwell's equations for a broad range of electromagnetic problems. Especially, in the last two decades, the problems posed by modeling plasma waves have attracted a great deal of attention. A lot of research efforts have been spent over many years in order to improve the FDTD-methods to model wave propagation in different types of media and in particular in magnetized plasma. These efforts highlighted the potential of the convolution (RC) method, the direct-integration (DI) method, the Z-transform method, the transmission line matrix method, the split-step, the fully explicit, the fully implicit and the hybrid FDTD methods. Fully explicit methods are straightforward and easy to implement but may suffer from restrictive stability conditions. Fully implicit methods are provably unconditionally stable but require computationally intensive matrix calculations. In this light, hybrid methods seem an attractive option : they are stable at the relatively nonrestrictive vacuum Courant limit (though to our knowledge no general-case proof of this is known), and require only the solution of very small sets of equations every time-step.

The objective of the work discussed in this dissertation is to develop a global FDTD model including a magnetized cold plasma algorithm that accounts the effects of the mode conversion. To generate this model, a three-dimensional cylindrical magnetized cold plasma algorithm is developed and first validation results in 1D and 2D have been obtained. This algorithm has the capacity to simulate wave behaviour in cold plasma under the influence of an externally applied magnetic field of arbitrary direction and magnitude.

Both in flux tubes of the solar corona and in fusion devices, the geometry is basically toroidal. In this work, wave propagation is studied adopting a toroidally symmetrical configuration.

In order to compare computational results with theoretical predictions (focusing on wave dynamics rather than wave interference), it is often convenient to suppress reflections of the waves at the edge of the simulation region. For this purpose, an effective absorbing layer that acts like as an accurate and computationally efficient damping condition is constructed.

Of special interest is the case of fusion plasma when the antennas can launch different electromagnetic modes into the nonuniform plasma where they can tunnel through the evanescent layers or convert to the other modes. The plasma density increases from a very low magnitude near the antenna and the chamber conductive wall to very high on the magnetic axis. Usually the problems of the wave propagation through such structures are solved in the frequency domain.

The other approach is to apply the FDTD method to study the problems in fusion plasma.

The FDTD hot plasma description requires the solution of the kinetic equations instead of the current equations for plasma species. Constructing the current equations from the plasma conductivity tensor is also always problematic since the conductivity tensor is known only in the frequency domain.

The cold plasma approximation is adopted, which provides a fully local time-domain description for the plasma currents. Curvature effects are included by using the appropriate expression for the curl operator in cylindrical coordinates. After having grasped the cold plasma wave dynamics and having tested the suitability of the FDTD method, kinetic corrections can be incorporated to upgrade the adopted model.

A special technique to terminate the simulations after the steady state is reached is also developed in this work.

An example of mode conversion simulations is presented in this dissertation.

The dissertation consists of 6 chapters. Chapter (1) presents a background information about the physics basis of plasma parameters and the electromagnetic cold plasma waves, and a short introduction to the Maxwell's equations together with the current equation. The formulations of the basic Yee algorithm and the fundamentals of FDTD method and previous related numerical studies are described in Chapter (2). Chapter (3) contains the detailed description of the developed numerical algorithm together with its characteriscs. Namely, two types of boundary conditions are developed in this code (see Section (3.4)): one models the power source that launches the wave into the plasma and the second one is designed to control the wave fields at the plasma edges. Besides boundary conditions, a special techinique to terminate the numerical simulations when the steady state is reached is also developed in this code. The calculation of the Poynting flux is used as criteria to check whether the steady state is reached. The results of this study can be found in Chapter (3.5).

The associated discretized dispersion relation is derived explicitely in Chapter (4), and special-case stability proofs are given. Section (4.2) justifies on why a derivation of the discrete dispersion relation in the cylindrical system is not straigtforward and why this analysis still can be performed in Cartesian coordinate system.

Chapter (5) provides the description of the process and the results of the validation of the developed numerical code, i.e. the accuracy and stability analysis, the comparison of the analytical and numerical solutions, the validation of the numerical dispersion relations and its comparison to the theory. The curvature effects are studied in Section (5.4). The results of the mode conversion simulations are presented in Section (5.5).

Finally, Chapter (6) concludes the dissertation. In Appendix A the alternative way to obtain the discrete dispersion relation is presented.

List of Abbreviations

3D	Three-Dimentional
2D	Two-Dimentional
1D	One-Dimentional
FDTD	Finite-Difference Time-Domain
IEEE	Institute of Electrical and Electronics Engineers

Notations

★ ★ ★

In this thesis the consistency of notations and definitions is respected. Tables below summarize the symbolic conventions throughout the document. Some symbols are used to denote different quantities, in which case the context and dimensions should remove any ambiguity. Temporary use of symbols outside or beyond these conventions, when required by calculations or reference to original work, will be clearly indicated. The International System of units (SI) is used in all formulas.

Mathematical symbols

j	imaginary unit
∇	nabla operator
$\Re$	real part
$\Im$	imaginary part
$\lvert\cdot\rvert$	magnitude
$\mathbf{x}$	a vector
$\perp$, $\parallel$	components perpendicular and parallel to the confining magnetic field
r, φ, ϑ	radial, toroidal and poloidal components in tokamak geometry

Electromagnetic symbols

c	speed of light $[m/sec]$
t	time $[sec]$
ω	frequency $[rad/sec]$
k	wavenumber $[rad/m]$
λ	wavelength $[m]$
ϵ_0	electric permittivity $[F/m]$
μ_0	magnetic permeability $[H/m]$
$\mathbf{E}$	electric field vector $[V/m]$
$\mathbf{H}$	magnetic field vector $[A/m]$

D	electric flux density $[C/m^2]$
B	magnetic flux density $[T]$
J	electric current density $[A/m^2]$

Plasma physics symbols

s	index denotes any particle specie
e	electron index
i	ion index
m_s	mass of the specie $[kg]$
q_s	specie charge $[C]$
n_s	particle density $[1/m^3]$
ϑ_s	collision frequency $[rad/sec]$

Plasma parameters

$\omega_{ps} = \sqrt{q^2 n_s/\epsilon_0 m_s}$	plasma frequency $[rad/sec]$
$\omega_p = \sqrt{\omega_{pe}^2 + \omega_{pi}^2}$	total plasma frequency $[rad/sec]$
$\Omega_{cs} = q_s B/m_s$	cyclotron frequency $[rad/sec]$
ω_{LH}	=low hybrid frequency $[rad/sec]$
$((\Omega_{ci}\Omega_{ce})^{-1}$	+
$\omega_{pi}^{-2})^{-1/2}$	

Special functions

J_n	n-th order Bessel function of the first kind
Y_n	n-th order Bessel function of the second kind

List of Publications

Articles in International Journals

- M. Surkova, W. Tierens, Y. Pavlenko, D. Van Eester, G. Van Oost and D. De Zutter, "3D discrete dispersion relation, numerical stability and accuracy of the hybrid FDTD model for cold magnetized plasma", *IEEE Transactions on Antennas and Propagation*, vol.62, issue 12, pp. 1-10, Dec. 2014.
- M. Surkova, Y. Pavlenko, D. Van Eester, G. Van Oost and D. De Zutter, "An analysis of the hybrid FDTD scheme for modelling the propagation of the electromagnetic waves in cold magnetized toroidal plasma", *Physica Scripta*, vol. T161, 014014, May. 2014.

Articles in Conference Proceedings

- M. Surkova, Y. Pavlenko, D. Van Eester, G. Van Oost and D. De Zutter, "An analysis of the hybrid FDTD scheme for modeling the propagation of the electromagnetic waves in cold magnetized toroidal plasma", *PLASMA-2013: International Conference on Research and Applications of Plasmas*, 2-6 Sept. 2013, Warsaw, Poland.

Poster Presentations

- M. Surkova, G. Van Oost, D. Van Eester, and D. De Zutter, "Hybrid Finite-Difference Time-Domain Method for Mode Conversion Simulations in Fusion Plasma", *IPAM Workshop: Computational Challenges in Magnetized Plasma*, 16-20 Apr. 2012, Los Angeles, USA.

Application of the Hybrid Explicit/Implicit Finite-Difference Time-Domain Method (FDTD) for Electromagnetic Computations in Cold Magnetized Toroidal Plasma

1

Introduction to cold plasmas and electromagnetic wave propagation therein

★ ★ ★

Plasma is a special class of gas that includes a large number of electrons, ionized atoms and molecules, on top of neutral atoms and molecules that are present in a normal gas. Plasma is a many-particle ensemble and is characterized by its collective behaviour. The plasma medium is often referred to as the fourth state of matter because it has properties profoundly different from those of the gaseous, liquid and solid states. Plasma is generally a high-temperature entity. However, a plasma is sometimes referred to as "cold plasma" if the thermal motion of the electrons and ions is negligible.
The following section describes the important concepts of the electromagnetic wave propagation in cold plasma.

1.1 The concept of plasma parameters

1.1.1 Particle density

Particle density is measured in particles per unit volume with n_e representing the electron density and n_i representing the ion density. A plasma is quasi-neutral when $n_e =< Z > n_i$, where $< Z >$ is the average charge state of the ions.

1.1.2 Plasma Frequency

Plasma frequency is the oscillation frequency of a charged particle species in a simple unmagnetized plasma when the charge distribution is locally pertubed from its equilibrium. The plasma frequency is given by

$$\omega_{pe} = \sqrt{q^2 n_e / \epsilon_0 m_e} \tag{1.1}$$

for electrons and

$$\omega_{pi} = \sqrt{q^2 n_i / \epsilon_0 m_i} \tag{1.2}$$

for ions. For a simple plasma consisting of electrons and one ion species, the total plasma frequency is then given by

$$\omega_p = \sqrt{\omega_{pe}^2 + \omega_{pi}^2} \tag{1.3}$$

which can be approximated by the electron plasma frequency ω_{pe} for many cases because of the large mass ratio of ions to electrons.

1.1.3 Cyclotron Frequency

The response of a charged particle to an applied magnetic field B is a spiral motion around the magnetic line of force with a specific angular frequency referred to as cyclotron frequency (also known as gyrofrequency). The raduis of the spiral motion is called Larmor radius. The cyclotron frequency of a charged particle species j is mathematically defined as $\omega_{cj} = q_i B / m_j$.

1.2 Overview of the electromagnetic wave propagation in a cold plasma

1.2.1 Dispersion relation in a uniform cold plasma

The dispersion relation of the electromagnetic way can be found by solving the wave equation, with the assumption that first-order quantities vary as $exp(j(\mathbf{k} \cdot \mathbf{r} - \omega \mathbf{t}))$ [1].

$$\mathbf{n} \times (\mathbf{n} \times \mathbf{E}) + \mathbf{K} \cdot \mathbf{E} = 0 \tag{1.4}$$

where the index of refraction $\mathbf{n}$ is defined as

$$\mathbf{n} = \frac{c}{\omega} \mathbf{k} \tag{1.5}$$

with **k** as a wave vector and the dielectric tensor is

$$\begin{pmatrix} S & -iD & 0 \\ iD & S & 0 \\ 0 & 0 & P \end{pmatrix} \tag{1.6}$$

with P, S and D are defined as

$$P = 1 - \sum_s \frac{\omega_{ps}^2}{\omega^2}, \tag{1.7}$$

$$S = \frac{R+L}{2}, \tag{1.8}$$

and

$$D = \frac{R-L}{2}, \tag{1.9}$$

where

$$R = 1 - \sum_s \frac{\omega_{ps}^2}{\omega(\omega + \Omega_{cs})} \tag{1.10}$$

and

$$L = 1 - \sum_s \frac{\omega_{ps}^2}{\omega(\omega - \Omega_{cs})}. \tag{1.11}$$

The letters P, S, D, R and L stand for the 'product', 'sum', 'difference', 'right-hand' and 'left-hand', respectively. The R and L terms arise in a derivation based on expressiong the fields in terms of rotating polarization. The second term of the R- and L-terms is usually called a susceptibility term. For more detail, the reader is referred to [1].

Since plasma is isotropic, the applied magnetic field can be expressed as $\mathbf{B} = B\mathbf{z}$. Defining θ as the angle between **B** and **n** and assuming that **n** is in the $x-z$ plane, the Equation (1.4) can be written in matrix form [1] as:

$$\begin{pmatrix} S - n^2\cos^2\theta & -iD & n^2\cos\theta\sin\theta \\ iD & S - n^2 & 0 \\ n^2\cos\theta\sin\theta & 0 & P - n^2\sin^2\theta \end{pmatrix} \begin{pmatrix} E_x \\ E_y \\ E_z \end{pmatrix} = 0 \tag{1.12}$$

where E_x, E_y and E_z are the electric field components.

The index s denotes the particle species. In order to have a nontrivial solution for Equation (1.6), one requires that the determinants of the coefficients vanish. The resulting equation is the dispersion equation.

This condition generates the biquadratic Equation (1.13):

$$An^4 - Bn^2 + C = 0 \tag{1.13}$$

where

$$A = Ssin^2\theta + Pcos^2\theta, \tag{1.14}$$

$$B = RLsin^2\theta + PS(1 + cos^2\theta) \tag{1.15}$$

and

$$C = PRL \tag{1.16}$$

The solution of Equation (1.13) may be written in terms of the angle θ as

$$tan^2\theta = -\frac{P(n^2 - R)(n^2 - L)}{(Sn^2 - RL)(n^2 - P)} \tag{1.17}$$

The dispersion relations for propagation at $\theta = 0$ and $\theta = \pi/2$ are quickly obtained from Equation (1.17). For $\theta = 0$:

$$P = 0, n^2 = R, n^2 = L \tag{1.18}$$

For $\theta = \pi/2$

$$n^2 = \frac{RL}{S}, n^2 = P \tag{1.19}$$

1.3 Cold plasma waves. Dispersion relations.

Plane waves in a cold plasma (one-specie plasma)

A special case of Equation (1.18), the $(\omega - k)$ dispersion relation of the plane waves in a cold collisionless one-specie plasma has the form:

$$\omega^2 = k^2c^2 + \omega_p^2 \tag{1.20}$$

These waves propagate in any direction and in the absence of plasma ($\omega_p^2 \propto n^2 \rightarrow 0$) the dispersion relation of these plasma waves takes the well-known form of that of light waves:

$$\omega = kc \tag{1.21}$$

Fig.(1.1) is the $\omega - k$ diagram for the plane waves in a cold homogeneous isotropic plasma. This figure shows that plane waves propagate in a plasma only for frequencies higher than the plasma frequency. In the vicinity of $\omega = \omega_p$, the wavelength becomes very large.

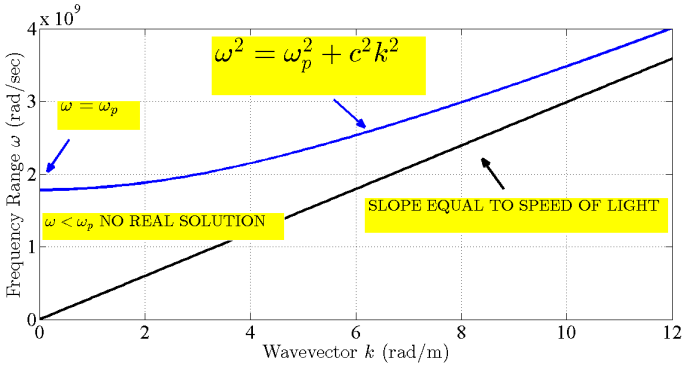

Figure 1.1: Frequency versus wave number diagram for plane electromagnetic waves in a cold collisionless plasma. For $\omega < \omega_p$ waves are evanescent.

1.3.1 Waves that propagate perpendicular to the magnetic field in a cold magnetized plasma

In many magnetically confined plasmas, waves are launched in a direction perpendicular to the strong, confining magnetic field. The wave with its **E** vector parallel to the magnetic field is called the ***ordinary wave***, because the dispersion relation is the same as if the magnetic field was zero. The wave with its **E** vector perpendicular to the magnetic axis is called the ***extraordinary wave*** [2], [3].

To obtain the dispersion relation of the high-frequency waves propagating perpendicular to the magnetic field, set $\theta = \pi/2$ [1].

For the ordinary wave $\mathbf{E}||\mathbf{B}_0$ the dispersion relation is (1.19)

$$k = \pm\frac{\omega}{c}\left(1 - \frac{\omega_p^2}{\omega^2}\right)^{1/2} \tag{1.22}$$

At high frequencies ($\omega >> \omega_p$) this electromagnetic wave takes no notice of the plasma, and $k = \omega/c$. For the extraordinary wave $\mathbf{E} \perp \mathbf{B}_0$ the dispersion relation (1.19) takes the form:

$$k = \pm\frac{1}{c}\left[\frac{(\omega^2 - \omega_1^2)(\omega^2 - \omega_2^2)}{\omega^2 - \omega_H^2}\right]^{1/2} \tag{1.23}$$

where ω_1 and ω_2 are the cutoff frequencies, i.e.

$$\omega_1 = \frac{\Omega_{ce}}{2}\left[-1+\left(1+\frac{4\omega_p^2}{\Omega_{ce}^2}\right)^{1/2}\right], \tag{1.24}$$

$$\omega_2 = \frac{\Omega_{ce}}{2}\left[1+\left(1+\frac{4\omega_p^2}{\Omega_{ce}^2}\right)^{1/2}\right] \tag{1.25}$$

A resonance appearing in this extraordinary wave dispersion relation is at $\omega = \omega_H$, where ω_H is an upper hybrid frequency and it is equal to

$$\omega_H = \left(\omega_p^2 + \omega_{ce}^2\right)^{1/2} \tag{1.26}$$

The frequency bands in which these waves exist and the velocities of these waves are seen in Fig. (1.2).

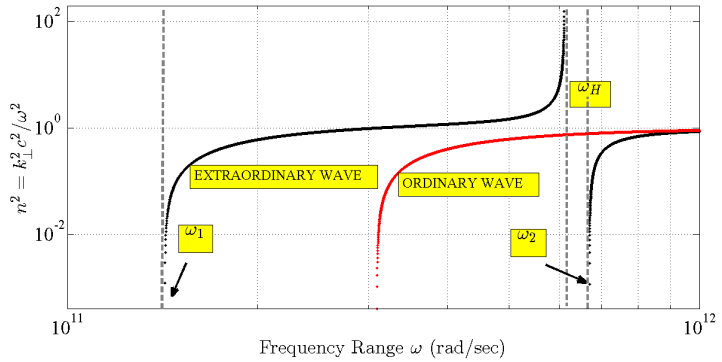

Figure 1.2: Index of refraction $n^2 = k^2c^2/\omega^2$ versus ω for the ordinary and extraordinary waves.

At high frequency $\omega \to kc$ for all the modes. The extraordinary mode has two distinct frequency ranges, with a characteristic index of refraction:

$$\omega >> \omega_H : n^2 = \left(\frac{kc}{\omega}\right)^2 = 1 \tag{1.27}$$

$$\omega \leq \omega_H : n^2 >> 1, \tag{1.28}$$

and there are two bands $\omega_H < \omega < \omega_2$ and $\omega < \omega_1$ in which the wave doesn't propagate.

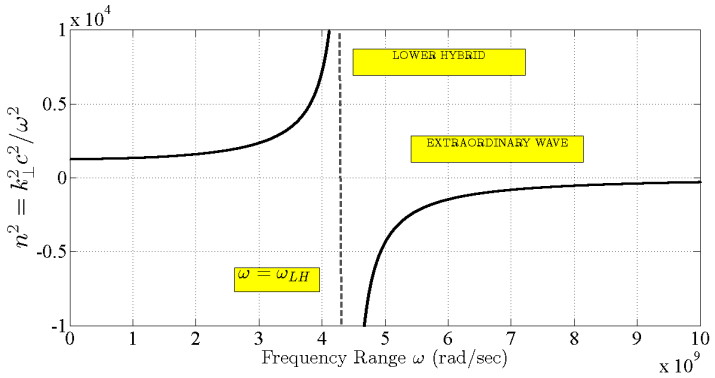

Figure 1.3: Index of refraction $n^2 = k^2c^2/\omega^2$ versus ω for the extraordinary waves.

1.3.2 Fast and slow waves

The Equation (1.6) can be rewritten in terms of parallel and perpendicular components of **n**. I.e., setting $n_{||} = n\cos\theta$ and $n_\perp = n\sin\theta$ the wave equation takes the form:

$$\begin{pmatrix} S - n_{||}^2 & -iD & n_{||}n_\perp \\ iD & S - n_{||}^2 + n_\perp^2 & 0 \\ n_{||}n_\perp & 0 & P - n_\perp^2 \end{pmatrix} \begin{pmatrix} E_x \\ E_y \\ E_z \end{pmatrix} = 0 \tag{1.29}$$

Analogously, if $n_{||}$ is set by plasma parameters then it is possible to solve Equation (1.29) for a non-trivial solution for $n_\perp$ by setting the determinant of the matrix to zero.

For waves with $\omega << \omega_{ps}$, $P >> n^2$ and the dispersion realtion can be simplified to a 4th order algebraic equation with solutions such as

$$n_\perp^2 = \frac{(S - n_{||}^2)^2 - D^2}{S - n_{||}^2} \tag{1.30}$$

$$n_\perp^2 = \frac{P(S - n_{||}^2)}{S} \tag{1.31}$$

Generally, the mode described by solution (1.30) is classified as the fast wave while (1.31) as the slow wave. The dispersion relationship of fast waves in the ion cyclotron frequency range (1.30) may be also rewritten in the following form [3]:

$$n_\perp^2 = \frac{\left(n_{||}^2 - R\right)\left(n_{||}^2 - L\right)}{S - n_{||}^2} \tag{1.32}$$

where R, L, S are 1.10, 1.11, 1.8, respectively. This solution indicates that there are regions of two cut-offs defined by $R = n_{||}^2$ and $L = n_{||}^2$ and one resonance defined by $S = n_{||}^2$ respectively. This resonance referred as the Alfven resonance, implying that the perpendicular wavenumber becomes infinite when the wave approaches this region.

The concept of the ion cyclotron resonant heating was first suggested by Stix [1] using the ion cyclotron mode. Frequency of this mode, referred as the 'slow wave' is a little bit lower than the ion cyclotron frequency. For tokamak and other systems Stix has shown that only another branch of wave with frequency higher than the ion cyclotron frequency can propagate into the central region of plasma, this branch is referred as the fast wave [1], [4].

Here, the extraordinary and ordinary waves are actually the fast and the slow wave, respectively, however, they work in the different ranges of frequency.

Below, a short introduction to the Maxwell's equations and the Lorentz equation of motion is given.

1.4 Maxwell's Equations and the Current Equation derived from the Lorentz Equation of Motion

★ ★ ★

In this section a short introduction to the Maxwell's equations and the current Equation derived from the Lorentz equation of motion which form the basis of the FDTD method for simulations of electromagnetic wave interactions [5] is presented.

1.4.1 Maxwell's equations

Considering a source-free region containing materials that may absorb electric energy, the time-dependent Maxwell's equations are given in differential form as follows:

Faraday's Law:

$$\nabla \times \mathbf{E} = -\partial \mathbf{B}/\partial t \tag{1.33}$$

Ampere's Law:

$$\nabla \times \mathbf{H} = -\partial \mathbf{D}/\partial t + \mathbf{J} \tag{1.34}$$

Gauss's Law for the electric field (charges are omitted):

$$\nabla \cdot \mathbf{D} = 0 \tag{1.35}$$

Gauss's Law for the magnetic field:

$$\nabla \cdot \mathbf{B} = 0 \tag{1.36}$$

These equations relate **E**, **H**, **D**, **B**, and **J**, all of which are functions of the space and time. For linear isotropic non-dispersive medium, electric flux density **D** is related to **E** by constitutive relationship $\mathbf{D} = \epsilon_0 \mathbf{E}$, **B** is related to magnetic field **H** by $\mathbf{B} = \mu_0 \mathbf{H}$. Substituting these three proportions into Equations (1.33) and (1.34) and writing out components of the curl operator ∇ in Cartesian coordinates yields the following coupled scalar equations:

$$\frac{\partial H_x}{\partial t} = \frac{1}{\mu_0}\left[\frac{\partial E_y}{\partial z} - \frac{\partial E_z}{\partial y}\right] \tag{1.37}$$

$$\frac{\partial H_y}{\partial t} = \frac{1}{\mu_0}\left[\frac{\partial E_z}{\partial x} - \frac{\partial E_x}{\partial z}\right] \tag{1.38}$$

$$\frac{\partial H_z}{\partial t} = \frac{1}{\mu_0}\left[\frac{\partial E_x}{\partial y} - \frac{\partial E_y}{\partial x}\right] \tag{1.39}$$

$$\frac{\partial E_x}{\partial t} = \frac{1}{\epsilon_0}\left[\frac{\partial H_z}{\partial y} - \frac{\partial H_y}{\partial z} - J_{sx}\right] \tag{1.40}$$

$$\frac{\partial E_y}{\partial t} = \frac{1}{\epsilon_0}\left[\frac{\partial H_x}{\partial z} - \frac{\partial H_z}{\partial x} - J_{sy}\right] \tag{1.41}$$

$$\frac{\partial E_z}{\partial t} = \frac{1}{\epsilon_0}\left[\frac{\partial H_y}{\partial x} - \frac{\partial H_x}{\partial y} - J_{sz}\right] \tag{1.42}$$

The above six coupled partial differential equations form the basis of the FDTD method for simulations of electromagnetic wave interactions.

1.4.2 Current equation

The equation of motion of a particle in electromagnetic field is given by the Lorentz force law

$$\mathbf{F} = q_s(\mathbf{E} + v \times \mathbf{B}) \tag{1.43}$$

The current equation derived from the Lorentz equation of motion has the following form:

$$(\frac{\partial}{\partial t} + \vartheta_s)\mathbf{J}_s = \epsilon_0 \omega_{ps}^2 \mathbf{E} - \boldsymbol{\Omega}_s \times \mathbf{J}_s. \tag{1.44}$$

As it is mentioned above, the set of Equations (1.33-1.34) and the Equation (1.44) lay the groundwork for the upcoming FDTD approach for simulations of the electro-magnetic waves.

References

[1] T. H. Stix, *Waves in plasmas*. Springer, 1992.

[2] N. A. Krall, A. W. Trivelpiece, and K. R. Symon, "Principles of plasma physics", *IEEE Trans. Plasma Sci.*, vol. 2, no. 3, pp. 196 –196, Sep. 1974.

[3] M. Brambilla, *Kinetic Theory of Plasma problems: Homogeneous Plasma*. Clarendon Press, 1998, vol. 1.

[4] T. H. Stix, "Fast wave heating of a two component plasma", vol. 15, no. 4, p. 737, Oct. 1975.

[5] A. Taflove and S. C. Hagness, *Computational Electrodynamics*. Artech House, 2005.

2

Introduction to the FDTD method

★ ★ ★

The finite-difference time-domain (FDTD) algorithm was originally proposed by Kane Yee [1] in 1966 and was later named and further developed by Taflove [2] and others for numerically solving Maxwell's equations.
*The FDTD algorithm is based on a central difference approximation of the spatial and time derivations of Maxwell's equations. The algorithm works by dividing the solution space along a regular grid and calculating the electric and magnetic field values at every location in the grid. The FDTD method is a time marching algorithm in which the values of the electric field are based on the values of the magnetic and the electric field at the previous time step and vice versa. As time progresses in the algorithm, time varying fields are propagated through the FDTD grid. In the FDTD algorithm the position of the field values are staggered in both space and time due to the use of central differences. Below Fig. 2.1 shows a standard Yee cell in which the distance between any field value along a Cartesian plane is one half of the length of the unit cell. The original FDTD technique directly discretized Ampere's and Faraday's laws into a system of difference equations based on the electric field (**E**) and the magnetic field (**H**). The FDTD method can be easily parallelized and scaled on high performance computing systems. In the following chapter the fundamentals of the FDTD method are briefly introduced.*

2.1 Formulations of the basic Yee algorithm

2.1.1 Yee mesh

To numerically discretize Maxwell's equations (see Chapter 1.4), Yee defined an orthogonal cubic lattice whose unit cell is illustrated in Fig. 2.1 to spatially allocate the field components. For this allocation, each field component is sampled and evaluated at a particular space position so that every **E** component is surrounded by four circulating **H** components, and every **H** component is surrounded by four circulating **E** components. This provides an elegant yet simple picture of three-dimentional (3D) space being filled by interlinked arrays of Faraday's and Ampere's law contours. The two Gauss's law are also simultaneously satisfied by this arrangement. Thus, it is possible to identify the **E** components linking with the **H** loops and, correspondingly the **H** components linking with the **E** loops as shown in Fig. 2.1. In the time domain, the **H**− and **E**− fields are obtained at time instant delays by half the sampling time step. The time advancing algorithm is explicit and can be easily adapted into computer programs to be solved numerically.

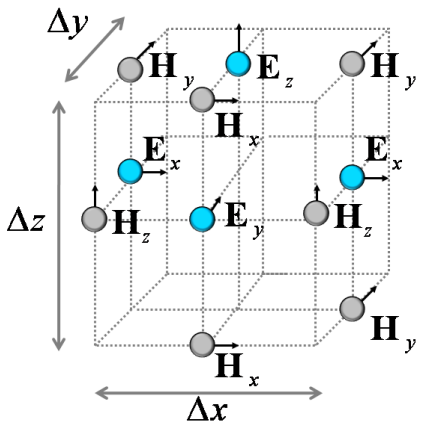

Figure 2.1: Orthogonal Yee cell.

2.1.2 Discretization of Maxwell's Equations

Yee's FDTD algorithm denotes any function f of space and time evaluated at a discrete point as $f(i\Delta x, j\Delta y, k\Delta z, n\Delta t) = f^n_{i,j,k}$, where Δt is the time increment and Δx, Δy and Δz are the lattice step increments in the x, y and z coordinate directions, respectively. The indices i, j, k and n are all integers. Utilizing the spatial gridding scheme defined in Fig. 2.1, Yee applied a second-order accurate central-difference scheme to both the space and time derivatives of Equations (1.37-1.42) based on Taylor's series expansion. For example, the first partial time derivative

$\frac{\partial E_x}{\partial t}$ of Equation (1.40) evaluated at $(i, j+1/2, k+1/2, n)$ can be expressed as

$$\frac{\partial E_x|^n_{i,j+1/2,k+1/2}}{\partial t} = \frac{E_x|^{n+1/2}_{i,j+1/2,k+1/2} - E_x|^{n-1/2}_{i,j+1/2,k+1/2}}{\Delta t} + O\left[(\Delta t)^2\right] \tag{2.1}$$

where the $\pm 1/2$ increment in the time-coordinate superscript n denotes a time domain finite-difference over $\pm 1/2\Delta t$. Similarly, the first partial space derivative $\frac{\partial H_z}{\partial z}$ and $\frac{\partial H_y}{\partial z}$ of Equation (1.40) evaluated at $(i, j+1/2, k+1/2, n)$ can be expressed as follows

$$\frac{\partial H_y|^n_{i,j+1/2,k+1/2}}{\partial z} = \frac{H_y|^n_{i,j+1/2,k+1} - H_y|^n_{i,j+1/2,k}}{\Delta z} + O[(\Delta z)^2] \tag{2.2}$$

$$\frac{\partial H_z|^n_{i,j+1/2,k+1/2}}{\partial y} = \frac{H_z|^n_{i,j+1,k+1/2} - H_z|^n_{i,j,k+1/2}}{\Delta y} + O[(\Delta y)^2] \tag{2.3}$$

where the $+1$ increment in the space-coordinate superscript j and k denotes a space domain finite-difference over Δy and Δz, respectively. The approximations of the partial derivatives in Equations (2.1-2.2) are said to be of second order accuracy. That means the second and higher order derivatives of the Taylor series, which are usually not computed, are treated as a rounding error of the order $O[(\Delta t)^2]$,$O[(\Delta y)^2]$ and $O[(\Delta z)^2]$, respectively.
The E_x values can be defined via the so-called semi-implicit approximation such as

$$E_x|^n_{i,j+1/2,k+1/2} = \frac{E_x|^{n+1/2}_{i,j+1/2,k+1/2} + E_x|^{n-1/2}_{i,j+1/2,k+1/2}}{2} \tag{2.4}$$

Next, using the approximations mentioned above the final explicit time-stepping relation for E_x can be obtained.Similarly, the time-stepping equations for all other field components E_y, E_x, H_x, H_y and H_z can be obtained by analogous procedures.

2.1.3 Courant Condition

The choice of space and time increments for the FDTD algorithm can affect the propagation characteristics of numerical waves in the FDTD lattice, and therefore the numerical error and stability. To avoid numerical instability, the time step Δt is required to have a specific bound relative to the lattice space increments Δx, Δy and Δz in accordance with the Courant-Fredrich-Levy stability condition [2] known as a Courant condition.

$$c\Delta t \sqrt{\frac{1}{\Delta x^2}\sin^2\left(\frac{\beta_x \Delta x}{2}\right) + \frac{1}{\Delta y^2}\sin^2\left(\frac{\beta_y \Delta y}{2}\right) + \frac{1}{\Delta z^2}\sin^2\left(\frac{\beta_z \Delta z}{2}\right)} \leq 1 \tag{2.5}$$

The rigorous derivation procedure of the Courant condition is based on complex-frequency analysis and can be found in [2]. According to this analysis, Equation (2.5) has to be hold to maintain the numerical solutions bounded in time, where β_x, β_y and β_z are the wavevector components. Equation (2.5) can always be satisfied if the Courant number **C** fulfills

$$\mathbf{C} \equiv c\Delta t \sqrt{\frac{1}{\Delta x^2} + \frac{1}{\Delta y^2} + \frac{1}{\Delta z^2}} \leq 1 \tag{2.6}$$

The Courant condition defining the upper bound of the time step Δt can then be derived as:

$$\Delta t \leq \frac{1}{c\sqrt{\frac{1}{\Delta x^2} + \frac{1}{\Delta y^2} + \frac{1}{\Delta z^2}}} \tag{2.7}$$

When $\Delta x = \Delta y = \Delta z = \Delta$, Equation (2.7) becomes $\Delta t \leq \Delta/(c\sqrt{n})$, where n is the dimension of the simulation domain. The Courant condition imposes an upper limit to the time increment which is related to the space increments. Enforcement of this upper bound on Δt guarantees the stability of the numerical algorithm. However, this condition can lead to small time increments for fine space discretization problems causing a highly computer intensive problem in terms of simulation time.

2.1.4 Cell-size Determination

In general, there are three key-points that have to be reached:
(1) the waves should be spatially well-resolved (which requires enough sampling points per wavelength),
(2) the waves should be temporally well-resolved (enough points per period),
(3) the Courant stability should be satisfied.
The first and second points determine accuracy, the third one determines stability.

The cell size must be much less than the smallest wavelength involved in the simulation. The number of points per wavelength is dependent on many factors. However, an often required constraint is 10 cells per wavelength [2], [3]. Also, the time step must be much smaller than the smallest period (highest frequency). But on one side, in 1D vacuum FDTD, (3) follows from (1) and (2): if there are $10\Delta x$ per wavelength ($\Delta x = \lambda/10$), and also $10\Delta t$ per period P ($\Delta t = P/10 = 1/(10 \cdot f) = \lambda/(10{\cdot}c)$), the Courant condition is obeyed : $\Delta x/\Delta t = (\lambda/10)/(\lambda/(10{\cdot}c)) = c$ but in general, (3) imposes limits on Δt above and beyond those demanded by accuracy, which can greatly increase the number of program steps needed, and which is why increasing the Courant limit (e.g. by using (partially) implicit methods) is considered to be advantageous.

2.2 Overview of existing FDTD methods for cold plasma

Many different FDTD techniques have been employed in the past to simulate the cold plasma medium such as the recursive convolution (RC) method [4], [5], [6], [7], [8], the direct integration (DI) method [9], [10], [11], [12],[13], [14], [15], the Z-transform method [16], [17], the transmission line matrix method [18] and the fully implicit method [19] which will be analyzed below. Among these many approaches the RC method and the DI method are the most widely used techniques because of their ease of implementation. A systematic analysis of these FDTD techniques has been detailed in [20] and [21].

The RC method utilizes the following property: the time-domain constitutive relation between displacement vector **D** and electric field **E** is given as a convolution integral whose time domain susceptibility function is known. An iteration derived from this time-domain convolution integral is then coupled with the difference approximations of Maxwell's equations to form the whole iteration set. For the RC method, a general algorithm can be derived that allows efficient simulation of any material with a complex electric permittivity that can be parameterized by means of a proper rational function of frequency. The major shortcoming, however, is that the accuracy can be influenced by using more or less exact algorithms for the numerical integration involved, which results in a trade-off between accuracy and computational efficiency. For studies requiring an extensive time interval to be considered, the accumulation of errors may be too large [22].

The DI method is based on direct finite-difference approximations of the complete field equations of the medium that consist of Maxwell's equations coupled with an auxiliary ordinary differential equation. Compared to the RC method, the DI method needs no changes in the algorithm when modeling materials with different permittivity functions, and the implementation is also much more straightforward.

2.2.1 DI methods for isotropic cold plasma

The theory describing EM wave propagation in cold plasma is known as magnetoionic theory [23] that assumes zero thermal velocity for the charged species. This is a good approximation as long as the thermal velocity is much less than the phase velocity of waves in cold plasma [24]. The governing equations for a source-free nonmagnetized cold plasma containing only electrons are shown as Equations (2.8-2.10). In this equation set, the Maxwell's Equations (2.8) and (2.9) are coupled with the auxiliary Equation (2.10) that relates the current **J** and the electric field **E**.

$$\nabla \times \mathbf{E} = -\mu_0 \frac{\partial \mathbf{H}}{\partial t} \tag{2.8}$$

$$\nabla \times \mathbf{H} = \epsilon_0 \frac{\partial \mathbf{E}}{\partial t} + \mathbf{J} \tag{2.9}$$

$$\frac{\partial \mathbf{J}}{\partial t} + \vartheta \mathbf{J} = \epsilon_0 \omega_p^2 \mathbf{E} \tag{2.10}$$

where ω_p is the plasma frequency and ϑ is the collision frequency. To numerically discretize Equations (2.8-2.10), many different leapfrog approximations have been developed as detailed in [21] and [20]. The following section will discuss the different requirements and simulation conditions for each of these developed techniques. For all of the methods listed below, J and E components occupy the same spatial locations in the Yee grid. H and E components are interleaved with a time-domain interval $\Delta t/2$ and a space domain interval $\Delta/2$.

Young's method

In Young's method [10], J and E components are interleaved with a time interval $\Delta t/2$, which means that J and H are collocated in time domain. For this reason, Young's method is also referred to as an $H - J$ collocated method. By central-differencing the derivatives of Equations (2.8-2.10) and central-averaging the ϑJ term of Equation (2.10), the resulting leapfrog approximations can be expressed as

$$\mathbf{H}^{n+1/2} = \mathbf{H}^{n-1/2} - \frac{\Delta t}{\mu_0} \nabla \times \mathbf{E}^n \tag{2.11}$$

$$\epsilon_0 \left[\frac{\mathbf{E}^{n+1} - \mathbf{E}^n}{\Delta t} \right] + \mathbf{J}^{n+1/2} = \nabla \times \mathbf{H}^{n+1/2} \tag{2.12}$$

$$\frac{\mathbf{J}^{n+1/2} - \mathbf{J}^{n-1/2}}{\Delta t} + \vartheta \frac{\mathbf{J}^{n+1/2} + \mathbf{J}^{n-1/2}}{2} = \epsilon_0 \omega_p^2 \mathbf{E}^n \tag{2.13}$$

Young's method requires only one time level storage of each field component, and uses significantly fewer multiplication and addition operations per time step than the other methods mentioned above.

Nickisch and Franke's Method

Different from Young's method, the J and E components in Nickisch and Franke's method [9] are collocated in time domain. As a result, the current derivative term $\partial J/\partial t$ of Equation (2.10) is then central-differenced as $(J^{n+1} - J^{n-1})/(2\Delta t)$. B y central-averaging the J term of Equation (2.9), Equations (2.8-2.10) are then discretized as

$$\mathbf{H}^{n+1/2} = \mathbf{H}^{n-1/2} - \frac{\Delta t}{\mu_0}\nabla \times \mathbf{E}^n \tag{2.14}$$

$$\epsilon \left[\frac{E^{n+1} - E^n}{\Delta t}\right] + \left[\frac{J^{n+1} + J^n}{2}\right] = \nabla \times H^{n+1/2} \tag{2.15}$$

$$\frac{\mathbf{J}^{n+1} - \mathbf{J}^{n-1}}{2\Delta t} + \nu \cdot \mathbf{J}^n = \epsilon_0 \omega_p^2 \mathbf{E}^n \tag{2.16}$$

Observed from Equations (2.15-2.16), the memory requirement of Nickisch and Franke's method is bigger than that of Young's method since two-levels of J must be stored now.

Cummer's method

In Cummer's method [20], the J and E components are collocated in both time and space domain so it is referred to as $E-J$ collocation method. Different from Nickisch and Franke's method, Equation (2.10) is now discretized at time step $n+1/2$ instead of n. By central-averaging the J terms of Equations (2.9) and (2.10) and the E term of Equation (2.10), the resulting leapfrog approximations of Equations (2.8-2.10) are

$$\mathbf{H}^{n+1/2} = \mathbf{H}^{n-1/2} - \frac{\Delta t}{\mu_0}\nabla \times \mathbf{E}^n \tag{2.17}$$

$$\epsilon_0 \left[\frac{\mathbf{E}^{n+1} - \mathbf{E}^n}{\Delta t}\right] + \left[\frac{\mathbf{J}^{n+1} + \mathbf{J}^n}{2}\right] = \nabla \times \mathbf{H}^{n+1/2} \tag{2.18}$$

$$\frac{\mathbf{J}^{n+1} - \mathbf{J}^n}{\Delta t} + \vartheta \cdot \frac{\mathbf{J}^{n+1} + \mathbf{J}^n}{2} = \epsilon_0 \omega_p^2 \left[\frac{\mathbf{E}^{n+1} + \mathbf{E}^n}{2}\right] \tag{2.19}$$

Cummer's exponential fitting method

Notice that the analytical solution of Equation (2.10) varies as $e^{-\vartheta t}$, indicating a growth per time step factor of $e^{-\vartheta \Delta t}$. To provide a more accurate approximation, Cummer [20] proposed a new discretization scheme shown as Equation (2.22) by applying a one step exponential fitting to Equation (2.10). The approximations of Equations (2.8) and (2.9) are kept the same as in Cummer's method described above. The resulting time stepping algorithm of Equations (2.8-2.10) can be written as

$$\mathbf{H}^{n+1/2} = \mathbf{H}^{n-1/2} - \frac{\Delta t}{\mu}\nabla \times \mathbf{E}^{n} \tag{2.20}$$

$$\epsilon_0 \left[\frac{\mathbf{E}^{n+1} - \mathbf{E}^{n}}{\Delta t}\right] + \left[\frac{\mathbf{J}^{n+1} + \mathbf{J}^{n}}{2}\right] = \nabla \times \mathbf{H}^{n+1/2} \tag{2.21}$$

$$\mathbf{J}^{n+1} = e^{-\vartheta \Delta t}\mathbf{J}^{n} + \frac{\epsilon_0 \omega_p^2}{\vartheta^2 \Delta t}\left[\left(\vartheta \Delta t + e^{-\vartheta \Delta t}\right)\mathbf{E}^{n+1} + (1 - e^{-\vartheta \Delta t} - \vartheta \Delta t e^{-\vartheta \Delta t})\mathbf{E}^{n}\right] \tag{2.22}$$

The homogeneous solution of the leapfrog approximation (2.22) has a growth per time step factor of $e^{\vartheta \Delta t}$ so it is exponentially fitted to the auxiliary differential Equation (2.10). For non-small $\nu \Delta t$ values, Cummer's exponential fitting method is considered as a more accurate numerical approach.

Smithe's method

Simulations of dense plasma in the radiofrequency range are typically performed in the frequency domain. This technique is well-suited for the study of linear heating and quasilinear evolution, but does not generalize well to the study of nonlinear phenomena. Conversely, a time-domain simulation in this range is difficult because the time scale is long compared to the electron plasma wave period, and in addition, the various cutoff and resonance behaviours within plasma leads to the fact that any explicit finite-difference scheme would be numerically unstable. To resolve this dilemma, explicit finite-difference Maxwell terms are maintained but a carefully time-centered locally implicit method is introduced to treat the plasma current, such that all linear plasma dispersion behaviour is reproduced at the available temporal and spatial resolution. Smithe's [25] algorithm requires that the time step abides by the vacuum Courant condition, and may be described as being explicit in vacuum wave propagation terms, and implicit in plasma wave terms.

The complete update set of equations for the time-domain plasma turns out to be:

Explicit:

$$\mathbf{B}^{n+1/2} = \mathbf{B}^{n} - (\Delta t/2)\nabla_{FD} \times M^{transpose} \cdot \mathbf{E}^{n} \tag{2.23}$$

Implicit:

$$\begin{aligned}\mathbf{J}_s^{n+1} = \mathbf{J}_s^n + \left(\epsilon_0 \omega_{ps}^2 \Delta t/2\right)\left(\mathbf{E}^{n+1} + \mathbf{E}^n\right) - \\ (\Delta t/2)\boldsymbol{\Omega}_s \times \left(\mathbf{J}_s^{n+1} + \mathbf{J}_s^n\right) - \\ \left(\nu_s \Delta t/2\right)\left(\mathbf{J}_s^{n+1} + \mathbf{J}_s^n\right)\end{aligned} \tag{2.24}$$

Implicit:

$$\begin{aligned}\mathbf{E}^{n+1} = \mathbf{E}^n - \left(\Delta t/\epsilon_0/2\right)\sum\nolimits_s \left(\mathbf{J}_s^{n+1} + \mathbf{J}_s^n\right) + \\ M \cdot \left[-\left(\Delta t/\epsilon_0\right) J_p^{n+1/2} + \left(c^2 \Delta t\right)\nabla_{FD} \times \mathbf{B}^{n+1/2}\right]\end{aligned} \tag{2.25}$$

Explicit:

$$\mathbf{B}^{n+1} = \mathbf{B}^{n+1/2} - (\Delta t/2)\nabla_{FD} \times M^{transpose} \cdot \mathbf{E}^{n+1} \tag{2.26}$$

where $\nabla_{FD}\times$ refers to the finite-difference curl operations, $\mathbf{B}$ are the Yee-cell magnetic field components localized to the faces of the unit cell, and provision has been made for future use of the usual half time step Yee-cell edge-component particle currents, $\mathbf{J}_p^{n+1/2}$. Here, $\mathbf{J}_p$ is set to zero. Since the fields $\mathbf{E}$ and $\mathbf{J}_s$ are localized at the nodes of a Yee-cell, it is necessary to map the two Yee-edge fields to the common node with a mapping M to be able to apply the other vector update equations [25].

The method of Smithe is applied in this work and the study on the application of this method to a magnetized toroidal plasma is discussed in Chapter 3.

2.2.2 Tierens' method

If Smithe solves the set of equations (2.23-2.26) in an explicit/implicit way by repeatedly interpolating from Yee-cell positions to collocated positions and back, then a fully implicit time-domain approach which is unconditionally stable such that the space and the time step can be chosen independently is developed by Tierens.

To give a particular example, a plasma wave beach, which is a slab configuration in which the density increases monotonically, simulation would be very difficult for Young's method, because Δt would have to resolve the very large plasma frequency. Smithe's method and Tieren's method can do plasma wave beaches easily, because the plasma frequency does not influence their Courant condition. Both Smithe's method and Young's method have trouble with phenomena whose wavelength is much smaller than c/f, because those force them to use a Δt which is much smaller than the period, and thus they need prohibitively many time steps

just to do a few periods. Tieren's method, on the other hand, has no problem with that either because you can just set Δt to whatever fraction of the period you prefer.

A more detailed explanation can be found in [19].

2.2.3 Analysis of the existing FDTD methods

Method	Courant condition
Young's method	$\Delta t < \frac{1}{\sqrt{\frac{c^2}{\Delta x^2}+\frac{\omega_p^2}{4}}}$
Nickisch and Franke's method	$\Delta t < \frac{1}{\sqrt{\frac{c^2}{\Delta x^2}+\frac{\omega_p^2}{4}}}$
Cummer's method	$\Delta t < \frac{\Delta x}{c}$
Cummer's Exponential Fitting method	$\Delta t < \frac{\Delta x}{c}$
Smithe's method	$\Delta t < \frac{\Delta x}{c}$
Tierens' method	∞ (implicit)

Table 2.1: Maximum numerical stability factors for different FDTD methods [20], [21], [25].

An important property of a numerical technique is its stability. For a stable algorithm, an error, whatever its cause, does not grow exponentially during the iteration, meaning that the solution changes by only a small amount for each time step. To the contrary, if a method is unstable, any small error generated during the iteration will grow to be a much larger error and it will overwhelm the desired solution. This will cause the algorithm to produce unrepresentable numbers (NaN) instead of real values. In other words, it should be noted that the Courant condition is not the condition under which the simulation approximates physics acceptably, it is the condition under which the simulation is stable. In time-domain, one typically takes stability to be a necessary condition (but not a sufficient one) for approximating physics, because instability implies the existence of exponentially-growing modes which are not physical. Accuracy is then obtained by choosing the space and time step small enough. The advantage of having a large Courant number is that it allows to choose the space and time steps independently, one purely based on the expected wavelengths, and one purely based on the expected periods. It does not mean that the arbitrarily large time steps can be taken- the arbitrarily large time steps can be taken without losing stability, but not without losing accuracy. Also it has to be mentioned that the discrete time-stepping operator in Tieren's method, as in all stable methods, has eigenvalues on the unit circle. The eigenvalues of the corresponding true continuous time-stepping operator are also

on the unit circle, but they have different arguments /"phases". And modifying the time step does move the eigenvalues along the unit circle, and making the time step too large will change the phases such that they no longer resemble the true physical phases. Depending on the method this may happen before or after stability is broken.

Table 2.1 summarizes the numerical stability properties of these methods in terms of their maximum Courant limits (defined as $c\Delta t/\Delta x$).

For Young's method, the maximum Courant number to keep the algorithm stable is $\sqrt{1-(\omega_p \Delta t/2)^2}$ for zero collision frequency. Cummer has proven through numerical stability analysis that this Courant number is also valid for $\vartheta \Delta t \neq 0$. Notice that, the maximum Courant number depends on the plasma frequency. This can result in an extremely small time step to ensure the stability of the whole system.

For Nickisch and Franke's method, the maximum Courant number to keep the algorithm stable is $\sqrt{1-(\omega_p \Delta t/2)^2}$ as well for zero collision frequency. However, this method will become unconditionally unstable if $\vartheta \Delta t \neq 0$, and the instability becomes more severe with increasing non-zero $\vartheta \Delta t$ values.

The maximum Courant number for both Cummer's and exponential fitting method is one for all of the possible collision frequencies. This unity Courant number does not depend on the plasma properties (ω_p and ϑ) and remains the same as for free space.

The second important property of a numerical technique is its accuracy. The errors produced in a particular algorithm depend on many issues such as the discretization of the derivatives. According to the dispersion analyses of [20], Young's method is the most accurate algorithm for lowloss plasma ($\vartheta \Delta t << 1$) among the aforementioned schemes. The accuracy property of Nickisch and Franke's method is identical to Young's method for lossless plasma ($\vartheta = 0$). However, as mentioned earlier, it becomes unconditionally unstable of $\vartheta \neq 0$. For a low-loss plasma, Cummer's method is the most accurate one.

In this dissertation, Smithe's technique is chosen as the discretization scheme to develop our 3D cold magnetized plasma algorithm.

References

[1] K. Yee, "Numerical solution of initial boundary value problems involving maxwell's equations in isotropic media", *IEEE Trans. Antennas Propag.*, vol. 14, no. 3, pp. 302 –307, 1966.

[2] A. Taflove and S. C. Hagness, *Computational Electrodynamics*. Artech House, 2005.

[3] D. M. Sullivan, *Electromagnetic simulation using the FDTD method*. John Wiley & Sons, 2013.

[4] R. J. Luebbers, F. Hunsberger, and K. S. Kunz, "A frequency-dependent finite-difference time-domain formulation for transient propagation in plasma", *IEEE Trans. Antennas Propag.*, vol. 39, no. 1, pp. 29 –34, Jan. 1991.

[5] D. F. Kelley and R. J. Luebbers, "Piecewise linear recursive convolution for dispersive media using fdtd", *IEEE Trans. Antennas Propag.*, vol. 44, no. 6, pp. 792 –797, Jun. 1996.

[6] R. Siushansian and J. LoVetri, "A comparison of numerical techniques for modeling electromagnetic dispersive media", *IEEE Microw. Guided Wave Lett.*, vol. 5, no. 12, pp. 426 –428, Dec. 1995.

[7] R. Luebbers, F. P Hunsberger, K. S. Kunz, R. B. Standler, and M. Schneider, "A frequency-dependent finite-difference time-domain formulation for dispersive materials", *IEEE Trans. Electromagn. Compat.*, vol. 32, no. 3, pp. 222 –227, Aug. 1990.

[8] R. J. Luebbers and F. Hunsberger, "Fdtd for n th-order dispersive media", *IEEE Trans. Antennas Propag.*, vol. 40, no. 11, pp. 1297 –1301, Nov. 1992.

[9] L. J. Nickisch and P. M. Franke, "Finite-difference time-domain solution of maxwell's equations for the dispersive ionosphere", *IEEE Antennas Propag. Mag.*, vol. 34, no. 5, pp. 33 –39, Oct. 1992.

[10] J. L. Young, "A full finite difference time domain implementation for radio wave propagation in a plasma", vol. 29, no. 6, pp. 1513 –1522, Nov. 1994.

[11] F. I. Kashiwa T., "A treatment by the finite-difference time-domain method of the dispersive characteristics associated with orientation polarization", vol. 3, pp. 203 –205, Jun. 1990.

[12] Y. N. Kashiwa T. and I. Fukai, "A treatment by the finite-difference time-domain method of the dispersive characteristics associated with orientation polarization", vol. E73, no. 8, pp. 1326 –1328, Aug. 1990.

[13] H. S. C. Joseph R. M. and A. Taflove, "Direct time integration of maxwell's equations in linear dispersive media with absorption for scattering and propagation of femtosecond electromagnetic pulses", vol. 16, no. 18, pp. 1412 –1414, 1991.

[14] O. P. Gandhi, B. Q. Gao, and J. Y. Chen, "A frequency-dependent finite-difference time-domain formulation for general dispersive media", *IEEE Trans. Microw. Theory Tech.*, vol. 41, no. 4, pp. 658 –665, Apr. 1993.

[15] Y. Takayama and W. Klaus, "Reinterpretation of the auxiliary differential equation method for fdtd", *IEEE Microw. Wireless Compon. Lett.*, vol. 12, no. 3, pp. 102 –104, Mar. 1994.

[16] D. M. Sullivan, "Frequency-dependent fdtd methods using z transforms", *IEEE Trans. Antennas Propag.*, vol. 40, no. 10, pp. 1223 –1230, Oct. 1992.

[17] D. Sullivan, "Z-transform theory and the fdtd method", *IEEE Trans. Antennas Propag.*, vol. 44, no. 1, pp. 28–34, Jan. 1996.

[18] T. Kashiwa, N. Yoshida, and I. Fukai, "Transient analysis of a magnetized plasma in three-dimensional space", *IEEE Trans. Antennas Propag.*, vol. 36, no. 8, pp. 1096 –1105, Aug. 1988.

[19] W. Tierens and D. De Zutter, "An unconditionally stable time-domain discretization on cartesian meshes for the simulation of nonuniform magnetized cold plasma", vol. 231, no. 15, pp. 5144 –5156, Jun. 2012.

[20] S. A. Cummer, "An analysis of new and existing fdtd methods for isotropic cold plasma and a method for improving their accuracy", *IEEE Trans. Antennas Propag.*, vol. 45, no. 3, pp. 392 –400, Mar. 1997.

[21] J. L. Young and R. O. Nelson, "A summary and systematic analysis of fdtd algorithms for linearly dispersive media", *IEEE Antennas Propag. Mag.*, vol. 43, no. 1, pp. 61 –126, Feb. 2001.

[22] J. Young, A. Kittichartphayak, Y. Kwok, and D. Sullivan, "On the dispersion errors related to fdtd type schemes", *IEEE Trans. Microw. Theory Tech.*, vol. 43, no. 8, pp. 1902 –1909, Aug. 1995.

[23] K. G. Budden, *The propagation of Radio Waves*. Cambridge Univ. Press, 1985.

[24] T. H. Stix, *Waves in plasmas*. Springer, 1992.

[25] D. N. Smithe, "Finite-difference time-domain simulation of fusion plasmas at radiofrequency time scales", vol. 14, no. 5, pp. 056 104–056 1047–, Apr. 2007.

3

3D Numerical Cold Plasma Algorithm and Its Characteristics

★ ★ ★

A three-dimensional hybrid explicit/implicit finite-difference time-domain (FDTD) numerical technique is proposed herein to simulate the electromagnetic (EM) wave propagation in a cold magnetized homogeneous/inhomogeneous (tokamak) plasma for an applied magnetic field. The 3D numerical code is built using a cylindrical coordinate system, and it can be applied for tokamak configurations. It is based on Maxwell's equations and the current equation for plasma species (the equation of motion). The hybrid explicit/implicit FDTD method is implemented. As is done classically for FDTD schemes, Faraday's law is solved here explicitly like in the classical FDTD scheme, while the Ampere's law is chosen to be solved implicitly.

3.1 Hybrid FDTD scheme

The cold plasma governing equations are expressed in terms of Maxwell's equations coupled with current equations derived from the Lorentz equation of motion. The resulting governing equation set in a time-domain is given in subsection 1.4 and by the set of Equations (1.33- 1.34) and the Equation (1.44).

Notice that the cyclotron frequency is a function of the applied magnetic field. Thus, the cross-product terms in (1.44) make the plasma anisotropic so that the wave behaviour depends on its propagation direction relative to the direction of

the applied magnetic field. This makes the whole system challenging to implement. Equation (1.44) contains a collision frequency term ϑ_s which describes the power dissipation of the plasma currents due to the collision processes between the plasma particles.

In cylindrical coordinates the governing differential set of equations is expanded into the following set of scalar expressions:

$$\frac{\partial B_r}{\partial t} = -\frac{1}{r}\frac{\partial E_z}{\partial \varphi} + \frac{\partial E_\varphi}{\partial z}, \tag{3.1}$$

$$\frac{\partial B_\varphi}{\partial t} = -\frac{\partial E_r}{\partial z} + \frac{\partial E_z}{\partial r}, \tag{3.2}$$

$$\frac{\partial B_z}{\partial t} = -\frac{1}{r}\left[\frac{\partial\left(rE_\varphi\right)}{\partial r} - \frac{\partial E_r}{\partial \varphi}\right], \tag{3.3}$$

$$\epsilon_0\frac{\partial E_r}{\partial t} = -\sum_s J_{sr} + \left[\frac{1}{r}\frac{\partial H_z}{\partial \varphi} - \frac{\partial H_\varphi}{\partial z}\right], \tag{3.4}$$

$$\epsilon_0\frac{\partial E_\varphi}{\partial t} = -\sum_s J_{s\varphi} + \left[\frac{\partial H_r}{\partial z} - \frac{\partial H_z}{\partial r}\right], \tag{3.5}$$

$$\epsilon_0\frac{\partial E_z}{\partial t} = -\sum_s J_{sz} + \frac{1}{r}\left[\frac{\partial\left(rH_\varphi\right)}{\partial r} - \frac{\partial H_r}{\partial \varphi}\right], \tag{3.6}$$

$$\frac{\partial J_{sr}}{\partial t} + \vartheta_s J_{sr} = \epsilon_0\omega_{ps}^2 E_r + \left[\Omega_{s\varphi}J_{sz} - \Omega_{sz}J_{s\varphi}\right], \tag{3.7}$$

$$\frac{\partial J_{s\varphi}}{\partial t} + \vartheta_s J_{s\varphi} = \epsilon_0\omega_{ps}^2 E_\varphi + \left[\Omega_{sz}J_{sr} - \Omega_{sr}J_{sz}\right], \tag{3.8}$$

$$\frac{\partial J_{sz}}{\partial t} + \vartheta_s J_{sz} = \epsilon_0\omega_{ps}^2 E_z + \left[\Omega_{sr}J_{s\varphi} - \Omega_{s\varphi}J_{sr}\right]. \tag{3.9}$$

The components of electric and magnetic fields and plasma currents are tightly coupled through Equations (3.1 - 3.9), which increases the numerical complexity of this algorithm. As a result, the plasma current terms cannot be explicitly eliminated from the equation system (3.1 - 3.9). Spatial- and temporal-average values of some of the field variables are therefore required for the algorithm implementation.

3.2 Hybrid FDTD Discretization Scheme

Time Discretization

We now introduce a finite- difference discretization of (1.33-1.34) and 1.44, and following Yee's notation [1], we denote a mesh point as $(i, j, k) = (i\Delta, j\Delta, k\Delta)$, where $\Delta = \Delta r, \Delta z$ is the space increment and $\Delta = \Delta\phi$ is the angular increment in the cylindrical coordinate system, and any function of space and time as $F^n(i, j, k) = F(i\Delta, j\Delta, k\Delta, n\Delta t)$, where Δt is the time increment. By positioning the field components of $\mathbf{E}, \mathbf{H}, \mathbf{J}$ on the mesh the way it will be described below, we evaluate the **E**-field and the current density **J**-field at integer time steps while the **H**-field is defined at half-integer time steps [2]. By central averaging the $\boldsymbol{J}$ terms of Equation (1.34) and Equation (1.44) and the $\boldsymbol{E}$ term of Equation (1.44), the resulting approximations of Equation (1.33) - (1.34) and 1.44 are:

$$\mu_0 \left[\frac{\mathbf{H}^{n+1/2} - \mathbf{H}^{n-1/2}}{\Delta t} \right] = -\nabla \times \mathbf{E}^n, \tag{3.10}$$

$$\epsilon_0 \left[\frac{\mathbf{E}^{n+1} - \mathbf{E}^n}{\Delta t} \right] + \left[\frac{\mathbf{J}_s^{n+1} + \mathbf{J}_s^n}{2} \right] = \nabla \times \mathbf{H}^{n+1/2}, \tag{3.11}$$

$$\left[\frac{\mathbf{J}_s^{n+1} - \mathbf{J}_s^n}{\Delta t} \right] + \nu_s \left[\frac{\mathbf{J}_s^{n+1} + \mathbf{J}_s^n}{2} \right] = \epsilon_0 \omega_{ps}^2 \left[\frac{\mathbf{E}^{n+1} + \mathbf{E}^n}{2} \right] - \left[\Omega_s \times \frac{\mathbf{J}_s^{n+1} + \mathbf{J}_s^n}{2} \right]. \tag{3.12}$$

Space Discretization

In the following subsection, the set of scalar Equations (3.1-3.9) is applied to the FDTD mesh. The modified Yee-cell describing the spatial positioning of the **E**, **H**, and $\mathbf{J}_s$ field-components is shown in Fig. 3.1. The components H_r, H_φ, H_z of the magnetic field **H** are localized at the center of the edges of the Yee-cell, as is typical in FDTD. The method proposed here initially locates the J_r, J_φ, and J_z components at the same positions as the E_r, E_φ, and E_z components, i.e. together at the center of the Yee-cell as in [2]. This simplifies the calculation of the cross product in Equation (1.44) while adding extra complexity to the calculation of the curl in Equation (1.33). Spatial averaging is required to calculate the central-difference derivatives. For example, to update the **H**- field components, four neighbouring field values of **E** should be averaged in order to find the field value at the centers of the faces of the Yee-cell. Thus, in order to interpolate the $(\nabla \times \mathbf{E})$, the twelve field values (four neighbouring values for each of the component) surrounding the desired position are then used to evaluate the corresponding derivative at that point. Unlike Equation (3.10) (which is initially explicit), the set (3.11) - (3.12) is implicit. In order to obtain explicit expressions, the term $\mathbf{J}^{n+1}$ is defined from

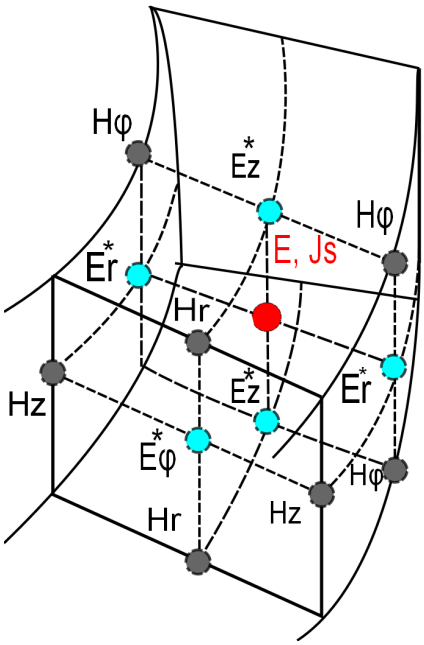

Figure 3.1: Modified Yee-cell for spatial positioning of the fields components. The components H_r, H_φ, H_z of the magnetic field **H** are localized at the center of the edges of the Yee-cell. The J_r, J_φ, J_z and E_r, E_φ, E_z components are collocated.

(3.12) and substituted in (3.11), which yields all field components of **E** at time step $(n+1)$ on the left side of (3.13) and all other values calculated at previous time steps on the right- hand side of (3.13). As such, Equation (3.13) becomes suitable for the FDTD implementation.

$$\begin{aligned}\mathbf{E}^{n+1} = \mathbf{M}_{E,E}\mathbf{E}^n - \mathbf{M}_{B,E}\sum_s \frac{1}{2}\left(\mathbf{M}_{2,s}+1\right)\mathbf{J}^n \\ + \mathbf{M}_{B,E}\left(\nabla\times\mathbf{H}\right)^{n+1/2}.\end{aligned} \tag{3.13}$$

Using (3.13), the set of equations is completed with:

$$\begin{aligned}\mathbf{J}^{n+1} = &\frac{\epsilon_0\omega_{ps}^2}{2}\mathbf{M}_{1,s}(\mathbf{M}_{E,E}+1)E^n \\ &- \frac{\epsilon_0\omega_{ps}^2}{2}\mathbf{M}_{1,s}\mathbf{M}_{B,E}\sum_s \frac{1}{2}\left(\mathbf{M}_{2,s}+1\right)J^n \\ &+ \frac{\epsilon_0\omega_{ps}^2}{2}\mathbf{M}_{1,s}\mathbf{M}_{B,E}\left(\nabla\times\mathbf{H}\right)^{n+1/2} + \mathbf{M}_{2,s}J^n,\end{aligned} \tag{3.14}$$

where

$$\mathbf{M}_{1,s} = \begin{pmatrix} \frac{1}{\Delta t} + \frac{\nu_s}{2} & -\frac{\Omega_z}{2} & \frac{\Omega_\varphi}{2} \\ \frac{\Omega_z}{2} & \frac{1}{\Delta t} + \frac{\nu_s}{2} & -\frac{\Omega_r}{2} \\ -\frac{\Omega_\varphi}{2} & \frac{\Omega_r}{2} & \frac{1}{\Delta t} + \frac{\nu_s}{2} \end{pmatrix}^{-1}, \tag{3.15}$$

$$\mathbf{M}_{2,s} = \mathbf{M}_{1,s} \begin{pmatrix} \frac{1}{\Delta t} - \frac{\nu_s}{2} & \frac{\Omega_z}{2} & -\frac{\Omega_\varphi}{2} \\ -\frac{\Omega_z}{2} & \frac{1}{\Delta t} - \frac{\nu_s}{2} & \frac{\Omega_r}{2} \\ \frac{\Omega_\varphi}{2} & -\frac{\Omega_r}{2} & \frac{1}{\Delta t} - \frac{\nu_s}{2} \end{pmatrix}, \tag{3.16}$$

$$\mathbf{M}_{E,E} = \left(\frac{\epsilon_0}{\Delta t} I + \sum_s \mathbf{M}_{1,s} \frac{\epsilon_0 \omega_{ps}^2}{2} \right)^{-1} \left(\frac{\epsilon_0}{\Delta t} I + \sum_s \mathbf{M}_{1,s} \frac{\epsilon_0 \omega_{ps}^2}{2} \right), \tag{3.17}$$

$$\mathbf{M}_{B,E} = \left(\frac{\epsilon_0}{\Delta t} I + \sum_s \mathbf{M}_{1,s} \frac{\epsilon_0 \omega_{ps}^2}{2} \right)^{-1}. \tag{3.18}$$

where I is a unit matrix [3], [4].

3.3 Characteristics of the Developed Numerical Code

3.4 Boundary Conditions

★ ★ ★

In this Section the description of the necessary boundary conditions for the computational domain is given. The boundary conditions were developed to describe two important phenomena. First, one has to model the power source that launches the wave into the plasma. Second one has to model the wave fields at the plasma edges.

3.4.1 Description of the boundary conditions

As a power source we use a so-called hard source [5] or a "point" source, which in our cylindrical case is really an infinitely thin cylindrical surface along the toroidal direction carrying a constant amplitude current with sinusoidal time-dependence at a particular frequency ω. It is switched on at $t = 0$ and flows until regime conditions are met. In more detail, the wave electric field is defined at a surface $r_a - N_{cells} = const$ which models, as is mentioned above, the Radio Frequency (RF) antenna or a power source condition (PSC) in the tokamak. Here, N_{cells} is the number of cells. Among the waves that are possibly excited by the hard source we choose to investigate only the wave mode that is used for plasma heating in the tokamak, i.e. only the mode that propagates towards the cylindrical axis.

In the presented study, the RF antenna is unrestricted in $\varphi-$ and z-directions to exclude the antenna edge effects on the wave propagation. The external confining magnetic field (uniform or nonuniform) is oriented along the φ-direction. The ordinary wave (the electric field is parallel to the external magnetic field) is launched by the PSC $E_\varphi = E_0 \sin(\omega t)$. The extraordinary wave (the electric field is perpendicular to the external magnetic field) is launched by the PSC $E_z = E_0 \sin(\omega t)$. Plasma media occupies the space of $[r_b, r_a]$ in the r- direction, where $r_a - r_b$ is the width of the plasma column.

One of the applied types of the boundary conditions is the Perfect Electric Conductor (PEC). Thus, the wave reaching the surface $r_b = const$ is reflected completely back to the antenna. Since at $r_a = const$, the PSC plays the role of PEC for the reflected waves, and we expect a process of multireflection between the surfaces $r_a = const$ and $r_b = const$. We would like to note that the multireflection process might evoke the unrestrained growth of the electromagnetic field amplitude and under these circumstances the steady state condition cannot be reached. However, including the collision frequency term ϑ_s (Equation (1.44)) will cause wave dissipation which allows the steady state to be reached. The magnitude of the collision frequency term defines the time needed to reach the steady state. Note, that there is a restriction on the collision frequency term value. It has to be large enough to minimize the wave reflection from the boundary r_b back to the antenna. In Section 3.4.2 such estimations of the collisional term values will be given.

A general frame of the simulation structure is illustrated in Fig. 3.2 together with the direction of the wave propagation and the location of the antenna.

3.4.2 Collision Frequency Term Effect

Here, the approximate analysis will be carried out to estimate the effect of the collision frequency term in Equation (1.44). In order to simplify the estimation the analysis will be done in a Cartesian coordinate system.

The fast wave propagates to the boundary $x = x_b$ according to the law $E_y(x) = E_0 exp(jk_x x)$, where E_0 is the wave amplitude defined by the antenna and k_x is

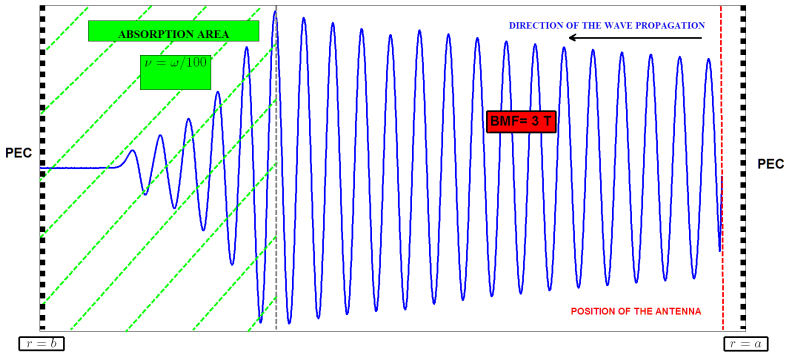

Figure 3.2: Illustration of the simulation structure. 1D case. Perfect electric conductor is used as a boundary condition. The power source is located close to the right edge of the simulation domain. The direction of the wave propagation is indicated in Fig. 3.2. The damping boundary condition indicated as an "absorbing area" is set at the distance that would allow to provide the effective damping of the wave. The collision frequency term that influences the process of damping is $\vartheta_s = \omega/100$. The background magnetic field is 3 T.

the x-component of the FW wave vector which is defined by the FW dispersion relation [6]. Reaching the boundary $x = x_b$ the FW is partially reflected with coefficient R and partially transmitted with coefficient T. Hence, the wave field in the range $[x_b, x_a]$ is defined as $E_y(x) = E_0(exp(jk_x x) + Rexp(-jk_x x))$. The wave field behind the boundary $x = x_b$ is defined by $E_y(x) = E_0 T exp(jk_x^{'} x)$, where $k_x^{'}$ stands for the FW wave vector in a plasma media with collisions. The well-known relation between the electric and magnetic fields of the FW is $\frac{\partial H_z}{\partial t} = -\frac{\partial E_y}{\partial x}$ (the problem is uniform along the y direction). Since the tangential components of the electromagnetic field have to be continues at the boundary $x = x_b$ it provides two equations:

$$1 + R = T, \tag{3.19}$$

$$k_x(1 - R) = k_x^{'} T. \tag{3.20}$$

These equations can be resolved for the transmission R and reflection T coefficients, respectively:

$$T = \frac{2}{1 + k_x^{'}/k_x}, \tag{3.21}$$

$$R = T - 1. \tag{3.22}$$

Since the time-averaged Poyting flux for plane waves is proportional to the square of the wave field amplitudes, the coefficient of the power transfer through the boundary is equal to $|T|^2$ and the coefficient of power reflection from the boundary is $1 - |T|^2$. In Fig. 3.3 the power reflection coefficient is calculated in a Cartesian coordinate system. It is compared with the penetration depth of the FW behind the boundary $x = r_b$ (it is defined from $Im(k_x^{'})$). The power reflection does not even reach 7% when the collisional frequency is equal to the antenna frequency. However, the wave penetration depth in this case is only 0.0641 (m) which does prevent the wave to reach the axis. The analysis shows that even $\vartheta_s = 0.1\omega$ with a power reflection of 0.1% is already enough for efficient damping of the electromagnetic wave.

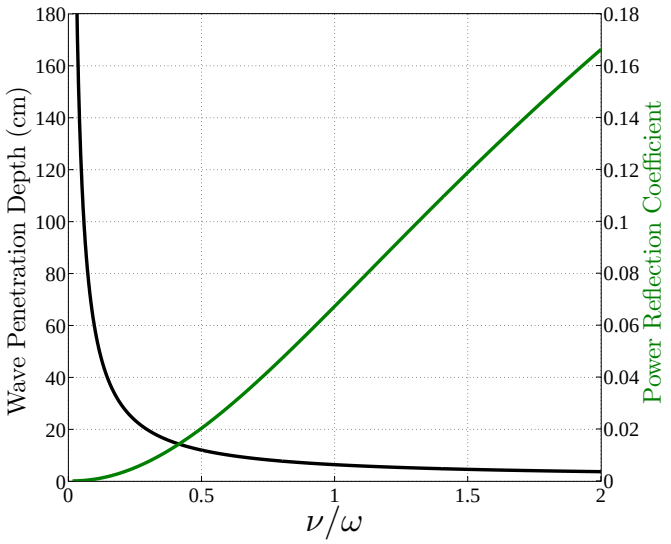

Figure 3.3: The dependence of the absolute value of the reflection coefficient R on the normalized value of the collisional frequency. The power reflection coefficient (green solid line) is compared to the wave penetration depth in cm (black solid line). It can be seen that even with the collision frequency term ν_s equal to 0.1ω the efficient damping of the electromagnetic wave is guaranteed.

Selection of the collision frequency term

As is mentioned above, a collision frequency term can be also used as an artificial cause of the damping of the wave and as a result the inclusion of the collision frequency term builds some sort of damping boundary condition. Therefore, it is interesting to analyse which value of the collision frequency term can be chosen

and how strong it damps the electromagnetic wave before it reaches the PEC. In Fig. 3.4 a sample of the propagation of the z-component of the electromagnetic wave is presented. The simulations are performed in homogeneous magnetized plasma with plasma density of $n_e = n_{DE} = 3 \cdot 10^{19}$ $(1/m^3)$ and background magnetic field of 3 T. The set of collision frequency terms is included in simulations in the form of $Const \cdot \omega$ where the source frequency ω is equal to $2.8 \cdot 10^9$ (rad/sec). On purpose, the length of the simulation domain is chosen to be rather long, i.e. $16m$. In Fig. 3.4 the most effective damping is observed when $Const = 1.9$. The

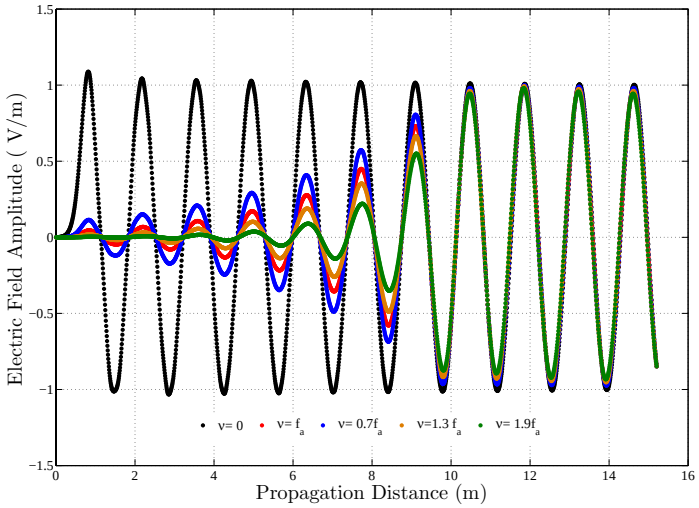

Figure 3.4: The effectiveness of the damping due to the chosen value of the collision frequency term.

other technique to choose the collision frequency term is based on the analysis of the imaginary part of the wavenumber k. Fig. 3.5 shows how $Im(k)$ depends on the collision frequency term. It can be seen that the peak of the collision frequency term is at about 10^{10} $(1/sec)$ independent from the initially chosen value. In Section 3.4.2 the collision frequency term is introduced as a part of the artificial damping boundary condition.

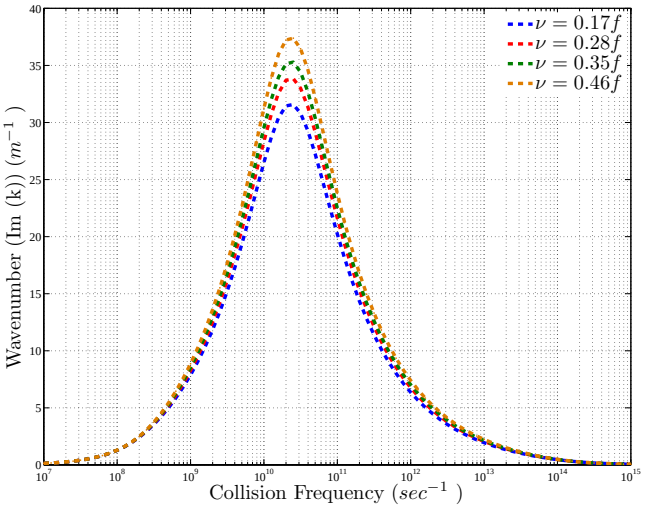

Figure 3.5: How to choose the value of the collision frequency term.

3.5 Steady State Criteria

★ ★ ★

An important issue in a simulation is a stopping criterion. The stopping criterion has to cover mainly the transition from the unsteady to the steady state. After the steady state there is no need to continue evaluating the variables at new time steps. In this CSection the Poynting flux is introduced as a criterion to terminate the simulation when the steady state is reached.

3.5.1 Poynting Flux. Averaged Energy Flux.

Here, the derivation of the Poynting flux is introduced in the FDTD simulation in plasma media. The calculation of the Poynting flux is used as a criterion to check whether the steady state is reached. For the wave propagation through the plasma column the steady state is reached when the averaged flux in front of the antenna becomes equal to the outgoing flux on the opposite side of the plasma column. The equality of the fluxes is used as an internal criterion to terminate calculations and to optimize the computational time.

The developed numerical technique can be described in the following way. The flux of the Poynting vector **S** (3.23) given by the vector product of an electric field (**E**) and a magnetic field **H** represents the flow of energy through a surface. Its

direction is that of the flow, and its magnitude is the intensity.

$$\mathbf{S} = \mathbf{E} \times \mathbf{H} \tag{3.23}$$

In order to find the components of the Poynting vector, the components H_r, H_φ, H_z of the magnetic field $\mathbf{H}$ should be interpolated at the location of the components of the electric field $\mathbf{E}$ and currents $\mathbf{J}_s$. Here, Equation 3.24 provides a sample of the calculation of the r-component of the Poynting vector.

$$\begin{aligned} S_r = E_\varphi|^{n+1/2}_{i+1/2,j+1/2,k+1/2} \tilde{H}_z|^{n+1/2}_{i+1/2,j+1/2,k+1/2} \\ - E_z|^{n+1/2}_{i+1/2,j+1/2,k+1/2} \tilde{H}_\varphi|^{n+1/2}_{i+1/2,j+1/2,k+1/2} \end{aligned} \tag{3.24}$$

The $\varphi-$ and $z-$ components of the Poynting vector are calculated in the same way.

The divergence of the Poynting vector in the cylindrical coordinate system is defined as:

$$\begin{aligned} \nabla \cdot \mathbf{S} = \frac{1}{i\Delta r} \left(i\Delta r \left(\frac{S_r|^n_{i+1/2,j,k} - S_r|^n_{i-1/2,j,k}}{\Delta r} \right) \right) \\ + \frac{1}{i\Delta r} \left(i\Delta r \left(\frac{S_\varphi|^n_{i,j+1/2,k} - S_\varphi|^n_{i,j-1/2,k}}{\Delta \varphi} \right) \right) \\ + \left(\frac{S_z|^n_{i,j,k+1/2} - S_z|^n_{i,j,k-1/2}}{\Delta z} \right) \end{aligned} \tag{3.25}$$

First, we choose to investigate the fast wave in an one-dimentional (1D) Cartesian coordinate system. Since the space is uniform in $y-$ and $z-$ directions, the expression of the Poynting flux takes the form:

$$S_x = E_y H_z \tag{3.26}$$

For this numerical simulation the following initial parameters have been chosen: the one-ion (HD) plasma is homogeneous with a density of $3 \cdot 10^{19}$ $(1/m^3)$. The background magnetic field is inhomogeneous and it decreases as $1/R$ with 3 Tesla at 3 m. The fast wave is excited by the antenna that is located at a distance of 4 m at a frequency $2 \cdot 10^8$ (rad/sec).

It has to be noted that the configuration of the simulation is chosen in such a way that the ion-cyclotron resonance would appear on the radial axis. At the high field side (HFS) the absorbing boundary condition is applied in order to damp a wave in a couple of wave periods. The result of the performed analysis is presented in Fig. 3.6. The blue line shows the behaviour of the averaged Poynting flux calculated near the antenna. The red line presents the averaged Poynting flux at the HFS. It can be seen that the steady state is reached at approximately $1.6 \cdot 10^-7$

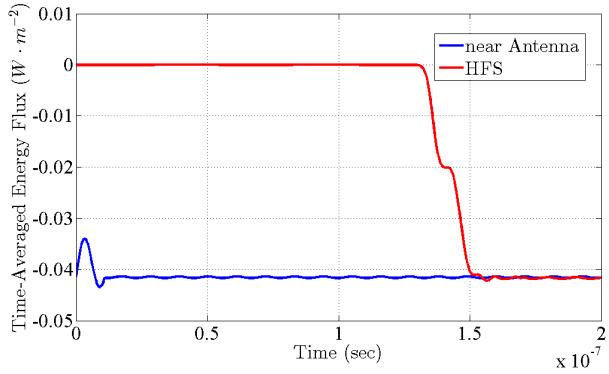

Figure 3.6: Time-averaged energy flux versus time.

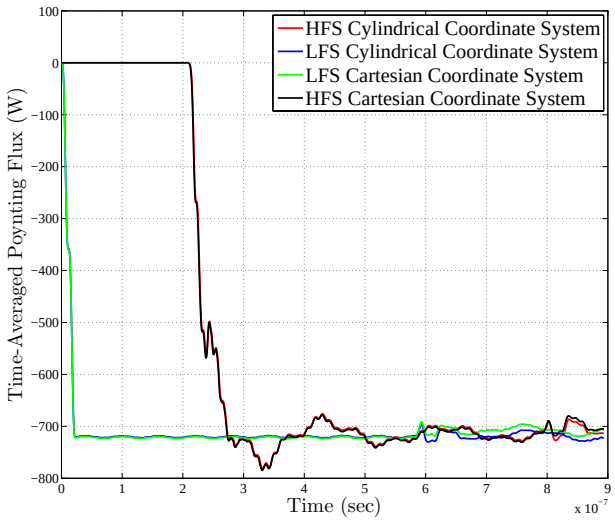

Figure 3.7: Comparison of the time-averaged energy fluxes in Cartesian and cylindrical coordinate systems.

(*sec*) when the averaged flux on one side of the simulation area becomes equal to the averaged flux on the other side.

Since the described above analysis is performed in the Cartesian coordinate system, the analogous approach is applied to calculate the averaged Poynting flux in the cylindrical geometry. The initial parameters of the performed simulation stay the same. In Fig. 3.7 the averaged Poynting flux is compared to the one calculated

in the cylindrical coordinate system. The green and blue lines show the comparison between the averaged Poynting fluxes at LFS (near antenna) in a Cartesian and cylindrical geometry, respectively. The black and red solid lines represent the averaged Poynting flux at HFS in Cartesian and cylindrical coordinate systems, respectively.

The results of the performed numerical test presented above show that the developed technique to recognize the steady state and therefore to terminate the simulation can be applied in both Cartesian and cylindrical coordinate systems.

References

[1] K. Yee, "Numerical solution of initial boundary value problems involving maxwell's equations in isotropic media", *IEEE Trans. Antennas Propag.*, vol. 14, no. 3, pp. 302 –307, 1966.

[2] D. N. Smithe, "Finite-difference time-domain simulation of fusion plasmas at radiofrequency time scales", vol. 14, no. 5, pp. 056 104–056 1047–, Apr. 2007.

[3] Y. Yu and J. J. Simpson, "An ej collocated 3-d fdtd model of electromagnetic wave propagation in magnetized cold plasma", *IEEE Trans. Antennas Propag.*, vol. 58, no. 2, pp. 469 –478, Dec. 2010.

[4] S. A. Cummer, "An analysis of new and existing fdtd methods for isotropic cold plasma and a method for improving their accuracy", *IEEE Trans. Antennas Propag.*, vol. 45, no. 3, pp. 392 –400, Mar. 1997.

[5] F. Costen, J.-P. Berenger, and A. K. Brown, "Comparison of fdtd hard source with fdtd soft source and accuracy assessment in debye media", *IEEE Trans. Antennas Propag.*, vol. 57, no. 7, pp. 2014 –2022, May 2009.

[6] M. Brambilla, *Kinetic Theory of Plasma problems: Homogeneous Plasma*. Clarendon Press, 1998, vol. 1.

4

Derivation of the full discrete dispersion relation

★ ★ ★

The fully discretized dispersion relation is given in this Chapter. The behaviour of the dispersion relation for a number of specific scenarios is studied.

4.1 Derivation of the full discrete dispersion relation

In a uniform medium the eigensolutions of Maxwell's equations are complex exponentials with a wavevector k and an (angular) frequency ω. Real sources do not excite just a single frequency, nor just a single wavevector, but nonetheless the understanding of the general-case behaviour of EM fields in the medium in terms of just these simple eigensolutions (a situation which is conveniently analogous to the well-known Fourier series) can be reached. For this reason the behaviour of the electromagnetic fields is often specified through its dispersion relation : how the wavevector k relates to the frequency ω. In order to understand the behaviour and applicability of computational models, it is needed to understand how this dispersion relation is affected : how does the discrete dispersion relation differ from the continuous one? To this end, it is proceeded much as it would be done in the continuous case and a complex exponential ersatz (4.1) is inserted into the discrete update equations (1.33-1.34) and (1.44):

$$E, H, J_s = exp(k_r r + n\varphi + k_z z - \omega t) \tag{4.1}$$

where k_r, k_z are the r, z components of the numerical wavevector and r is a radial coordinate. Substituting the wave expression of (4.1) into the finite-difference set of equations of (1.33-1.34) and (1.44) yields, after simplification, the following set of equations:

$$\frac{1}{r\Delta\varphi}\cot\left(k_z\frac{\Delta z}{2}\right)\tan\left(n\frac{\Delta\varphi}{2}\right)E_z-\frac{1}{\Delta z}E_\varphi=\frac{1}{\Delta t}\frac{\sin\left(\omega\frac{\Delta t}{2}\right)}{\cos\left(n\frac{\Delta\varphi}{2}\right)\sin\left(k_z\frac{\Delta z}{2}\right)}H_r, \tag{4.2}$$

$$\frac{1}{\Delta z}\cot\left(k_r\frac{\Delta r}{2}\right)\tan\left(k_z\frac{\Delta z}{2}\right)E_r-\frac{1}{\Delta r}E_z=\frac{1}{\Delta t}\frac{\sin\left(\omega\frac{\Delta t}{2}\right)}{\sin\left(k_r\frac{\Delta r}{2}\right)\cos\left(k_z\frac{\Delta z}{2}\right)}H_\varphi, \tag{4.3}$$

$$\left[\frac{2}{\Delta r}\sin\left(k_r\frac{\Delta r}{2}\right)-\frac{j}{r}\cos\left(k_r\frac{\Delta r}{2}\right)\right]\cot\left(n\frac{\Delta\varphi}{2}\right)E_\varphi-\frac{2}{r\Delta\varphi}\cos\left(k_r\frac{\Delta r}{2}\right)E_r=\frac{2}{\Delta t}\frac{\sin\left(\omega\frac{\Delta t}{2}\right)}{\sin\left(n\frac{\Delta\varphi}{2}\right)}H_z, \tag{4.4}$$

$$\frac{2}{r\Delta\varphi}\sin\left(n\frac{\Delta\varphi}{2}\right)H_z-\frac{2}{\Delta z}\sin\left(k_z\frac{\Delta z}{2}\right)H_\varphi=-\frac{2}{\Delta t}\frac{\sin\left(\omega\frac{\Delta t}{2}\right)}{\cos\left(k_r\frac{\Delta r}{2}\right)}E_r-j\frac{\cos\left(\omega\frac{\Delta t}{2}\right)}{\cos\left(k_r\frac{\Delta r}{2}\right)}J_r, \tag{4.5}$$

$$\frac{2}{\Delta z}\sin\left(k_z\frac{\Delta z}{2}\right)H_r-\frac{2}{\Delta r}\sin\left(k_r\frac{\Delta r}{2}\right)H_z=-\frac{2}{\Delta t}\frac{\sin\left(\omega\frac{\Delta t}{2}\right)}{\cos\left(n\frac{\Delta\varphi}{2}\right)}E_\varphi-j\frac{\cos\left(\omega\frac{\Delta t}{2}\right)}{\cos\left(n\frac{\Delta\varphi}{2}\right)}J_\varphi, \tag{4.6}$$

$$\left[\frac{2}{\Delta r}\sin\left(k_r\frac{\Delta r}{2}\right)-\frac{j}{r}\cos\left(k_r\frac{\Delta r}{2}\right)\right]H_\varphi-\frac{2}{r\Delta\varphi}\sin\left(n\frac{\Delta\varphi}{2}\right)H_r=-\frac{2}{\Delta t}\frac{\sin\left(\omega\frac{\Delta t}{2}\right)}{\cos\left(k_z\frac{\Delta\varphi}{2}\right)}E_z-j\frac{\cos\left(\omega\frac{\Delta t}{2}\right)}{\cos\left(k_z\frac{\Delta z}{2}\right)}J_z, \tag{4.7}$$

$$-\frac{2j}{\Delta t}J_r \tan\left(\omega\frac{\Delta t}{2}\right) + \vartheta_s J_r = \omega_{ps}^2 E_r + \left(J_\varphi \Omega_z - J_z \Omega_\varphi\right), \tag{4.8}$$

$$-\frac{2j}{\Delta t}J_\varphi \tan\left(\omega\frac{\Delta t}{2}\right) + \vartheta_s J_\varphi = \omega_{ps}^2 E_\varphi + \left(J_z \Omega_r - J_r \Omega_z\right), \tag{4.9}$$

$$-\frac{2j}{\Delta t}J_z \tan\left(\omega\frac{\Delta t}{2}\right) + \vartheta_s J_z = \omega_{ps}^2 E_z + \left(J_r \Omega_\varphi - J_\varphi \Omega_r\right). \tag{4.10}$$

The solution may be found if the determinant (D) of (4.2-4.10) is set to zero.

$$D = \begin{bmatrix}
0 & -1/\Delta z & \xi_{1Ez} & -\xi_{1Hr} & 0 & 0 & 0 & 0 & 0 \\
\xi_{2Er} & 0 & 1/\Delta r & 0 & -\xi_{2H\varphi} & 0 & 0 & 0 & 0 \\
\xi_{3Er} & \xi_{3E\varphi} & 0 & 0 & 0 & -\xi_{3Hz} & 0 & 0 & 0 \\
-\xi_{4Er} & 0 & 0 & 0 & \xi_{4H\varphi} & \xi_{4Hz} & -\xi_{4Jr} & 0 & 0 \\
0 & -\xi_{5E\varphi} & 0 & \xi_{5Hr} & 0 & \xi_{5Hz} & 0 & -\xi_{5J\varphi} & 0 \\
0 & 0 & -\xi_{6Ez} & \xi_{6Hr} & \xi_{6H\varphi} & 0 & 0 & 0 & -\xi_{6Jz} \\
-\omega_{ps}^2 & 0 & 0 & 0 & 0 & 0 & \xi_{7Jr} & -\Omega_z & \Omega_\varphi \\
0 & -\omega_{ps}^2 & 0 & 0 & 0 & 0 & \Omega_z & \xi_{8\varphi} & -\Omega_r \\
0 & 0 & -\omega_{ps}^2 & 0 & 0 & 0 & -\Omega_\varphi & \Omega_r & \xi_{9Jz}
\end{bmatrix}$$

where

$$\xi_{1Ez} = \frac{1}{\Delta r \Delta \varphi}\cot(k_z\frac{\Delta z}{2})\tan(n\frac{\varphi}{2}) \tag{4.11}$$

$$\xi_{1Hr} = \frac{1}{\Delta t}\frac{\sin(\omega\frac{\Delta t}{2})}{\cos(n\frac{\Delta\varphi}{2})\sin(k_z\frac{\Delta z}{2})} \tag{4.12}$$

$$\xi_{2Er} = \frac{1}{\Delta z}\cot(k_r\frac{\Delta r}{2})\tan(k_z\frac{\Delta z}{2}) \tag{4.13}$$

$$\xi_{2H\varphi} = \frac{1}{\Delta t}\frac{\sin(\omega\frac{\Delta t}{2})}{\sin(k_r\frac{\Delta r}{2})\cos(k_z\frac{\Delta z}{2})} \tag{4.14}$$

$$\xi_{3E\varphi} = (\frac{2}{\Delta r}\sin(k_r\frac{\Delta r}{2}) - \frac{j}{r}\cos(k_r\frac{\Delta r}{2}))\cot(n\frac{\Delta\varphi}{2}) \tag{4.15}$$

$$\xi_{3Er} = \frac{2}{r\Delta\varphi}\cos(k_r\frac{\Delta r}{2}) \tag{4.16}$$

$$\xi_{3Hz} = \frac{2}{\Delta t}\frac{\sin(\omega\frac{\Delta t}{2})}{\sin(n\frac{\Delta\varphi}{2})} \tag{4.17}$$

$$\xi_{4Hz} = \frac{2}{r\varphi}\sin(n\frac{\Delta\varphi}{2}) \tag{4.18}$$

$$\xi_{4H\varphi} = \frac{2}{\Delta z}\sin(k_z\frac{\Delta z}{2}) \tag{4.19}$$

$$\xi_{4Er} = -\frac{2}{\Delta t}\frac{\sin(\omega\frac{\Delta t}{2})}{\cos(k_r\frac{\Delta r}{2})} \tag{4.20}$$

$$\xi_{4Jr} = j\frac{\cos(\omega\frac{\Delta t}{2})}{\cos(k_r\frac{\Delta r}{2})} \tag{4.21}$$

$$\xi_{5Hr} = \frac{2}{\Delta z}\sin(k_z\frac{\Delta z}{2}) \tag{4.22}$$

$$\xi_{5Hz} = \frac{2}{\Delta r}\sin(k_r\frac{\Delta r}{2}) \tag{4.23}$$

$$\xi_{5E\varphi} = -\frac{2}{\Delta t}\frac{\sin(\omega\frac{\Delta t}{2})}{\cos(n\frac{\Delta\varphi}{2})} \tag{4.24}$$

$$\xi_{5J\varphi} = -j\frac{\cos(\omega\frac{\Delta t}{2})}{\cos(n\frac{\Delta\varphi}{2})} \tag{4.25}$$

$$\xi_{6H\varphi} = \frac{2}{\Delta r}\sin(k_r\frac{\Delta r}{2}) - \frac{j}{r}\cos(k_r\frac{\Delta\varphi}{2}) \tag{4.26}$$

$$\xi_{6Hr} = \frac{2}{r\Delta\varphi}\sin(n\frac{\Delta\varphi}{2}) \tag{4.27}$$

$$\xi_{6Ez} = -\frac{2}{\Delta t}\frac{\sin(\omega\frac{\Delta t}{2})}{\cos(k_z\frac{\Delta\varphi}{2})} \tag{4.28}$$

$$\xi_{6Jz} = -j\frac{\cos(\omega\frac{\Delta t}{2})}{\cos(k_z\frac{\Delta z}{2})} \tag{4.29}$$

$$\xi_{7Jr} = -\frac{2j}{\Delta t}\tan(\omega\frac{\Delta t}{2}) + \nu_s \tag{4.30}$$

$$\xi_{8J\varphi} = -\frac{2j}{\Delta t}\tan(\omega\frac{\Delta t}{2}) + \nu_s \tag{4.31}$$

$$\xi_{9Jz} = -\frac{2j}{\Delta t}\tan(\omega\frac{\Delta t}{2}) + \nu_s \tag{4.32}$$

Assuming r is sufficiently large, i.e. the studied region is far from the cylindrical axis where the limiting case of the Cartesian coordinate system is still valid, the r-dependent terms of D become negligible and the discrete dispersion relation may be obtained under a specific condition (4.33) with n equal to 0.

$$\frac{2}{\Delta r}sin(k_r\frac{\Delta r}{2}) >> \frac{cos(k_r\frac{\Delta r}{2})}{r}, \tag{4.33}$$

which means that for sufficiently small Δr, if the wavelength is significantly shorter than the distance from the point of consideration to the cylindrical axis, i.e $k_r >> 1/r$ (where r is a distance from the point of consideration to the cylindrical axis), the cylindrical dispersion relation approximates the cartesian one.

★ ★ ★

To support the choice of the coordinate system in the mathematical analysis, below, the comparison of the analytical dispersion relations in Cartesian and cylindrical coordinate systems is performed.

In the 1D cylindrical coordinate system where space in ϕ- and z- direction is chosen to be uniform, the analytical expression of the dispersion relation of the fast wave is the following:

$$\frac{c^2}{\omega^2}k_r\left(\frac{1}{r} + jk_r\right) - j\frac{\epsilon_1^2 - \epsilon_2^2}{\epsilon_1} = 0 \tag{4.34}$$

where

$$\epsilon_1 = 1 - \frac{\omega_{pe}^2}{\omega_{pe}^2 - \Omega_{ce}^2} - \frac{\omega_{pi}^2}{\omega^2 - \Omega_{ci}^2} \tag{4.35}$$

$$\epsilon_2 = -\frac{1}{\omega}\left(\frac{\omega_{pe}^2 \Omega_{ce}}{\Omega_{ce}^2 - \omega^2}\right) + \frac{\omega_{pi}^2 \Omega_{ci}}{\Omega_{ci}^2 - \omega^2} \tag{4.36}$$

To carry out this analytical analysis the following test case was chosen: the dispersion relation of the fast wave in homogeneous collisionless plasma is investigated. The density of plasma ($n_e = n_{HD}$) is $3 \cdot 10^{19}$ $1/m^3$. The background magnetic field is homogeneous and it is equal to 3 T. The source frequency ω is $2.87 \cdot 10^8$ rad/sec.

Fig. 4.1 shows the result of the performed analysis. As it can be observed, the curvature effects appear at a radius of the order of the wavelength. In this particular case, the wavelength λ is equal to 0.0026 m. Coming back to the discretization of

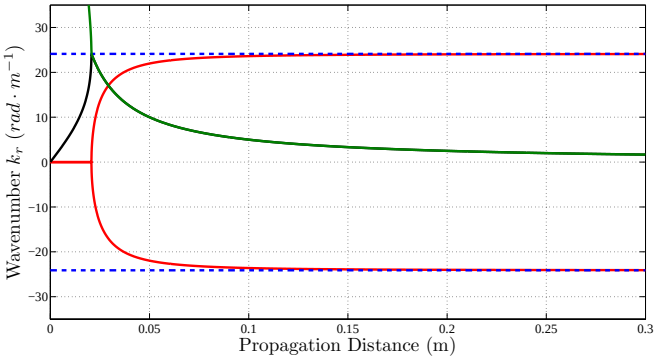

Figure 4.1: Comparison of the analytical dispersion relation in the cylindrical and Cartesian coordinate systems. The curvature effects appear at a radius (0.2 m) of the order of the wavelength. In this particular case, the wavelength λ is equal to 0.0026 m. The blue dashed lines show the two roots of the dispertion relation in the Cartesian coordinate system. The black, red and green solid lines are the roots of the dispersion relation in cylindrical coordinates.

the Maxwell's equations, the expression for the 3D discrete dispersion relation is:

$$\begin{gathered}\left[a_1^2 a_2^2 b_3^2 \epsilon_1 + a_1^2 a_3^2 b_2^2 \epsilon_3 + a_2^2 a_3^2 b_1^2 \epsilon_1\right] \tilde{k}^2 - \\ \left[a_1^2 (b_2^2 + b_3^2)\epsilon_1 \epsilon_3 + a_2^2 (b_1^2 + b_3^2)(\epsilon_1^2 - \epsilon_2^2) + \right. \\ \left. a_3^2 (b_1^2 + b_2^2)\epsilon_1 \epsilon_3\right] b_4^2 + \epsilon_3 (\epsilon_1^2 - \epsilon_2^2) b_4^4 = 0.\end{gathered} \tag{4.37}$$

where

$$\epsilon_1 = 1 - \sum_s \frac{\omega_{ps}^2 \tilde{\omega}}{\omega^*(\tilde{\omega}^2 - \Omega_s^2)},$$

$$\epsilon_2 = -\sum_s \frac{\omega_{ps}^2 \Omega_s}{\omega^*(\tilde{\omega}^2 - \Omega_s^2)},$$

$$\epsilon_3 = 1 - \sum_s \frac{\omega_{ps}^2}{\omega^* \tilde{\omega}},$$

with

$$\omega^* = \frac{2}{\Delta t} tan(\omega \frac{\Delta t}{2}),$$
$$\tilde{\omega} = \omega^* + i\nu_s,$$

and $\tilde{k}^2 \equiv b_1^2 + b_2^2 + b_3^2$ is the square of the discretized wave vector.

To simplify the equation, the following notations are used:

$$\begin{aligned}
a_1 &\equiv cos(k_r \frac{\Delta r}{2}), \quad b_1 \equiv \frac{2}{\Delta r} sin(k_r \frac{\Delta r}{2}), \\
a_2 &\equiv cos(n \frac{\Delta \varphi}{2}), \quad b_2 \equiv \frac{2}{r \Delta \varphi} sin(n \frac{\Delta \varphi}{2}), \\
a_3 &\equiv cos(k_z \frac{\Delta z}{2}), \quad b_3 \equiv \frac{2}{\Delta z} sin(k_z \frac{\Delta z}{2}), \\
a_4 &\equiv cos(\omega \frac{\Delta t}{2}), \quad b_4 \equiv \frac{2}{c \Delta t} sin(\omega \frac{\Delta t}{2}),
\end{aligned} \tag{4.38}$$

To validate the obtained discrete dispersion relation, a number of specific scenarios is studied below.

4.1.1 Vacuum case

For a vacuum, when the plasma density is zero, the discrete dispersion relation (4.37) becomes:

$$\left[a_1^2a_2^2b_3^2 + a_1^2a_3^2b_2^2 + a_2^2a_3^2b_1^2\right]\tilde{k}^2$$
$$-\left[a_1^2(b_2^2+b_3^2) + a_2^2(b_1^2+b_3^2) + a_3^2(b_1^2+b_2^2)\right]b_4^2 + b_4^4 = 0. \tag{4.39}$$

Ensuring that the problem is well-resolved (Δr, $r\Delta\varphi$, $\Delta z << \lambda$) and using the Taylor series expansion of the sine and cosine for a small parameter, a_1, a_2, a_3 are 1 to first order, and we obtain the vacuum dispersion relation:

$$k_r^2 + (\frac{n}{r})^2 + k_z^2 \equiv k^2 = \frac{\omega^2}{c^2}. \tag{4.40}$$

Demanding that real k always map to real ω leads to the Courant condition:

$$c\Delta t < \frac{1}{\sqrt{(\frac{1}{\Delta r})^2 + (\frac{1}{r\Delta\varphi})^2 + (\frac{1}{\Delta z})^2}}. \tag{4.41}$$

Equation (4.40) is the well-known dispersion relation for electromagnetic waves in vacuum, when the frequency is proportional to the wavenumber [1], [2].

4.1.2 Nonmagnetized plasma

In the absence of a background magnetic field, the term in ϵ_1 in equation (4.37) becomes equal to the term in ϵ_3, and the term in ϵ_2 is zero. The full discrete dispersion relation (4.37) reduces to:

$$\left[a_1^2a_2^2b_3^2 + a_1^2a_3^2b_2^2 + a_2^2a_3^2b_1^2\right]\epsilon_3\tilde{k}^2$$
$$-\left[(a_1^2(b_2^2+b_3^2) + a_2^2(b_1^2+b_3^2) + a_3^2(b_1^2+b_2^2)\right]\epsilon_3^2b_4^2 \tag{4.42}$$
$$+\epsilon_3^3b_4^4 = 0.$$

Neglecting the higher order terms of the Taylor series expansion, the nonmagnetized plasma dispersion relation (4.42) becomes

$$\tilde{k}^2 = \epsilon_3 b_4^2. \tag{4.43}$$

If the collisional frequency term is neglected, $\tilde{\omega}$ becomes equal to ω^* and ϵ_3 takes the form

$$\epsilon_3 = 1 - \left(\frac{\Delta t}{2}\right)^2 \cot^2\left(\frac{\omega\Delta t}{2}\right)\sum_s \omega_{ps}^2. \tag{4.44}$$

Now Equation (4.43) can be solved for $\sin(\omega\Delta t/2)$:

$$\tilde{k}^2 = \left(\frac{2}{c\Delta t}\right)^2 \sin^2(\omega\frac{\Delta t}{2}) - \frac{1}{c^2}\cos^2(\omega\frac{\Delta t}{2})\sum_s \omega_{ps}^2. \tag{4.45}$$

Here, only the terms of the first order of the Taylor series expansion are retained, and we obtain the slow wave dispersion relation [2]:

$$k^2 = \frac{\omega^2}{c^2}\left(1 - \sum_s \frac{\omega_{ps}^2}{\omega^2}\right) = \epsilon_3 \frac{\omega^2}{c^2}. \tag{4.46}$$

The stability condition in case of non-magnetized plasma can be found in the following way. The dispersion relation (4.45) can be rewritten as

$$\begin{aligned}[(\tfrac{2}{\Delta r}))^2 \sin^2(k_r\tfrac{\Delta r}{2} + (\tfrac{2}{r\Delta\varphi})^2 \sin^2(n\tfrac{\Delta\varphi}{2}) + (\tfrac{2}{\Delta z})^2 \sin^2(k_z\tfrac{\Delta z}{2})]c^2 \\ = [1 - (\tfrac{\Delta t}{2})^2 \tfrac{\cos^2(\omega\Delta t/2)}{\sin^2(\omega\Delta t/2)} \textstyle\sum \omega_{ps}^2](\tfrac{2}{\Delta t})^2 \sin^2(\omega\Delta t/2)\end{aligned} \tag{4.47}$$

After $\cos^2(\omega\Delta t/2)$ is replaced by $1 - \sin^2(\omega\Delta t/2)$ the Equation (4.47) can be simplified to

$$\begin{aligned}[(\tfrac{2}{\Delta r}))^2 \sin^2(k_r\tfrac{\Delta r}{2} + (\tfrac{2}{r\Delta\varphi})^2 \sin^2(n\tfrac{\Delta\varphi}{2}) + (\tfrac{2}{\Delta z})^2 \sin^2(k_z\tfrac{\Delta z}{2})]c^2 \\ = \sin^2(\omega\Delta t/2)[(\tfrac{2}{\Delta t})^2 + \textstyle\sum \omega_{ps}^2] - \textstyle\sum \omega_{ps}^2\end{aligned} \tag{4.48}$$

The range of the values on the left-hand side of the Equation (4.48) must be constrained within the range of the values that the right-hand side of the Equation (4.48) can take, hence

$$2c^2[(\frac{1}{\Delta r})^2 + (\frac{1}{r\Delta\varphi})^2(\frac{1}{\Delta z})^2] < (\frac{2}{\Delta t})^2 \tag{4.49}$$

Analysis of the Equation (4.49) shows that the Courant condition for a nonmagnetized plasma is completely equivalent to the vacuum Courant condition (4.41).

4.1.3 Magnetized plasma

3D

Equation 4.37 represents the general form of the numerical dispersion relation in the full three-dimensional case.

2D and 1D dispersion relations

Neglecting the terms of second order of the Taylor series expansion in the grid step, Equation (4.37) becomes:

$$\begin{aligned}&\left[(b_1^2+b_3^2)\epsilon_1+b_2^2\epsilon_3\right]\tilde{k}^2\\&-\left[(b_1^2+2b_2^2+b_3^2)\epsilon_1\epsilon_3+(b_1^2+b_3^2)(\epsilon_1^2-\epsilon_2^2)\right]b_4^2\\&+\epsilon_3\left[\epsilon_1^2-\epsilon_2^2\right]b_4^4=0.\end{aligned}\tag{4.50}$$

When the problem is uniform along the z- direction ($b_3 = 0$), the magnetized dispersion relation (4.50) becomes:

$$\begin{aligned}&\left[b_1^2\epsilon_1+b_2^2\epsilon_3\right]\tilde{k}^2\\&-\left[(b_1^2+2b_2^2)\epsilon_1\epsilon_3+b_1^2(\epsilon_1^2-\epsilon_2^2)\right]b_4^2\\&+\epsilon_3\left[\epsilon_1^2-\epsilon_2^2\right]b_4^4=0.\end{aligned}\tag{4.51}$$

When the problem is uniform along z- and $\varphi-$ directions $b_2 = b_3 = 0$ and the wave is transverse, Equation (4.51) can be further simplified to:

$$\begin{aligned}&\epsilon_1\tilde{k}^4-\left[\epsilon_1\epsilon_3+(\epsilon_1^2-\epsilon_2^2)\right]b_4^2\tilde{k}^2\\&+\epsilon_3\left[\epsilon_1^2-\epsilon_2^2\right]b_4^4=0.\end{aligned}\tag{4.52}$$

Equation (4.52) gives two well-known solutions. One of them is the slow wave dispersion relation (4.43) $\tilde{k}^2 = \epsilon_3 b_4^2$ and the second one is:

$$\tilde{k}^2=\frac{\epsilon_1^2-\epsilon_2^2}{\epsilon_1}b_4^2=\alpha b_4^2.\tag{4.53}$$

Keeping the terms of the first order of the Taylor series expansion, Equation (4.53) gives the dispersion relation of the extraordinary wave [2]:

$$k^2=\frac{\epsilon_1^2-\epsilon_2^2}{\epsilon_1}\frac{\omega^2}{c^2}=\alpha\frac{\omega^2}{c^2}.\tag{4.54}$$

In this Chapter, a full discrete disprsion relation in vacuum, non-magnetized and magnetized cases is obtained. It is shown that under certain assumptions the discrete dispersion realtion conincides with the theoreticall obtaines ones. However,

the reader may notice that the numerical model has been developed in the cylindrical coordinates whereas the mathematical analysis of the discrete dispersion relation has been performed in the Cartesian coordinate system. Below an ample justification of why a dispersion analysis can't be performed in the cylindrical coordinates and why it still can be done in a Cartesian one is demonstrated.

4.2 Justification on the choice of the coordinate system

★ ★ ★

As pointed out in the previous section the developed numerical code is build in cylindrical coordinates, but in the end all mathematical analysis is performed in the cartesian ones. Despite given justification that the cartesian results will be applicable in certain limits (4.33), the additional analysis on why a derivation of the discrete dispersion relation in the cylindrical system is not straigtforward and why this analysis still can be done in Cartesian coordinates and it is presented in this Section.

4.2.1 Purpose of the substudy

To explain the purpose of this substudy it is important to give a 'definition' of what a discrete dispersion relation is. The discrete dispersion relation is not just a local condition for non-trivial solutions of the sourceless wave equation, it is a description of the properties of the global solutions of the time-stepping operator. And therefore it is important to derive a stability condition of the discrete dispersion relation. In a Cartesian coordinate system in a uniform linear medium the discrete solutions can be transformed straightforward to the exact solutions, in other words, the knowledge of the eigenfunctions of the spatial operator k maps to the knowledge of the eigenfunctions of the time-stepping operator. And therefore the derivation of the discrete dispersion relation and its stability condition is rather straighforward. After the discrete dispersion relation is derived, the FULL knowledge of the behaviour of the waves in the continuous and discrete physics is obtained. In other words, a full description of the properties of the global solutions of the time-stepping operator is gained. However in the cylindrical coordinate system in the same uniform media the derivation of the discrete dispersion relation based on eigensolutions cannot be performed by just deforming the continuous dispersion relation: the eigensolutions do not correspond to the ones in the continuous physics. And therefore it is desirable to find out whether it is possible to construct a discrete dispersion relation in the cylindrical coordinate system. The following substudy attempts to show a fundamental difference between Cartesian discretisation and non-Cartesian one, i.e. that the acceptance of the coordinate-dependent dispersion relation is going to reduce the disperion relation from an

exact description of global solutions of discretized physics to an approximate dispersion relation that can predict wavelength in areas where the dispersion relation varies slowly.

4.2.2 Origin of justification

In cartesian coordinates, it happens to be the case that the solutions $exp(jkx - j\omega t)$ can be inserted in the discrete equations and it can be found that they are indeed exact solutions of the discrete equations provided some condition $f(k,w) = 0$ holds. This procedure is exactly analogous to the procedure for obtaining the continuous (exact) dispersion relation $g(k,w) = 0$ therefore the effectiveness of a certain discretisation scheme by comparing f(k,w) and g(k,w) can be judged. As it is a rather convenient assumption, it has become background knowledge that some people take for granted, forgetting its justification, and just assuming it will always work. Unfortunately, this is not the case: in some other sufficiently regular coordinate systems, such as spherical and cylindrical coordinates, the exact solutions of the exact equations still can be written down, but still have two parameters : a spatial scale parameter analogous to k, and a frequency parameter ω. In cylindrical coordinates these exact solutions would involve Bessel functions. But, in general, these exact solutions are not exact solutions of the discretized equations (not even if the dispersion relation is changed), which means that the construction of the discrete dispersion relation in the same way as it is done in the cartesian coordinates is not possible.

Here, it is intended to show that the exact solutions of the discrete equations in cylindrical coordinates are not exactly Bessel functions.

4.2.3 Justification

Consider the Bessel functions $J_\nu(kr)$, which are the solutions for E_φ in cylindrical coordinates if $k_\varphi = 0$. In a cylindrical geometry with radius R the boundary condition $J_\nu(kR) = 0$ is present, which gives possible values of k (and with it, the resonant frequencies). Assuming k_i is the set of k for which $J_\nu(k_i R) = 0$, the functions $J_\nu(k_i r)$ are linearly independent, and in fact orthogonal under a certain inner product [3], [4], [5]. This means that (almost) any function on $[0,R]$ can be written as a linear combination of $J_\nu(k_i r)$. In particular, an eigensolution of the cylindrical FDTD time stepping operator can be written as a linear combination of $J_\nu(k_i r)$ and the coefficients can be looked at : an exact Bessel function will have all coefficients 0 except one, and an approximate Bessel function will have a peak surrounded by small values (much like an approximate sin function has a peak in its Fourier spectrum) The description of the procedure and the obtained results are given below.

Description of the procedure

A general scheme of the proposed analysis is the following. The first step is to write down the time-stepping operator and to obtain the eigenvalues λ_i and the eigenvectors v_i. The eigenvectors v_i can be interpreted as the frequency-domain solution for an angular frequency $\arg(\lambda_i)/\Delta t$. Then, a λ_i and a v_i of interest are picked up (in this case, well-resolved and ill-resolved ones). Finally, the chosen v_i can be written as a linear combination of continuous eigensolutions f_k (i.e. Bessel function in the cylindrical case and sine in the Cartesian coordinate system):

$$v_i = \sum (a_k f_k(r)) \tag{4.55}$$

Below it is shown that in case a Cartesian coordinate system this is always possible, and, if the discrete solution coincides with a continuous solution, all but one of the a_k will be 0. In a cylindrical coordinate system, if the discrete solution merely approximates a continuous solution, many a_k will be nonzero, though one will be much larger than the others.

4.2.4 case A: Cartesian

In a Cartesian coordinate system 1D box in $[0,1]$ a continuous solution with $E_y = \sin(n\pi x)exp(j\omega_c(n)t)$ exists and a discrete solution with $E_y = \sin(n\pi x)exp(j\omega_d(n)t)$ also exists, where $\omega_c(n)$ is the continuous resonant frequency, a function of a mode number n and $\omega_d(n)$ is the discrete resonant frequency as a function of the mode number n. It can be seen that the discrete solution coincides with a continuous one and the discretisation has caused a deformation of the $\omega - k$ plane (dispersion relation): $\omega_c(n) \neq \omega_d(n)$ (see Fig. 4.3 and Fig. 4.2).

4.2.5 Case B: cylindrical system

In a cylindrical 1D box in $[0,1]$ a continuous solution with $E_\varphi = J_1(kr)exp(j\omega_c(n)t)$ exists and a discrete solution with $E_\varphi = J_1(kr)exp(j\omega_d(n)t)$ does not exist. A discrete solution with $E_\varphi = f(r)exp(j\omega_d(n)t)$ exists, though $f(r)$ is not of the form $J_1(kr)$ for any k. It can be seen that $J_1(kr) \neq f(x)$,i.e. the discrete solution does not coincide with a continuous solution and the discretisation influences the solution beyond merely deforming the $\omega - k$ plane (see Fig. 4.4- Fig. 4.5).

Conclusion

What does this all imply? In Cartesian system it is rather easy to prove the statement of the form if $f(kx)exp(j\omega t)$ is an exact eigensolution of the continuous physics, then $(f(g(k)x) + 0)exp(jh(\omega)t)$ is an exact eigensolution of the discretized physics. The accuracy of the approximation would then be judged by how closely $g(k)$ approximates k, and $h(\omega)$ approximates ω. This

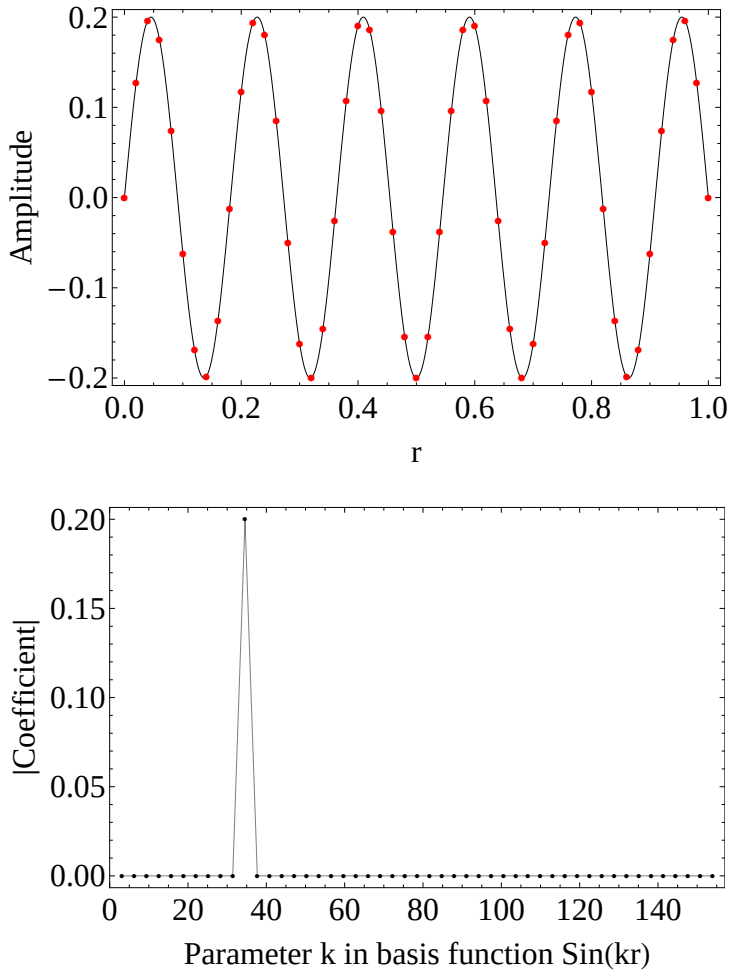

Figure 4.2: Upper figure: well-resolved eigensolution of FDTD time-stepping operator in Cartesian coordinates. Lower figure: Expansion of this solution in orthogonal Sine functions.

statement can be simplified to if $d(k,\omega) = 0$ is the continuous dispersion relation, then $d(g(k),h(\omega)) = 0$ is the discrete dispersion relation. However, in the cylindrical system, it may be possible to prove the statement of the form: if $f(kr)exp(j\omega t)$ is an exact eigensolution of the continuous physics, then $(f(g(k)r) + e(r,k,\omega))exp(jh(\omega)t)$ is an exact eigensolution of the discretized physics. The accuracy of the approximation would then be judged by how closely $g(k)$ approximates k, and $h(\omega)$ approximates ω and $e(r,k,\omega)$ approximates 0,

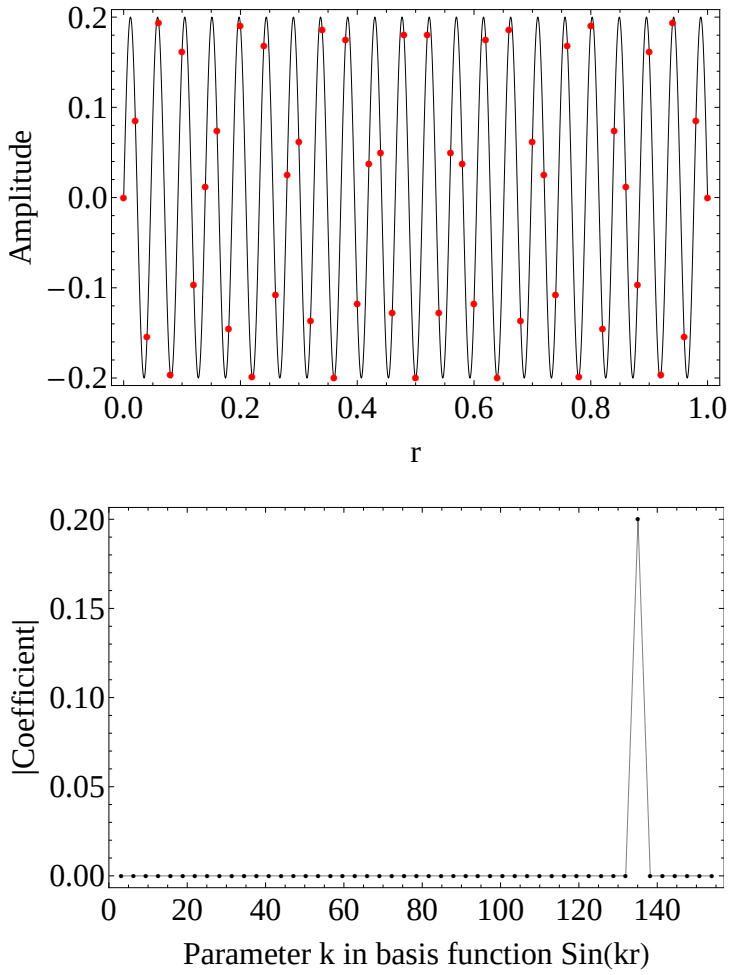

Figure 4.3: Upper figure: ill-resolved eigensolution of FDTD time-stepping operator in Cartesian coordinates. Lower figure: Expansion of this solution in orthogonal Sine functions.

perhaps $|e| \ll |f|$. Generally, it can be concluded that the results are as expected: the discrete solutions are not exact Bessel function (contrast with the cartesian case, where the discrete solutions are exact complex exponentials). And this gives a justification for why it is rather complex to perform a dispersion analysis in the cylindrical coordinate system the way it is possible to do it in cartesian : in cartesian, the only effect of the discretisation is a deformation of the dispersion curve, while in cylindrical coordinates, the expression for the solutions itself

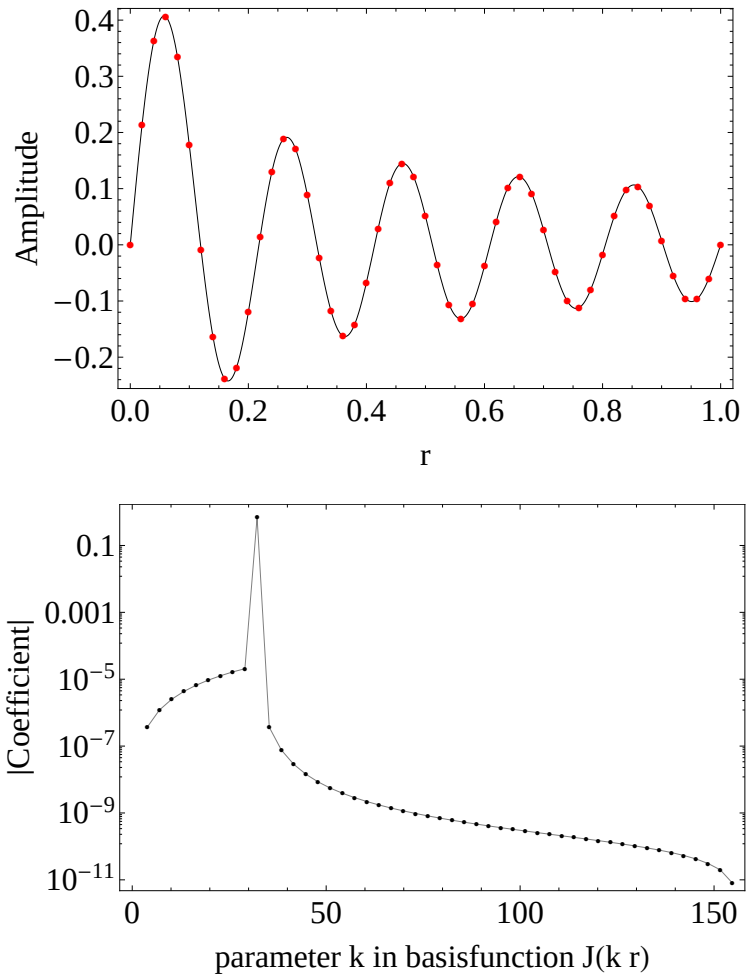

Figure 4.4: Upper figure: well-resolved eigensolution of FDTD time-stepping operator in cylindrical coordinates. Lower figure: Expansion of this solution in orthogonal Bessel functions.

changes from a pure Bessel to something that approximates a pure Bessel, which is an effect that cannot be described by dispersion curve deformation alone.

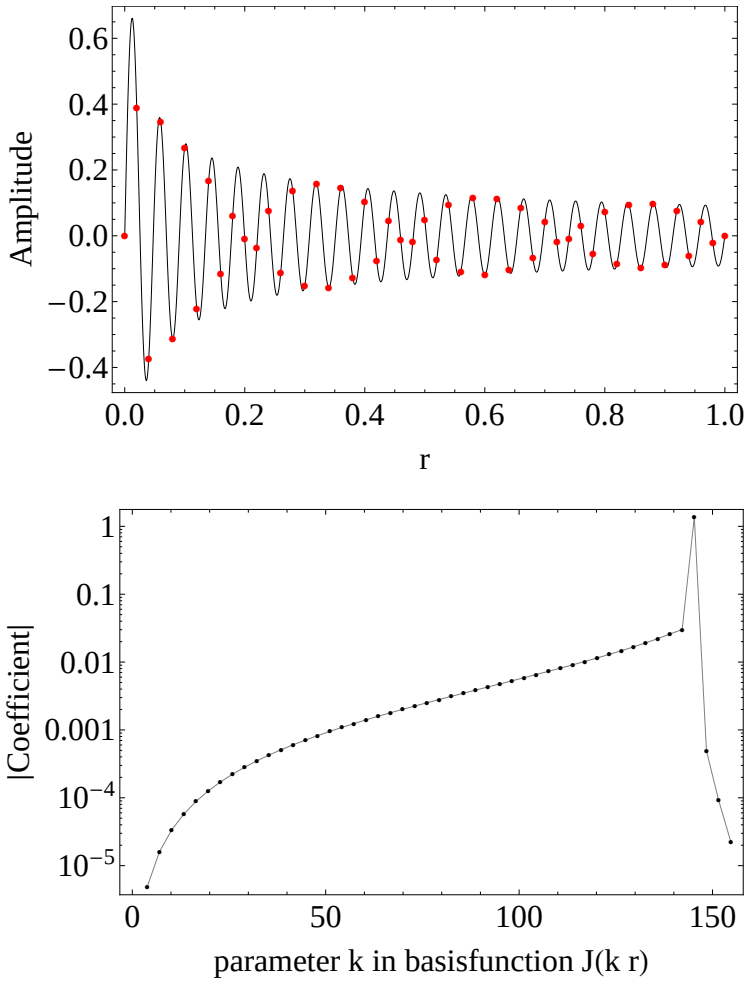

Figure 4.5: Upper figure: ill-resolved eigensolution of FDTD time-stepping operator in cylindrical coordinates. Lower figure: Expansion of this solution in orthogonal Bessel functions.

References

[1] T. H. Stix, *Waves in plasmas*. Springer, 1992.

[2] M. Brambilla, *Kinetic Theory of Plasma problems: Homogeneous Plasma*. Clarendon Press, 1998, vol. 1.

[3] J. Schroeder, "Signal processing via fourier-bessel series expansion", vol. 3, no. 2, pp. 112 –124, Apr. 1993.

[4] W. Magnus, *Formulas and Theorems for Special Functions of Mathematical Physics*. Berlin: Springer, 1966.

[5] W. R. Smythe, *Static and Dynamic Electricity*, 3rd ed. New York: McGraw-Hill, 1968.

5

Validation of the Developed Numerical Code

5.1 Accuracy and Stability Analysis

★ ★ ★

Before employing the proposed numerical algorithm, it is needed to determine if it is applicable to the problem at hand. Tackling any problem numerically (rather than analytically) inevitably introduces discretization errors. In this Section the accuracy and stability analysis of the developed numerical algorithm is presented. A stability proof is provided for nonmagnetized uniform plasma, in which case the stability condition is the vacuum Courant condition. For magnetized cold plasma the stability condition is investigated numerically using the von Neumann technique [1].

5.1.1 Accuracy

The study of a numerical algorithm's accuracy involves studying, and imposing, bounds on these errors. An analysis of the discretization error can be performed by comparing numerical and exact dispersion relations, as in [2], [3], [4], [5]. The approach followed by [2] is based on comparing the numerically calculated dispersion which expresses how the index of refraction depends on the wave frequency with the analytically predicted dispersion. Subsequently the numerical errors are calculated as the deviation of the numerical results with respect to the corresponding values obtained analytically. However, rather than using the relative error on the dispersion (as [2] did) we propose to use the relative dispersion

error defined as :

$$\delta = |Re\left(N_{num} - N_{anal}\right)/Re\left(N_{anal}\right)|, \tag{5.1}$$

where N_{num} and N_{anal} are the numerically and analytically obtained indexes of refraction. In order to evaluate the relative dispersion error we choose to investigate the dispersion relation of the extraordinary wave [6]. This particular plasma mode is selected because the range of the propagation of this wave contains ion-cyclotron frequencies ($\Omega_{ci} = q_i B/m_i$), The numerical tests were conducted in the frequency range from 0 to the low hybrid frequency ($\omega_{LH} = ((\Omega_{ci}\Omega_{ce})^{-1} + \omega_{pi}^{-2})^{-1/2}$), because exactly in this range the values of the wave vector are real and the wave itself propagates through the simulation region (see Fig.5.1). The

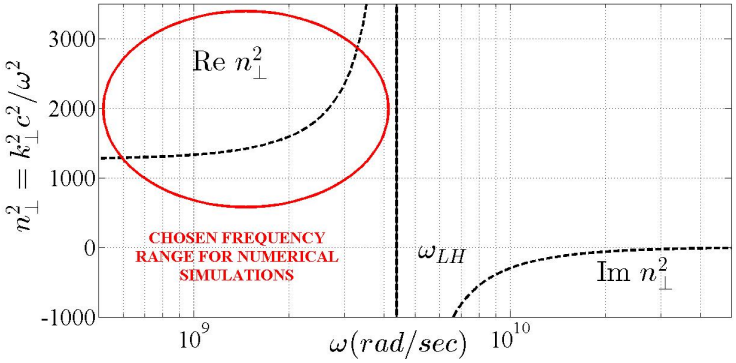

Figure 5.1: Analytical dispersion relation of the extraordinary wave. The frequency range from 0 to ω_{LH} marked in red is chosen for numerical simulations.

considered time-steps lie in an interval from 0 to π/ω. The numerical simulations are conducted in the collisionless homogeneous media with initial plasma parameters $n_e = n_D = 10^{19}$ $(1/m^3)$ and background magnetic field B_0 equal to $3(T)$. On Fig. 5.2 the contour plot shows the relative dispersion error (see Eq. (5.1)), as a function of frequency ω and time-step Δt. The contour lines (of this contour plot) demarcate the borders of the areas in the (ω, Δt) plane where the relative dispersion error is below a certain numerical value of the dispersion error. This will give us guidance on how to choose Δt for a certain frequency range provided that we require a certain accuracy. For example, if the values of the frequency and time-step are chosen within the area demarcated by the contour labeled "0.01", it is guaranteed that the dispersion error will not exceed 1 %. The conclusion from the discussion is that in order to get a sufficient accuracy (i.e. a relative dispersion error of less than, e.g. 1%) the time-step has to be chosen such that the point $(\omega, \Delta t)$ lies in an area demarcated by and below the two '0.01' contours as illustrated in Fig. (5.2).

In what follows extra attention is devoted to the result shown in Fig. (5.2). Each point in the figure is obtained by selecting a particular frequency ω and a corre-

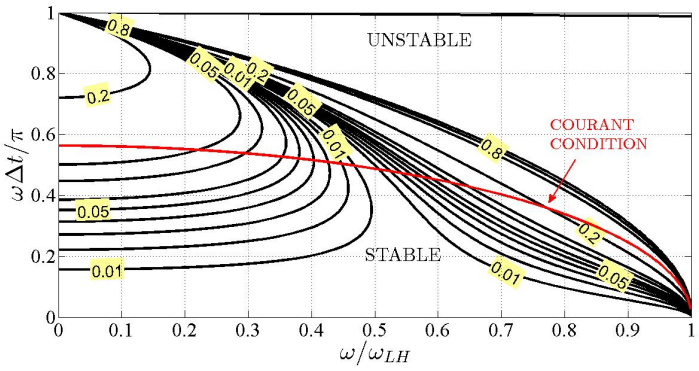

Figure 5.2: A contour plot of the dispersion error as a function of ω and Δt. The lines of the contour plot demarcate the borders of the areas corresponding to a certain accuracy. The Courant limit (red solid line) shows the border between stable and unstable simulation areas.

sponding time-step Δt. Using ω, the dispersion relation is invoked to determine the space-step Δr as a fraction of the relevant wavelength (e.g. $1/100$ of that wavelength). In this way, one can make sure that time- and space-steps are sufficiently small, such that the simulated wave phenomena are well-resolved both in time and space. It is clear that, when increasing the time step (points located higher on the y-axis of the figure), accuracy can be expected to decrease. However, it is unclear and puzzling that for points closer to ω_{LH} but still very small Δt, i.e. points located near the lower right corner of the figure, accuracy is poor, regardless of the Courant limit.

We would like to that W. Tierens for suggesting the following possible explanation. When approaching ω_{LH}, the resonant behaviour becomes dominant. It could very well happen that the numerical discretization of the problem gives rise to a slightly different resonance frequnecy then the analytical one and that this numerical resonance frequnecy is higher than the analytical one. In that case, when approaching ω_{LH}, N_{anal} increases dramatically when approaching ω_{LH}, while N_{num} does not, and hence the relative error goes to 1.

It has further be noted that in [7], Y. Pavlenko discusses a very similar problem. He suggests that a nondissipative FDTD method cannot correctly treat the wave processes near the resonance frequency. Without going into further discussion on this point, it is clear that when N_{anal} no longer becomes infinite at the resonance frequency, the effect of a possible difference between analytical and numerical resonance frequency will also be less dramatic.

5.1.2 Stability

Theoretically, each difference scheme has an exact solution. However, when explicit calculations are carried out in a computer, errors are commited due to the finite precision of the arithmetic operations.

One of the standard analytical approaches to examine the stability of a numerical technique is a method developed by von Neumann [8]. Stability approach means that an explicit solution is stable if it produces a bounded result giving a bounded input. The numerical solution is unstable if it produces an unbounded result given a bounded input. The Von Neumann method expresses the error in a numerical solution at any point in time as a finite spatial Fourier series. Numerical stability results if each Fourier term has a unity-or-less growth factor over one time-step. Then, assuming that each Fourier term is initially bounded, each term remains bounded at all subsequent time-steps. Since the system is linear, the total error represented by the finite sum of the Fourier terms must also be bounded at any time-step.

In other words, if the method is stable, its source-free solutions will not diverge no matter what the initial fields are. Because the simulation region is finite, any initial field configuration can be expanded as a linear combination of complex exponentials with real wavenumbers k. Because the time-stepping operator is linear, the stability can be verified for every one of these compex exponentials. In uniform Cartesian cases, these complex exponentials are eigenvectors of the time-stepping operator, which makes verifying their stability rather straighforward: it has to be ensured that the corresponding eigenvalues lie in or on the unit circle. If there are eigenvalues outside the unit circle, the associated solution will increase exponentially with time.

The 1D problem with the wave propagating in the r- direction with non-zero components $E_r, E_z, H_\varphi, J_r, J_z$ in magnetized plasma is considered. The difference equations can be written in the general form:

$$\underbrace{F^{t+1}}_{future} = M \underbrace{F^{t}}_{past}, \tag{5.2}$$

where F represents a column vector containing all discretized electric, magnetic and current field components and where M is the amplification matrix. The numerical scheme is stable if the eigenvalues of M lie on the unit circle in the complex plane. Only when there are losses either due to the nature of the material or due to radiation escaping from the simulation region, some of the eigenvalues may fall inside the unit circle [9]. In Fig. 5.3 the eigenvalues of the amplification matrix of the applied FDTD method for magnetized plasma are presented.

In this particular case the simulation parameters are: $n_{e^-} = 3 \cdot 10^{19}$ $(1/m^3)$, $n_D = 0.98 n_{e^-}$ $(1/m^3)$, $n_H = 0.02 n_{e^-}$ $(1/m^3)$. The background magnetic field is uniform and it is equal to 3 T. The space step Δr is calculated based on the

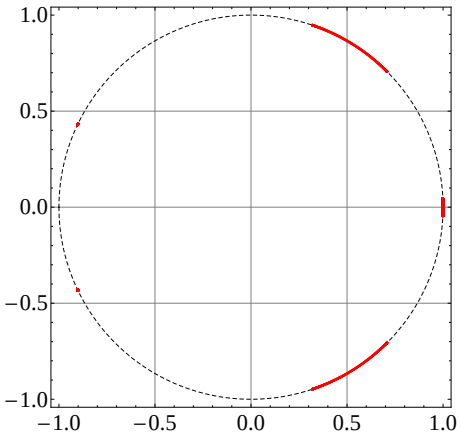

Figure 5.3: Numerical stability test. The eigenvalues of the amplification matrix M are located on the unit circle in the complex plane. The initial simulation parameters are: $n_{e^-} = 3{\cdot}10^{19}\ (1/m^3)$, $n_D = 0.98 n_{e^-}\ (1/m^3)$, $n_H = 0.02 n_{e^-}\ (1/m^3)$. The background magnetic field is uniform and it is equal to 3 T.

analytical dispersion relation [10], [6]. The time-step Δt is determined in agreement with the Courant stability condition [8]. This numerical analysis shows that the developed technique is indeed stable at these parameters. In particular, we find that the time-step has to be suffciently small, i.e. it must satisfy the vacuum Courant condition. If it exceeds the Courant limit, instability could occur [11].

5.2 Validation of the developed numerical code

★ ★ ★

Having developed a global cold magnetized toridal plasma numerical model, this FDTD algorithm is validated, firstly, by comparing analytical and numerical electromagnetic wave solutions in vacuum, nonmagnetized and magnetized plasma. The results of these simulations are presented below. Then, numerical simulations are performed to check whether the numerical dispersion relations for the above mentioned cases coincide with the dispersion relations predicted analytically. The performed analysis shows a very good agreement with the theoretically obtained results.

5.2.1 Vacuum Case

It is well-known that the analytical solution to Maxwell's differential equation may be written in terms of Bessel functions. In order to demonstrate the reliability of the developed numerical code, a set of simple numerical tests were conducted. First, the behaviour of the electromagnetic waves in vacuum is validated. To initial conditions of the simulations are the following: the electromagnetic wave is generated by a hard source in the middle of the computational domain. The total number of cells is $N_{cells} = 700$. The source frequency is $\omega = 2.7 \cdot 10^9$ (rad/sec). The size of the space step is chosen with regard to the analytically obtained wavelength λ ($k_0 = \omega/c$) and it is equal to $\Delta r = \lambda/10 = 0.031$ (m).

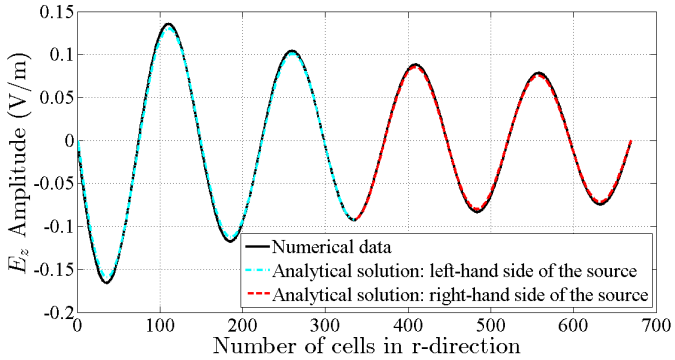

Figure 5.4: Validation of the developed numerical algorithm. Comparison of the analytical and numerical electromagnetic wave solution in the vacuum case. The total number of cells is $N_{cells} = 70$. The source frequency is $\omega = 2.7 \cdot 10^9$ (rad/sec). The size of the space step is chosen with regard to the analytically obtained wavelength ($k_0 = \omega/c$) and it is equal to $\Delta r = 0.031$ (m).

In Fig. 5.4 a numerically obtained behaviour of the z-component of the electric field **E** in vacuum is compared to the analytical solution of Maxwell's equations. The black dashed line shows the numerical solution. As the source is located in the middle of the simulation area, two analytical solutions are plotted: the cyan dashed line represents the left-hand side of the predicted solutions, the red dashed line stands for the right-hand side. In this case the numerical error is about 0.5 %. Fig. 5.4 shows a good agreement between analytically and numerically obtained solutions.

5.2.2 Nonmagnetized plasma case

Analogously, the developed numerical code is validated in case of nonmagnetized plasma. Fig. 5.5 presents a sample of the z-component of the electric field. The numerically obtained data is compared to the analytically calculated solution. The electromagnetic wave is excited in the middle of the simulation domain. In Fig. 5.5

the black dashed line represents the numerical solution. The green solid line and the pink dashed line show the right-hand side and the left-hand side analytical solutions, respectively. The initial parameters of this test are: the frequency of the source is $\omega = 1.4 \cdot 10^9$ (rad/s), the space lattice increment is $\Delta r = 0.0099$ (m). The density of plasma is $n_e = n_{DE} = 3 \cdot 10^9$ $(1/m^3)$. The number of cells in the r-direction is 346. Fig. 5.5 shows that the numerically obtained data coincide well with the predicted solution (numerical error is about 2 %).

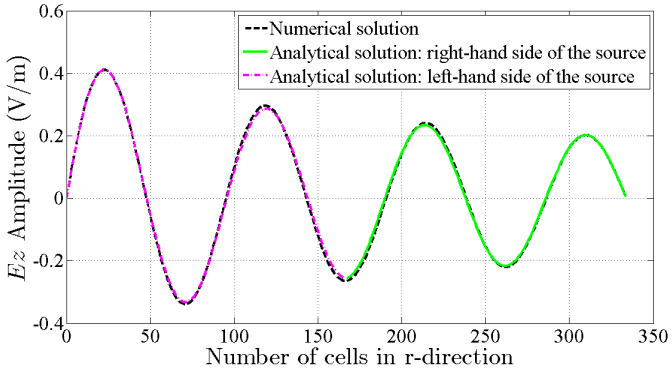

Figure 5.5: Validation of the numerical algorithm. Comparison of the analytical and numerical electromagnetic wave solution in nonmagnetized case. The frequency of the source is $\omega = 1.4 \cdot 10^9$ (rad/s), the space lattice increment is $\Delta r = 0.0099$ (m). The density of the plasma is $n_e = n_{DE} = 3 \cdot 10^9$ $(1/m^3)$.

5.2.3 Magnetized plasma case

The method to validate the constructed numerical code was described above. The same approach is applied for the analysis of the electromagnetic waves in magnetized plasma. Fig. 5.6 compares the analytical and numerical solution of electromagnetic waves. The source is located in the middle of the simulation area. The red dashed line shows the numerically obtained solution. The black solid line illustrates the right-hand side behaviour of the analytical solution and the green dot-dashed line stands for the left-hand side solution. The initial parameters are: the source frequency is $\omega = 2.7 \cdot 10^9$ (rad/s), the space lattice increment is $\Delta r = 0.0026$ (m). The density of the plasma is $n_e = n_{DE} = 3 \cdot 10^{19}$ $(1/m^3)$. The background magnetic field is equal to 3 T. The number of cells is 670. Fig. 5.6 shows a very good agreement (0.5 % numerical error) with the theory.

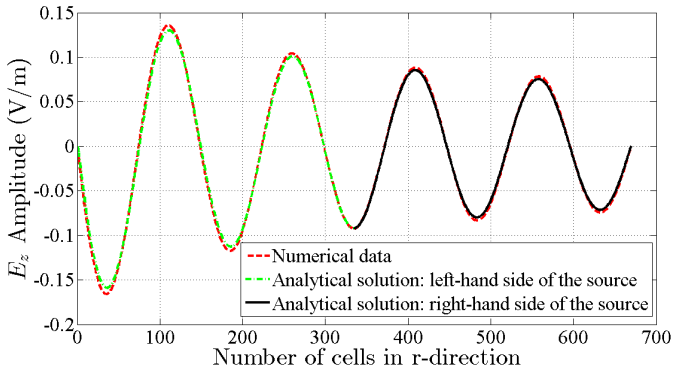

Figure 5.6: Validation of the numerical algorithm. Comparison of the analytical and numerical electromagnetic wave solution in the magnetized plasma case. The source frequency is $\omega = 2.7 \cdot 10^9$ (rad/s), the space lattice increment is $\Delta r = 0.0026$ (m). The density of the plasma is $n_e = n_{DE} = 3 \cdot 10^{19}$ $(1/m^3)$. The background magnetic field is equal to 3 T.

5.3 Dispersion relations

In the section 4.1 it is proven that the dispersion relation of the actual problem and its FDTD counterpart obtained when using the hybrid FDTD method [12] will become identical for a sufficiently small time step. In the following section, this claim is further substantiated by providing numerical data from the developed numerical FDTD code. As was mentioned above, this code is based on [12], but adapted to a cylindrical coordinate system (r, φ, z) and is particularly suited for tokamak/stellarator configurations.

5.3.1 Nonmagnetized plasma dispersion relation

Fig. 5.7 compares the theoretical dispersion curve of the hybrid explicit/implicit method to the numerical one. The numerical results are obtained for the 1D case, the model is invariant in φ- and z-direction. The blue and the green starred lines represent the analytical and the numerical dispersion relation of the electromagnetic wave in a nonmagnetized plasma, respectively. The slope of the red dashed line is equal to the speed of light. The initial parameters of the presented analysis are: the density of electrons n_e is $3 \cdot 10^{19}$ $(1/m^3)$, the plasma frequency is equal to $3.08 \cdot 10^{11}$ (rad/sec).

The numerical dispersion curve is obtained in the following way. As a source a "point" source is used, which in this cylindrical case is really an infinitely thin cylindrical surface along the toroidal direction carrying a constant amplitude current with sinusoidal time-dependence at a particular frequency ω. This current

is switched on at $t = 0$ and flows until regime conditions are met. The source is also called a hard source [13]. Observing the fields sufficiently far from the origin the wavelength λ can be found from consecutive maxima and minima and $k(\omega) = 2\pi/\lambda$ (for real k). This procedure is repeated to cover the complete frequency range of interest. To be sure that FDTD simulations are sufficiently accurate, the space increment Δr is chosen to be $\lambda/100$ (1/100-th of the theoretically determined wavelength λ) and the time-step Δt equal to $\Delta r/2c$, where c is the speed of light in vacuum. Fig. 5.7 clearly shows that the numerical results are in a good agreement with analytical predictions.

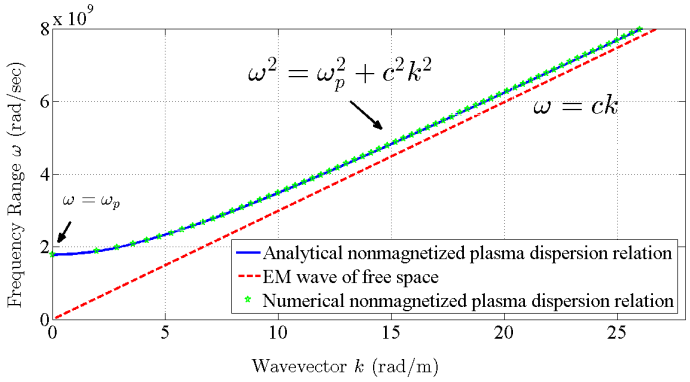

Figure 5.7: Validation of the developed numerical algorithm. Comparison of the analytical and numerical dispersion relations in nonmagnetized plasma. The initial parameters are the following: n_e is $3 \cdot 10^{19}$ $(1/m^3)$, the plasma frequency is equal to $3.08 \cdot 10^{11}$ (rad/sec).

5.3.2 Homogeneous magnetic field. Magnetized plasma

Fig. 5.8 and Fig. 5.9 compare the theoretical dispersion curve of the hybrid explicit/implicit method to the numerical one over a wide frequency range. In Fig. 5.8 the blue line illustrates the behaviour of the analytical dispersion relation of the extraordinary wave. The starred red line stands for the numerical dispersion relation. In Fig. 5.9 the red line represents the dispersion relation of the ordinary wave and the black triangled line shows its numerical dispersion relation. The numerical results are obtained for the 1D case, the model is invariant in φ- and z-direction. A one-ion homogeneous collisionless plasma is considered. The initial simulation parameters are the following: $n_e = n_{De} = 3 \cdot 10^{19}$ $(1/m^3)$. The background magnetic field is equal to 3 T. The plasma specie frequencies are $\omega_{pe} = 3.08 \cdot 10^{11}$ (rad/sec), $\omega_{pDe} = 5.09 \cdot 10^9$ (rad/sec). The electron cyclotron frequency is $\Omega_{ce} = 5.27 \cdot 10^{11}$ (rad/sec). The ion cyclotron frequency is $\Omega_{ci} = 1.43 \cdot 10^8$ (rad/sec). The real solutions of the numerical dispersion relation in case of a homogeneous magnetized plasma are obtained analogously to

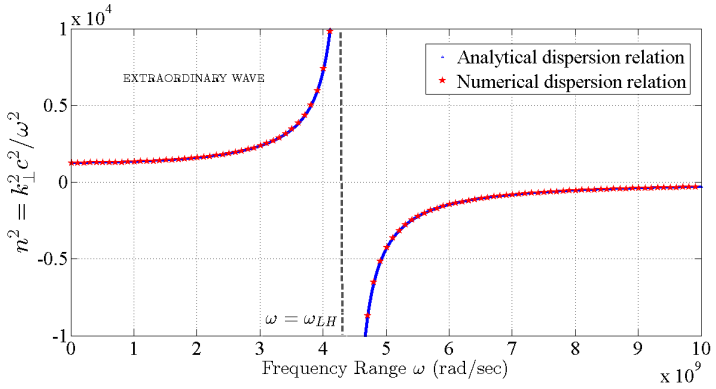

Figure 5.8: Validation of the developed numerical algorithm. Comparison of the analytical and numerical dispersion relations in case of magnetized plasma in a homogeneous background magnetic field. The initial simulation parameters are the following: $n_e = n_{De} = 3 \cdot 10^{19}$ $(1/m^3)$. The background magnetic field is equal to 3 T. The plasma specie frequencies are $\omega_{pe} = 3.08 \cdot 10^{11}$ (rad/sec), $\omega_{pDe} = 5.09 \cdot 10^9$ (rad/sec). The electron cyclotron frequency is $\Omega_{ce} = 5.27 \cdot 10^{11}$ (rad/sec). The ion cyclotron frequency is $\Omega_{ci} = 1.43 \cdot 10^8$ (rad/sec).

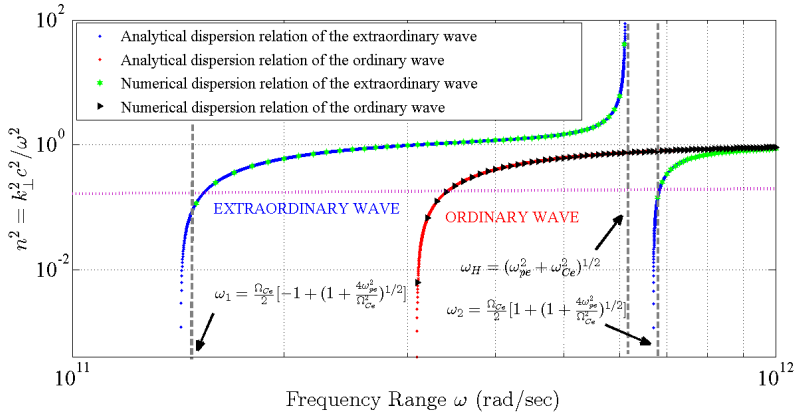

Figure 5.9: Validation of the developed numerical algorithm. Comparison of the analytical and numerical dispersion relation of the ordinary and extraordinary waves in magnetized plasma in a homogeneous background magnetic field. The initial simulation parameters are the same as in Fig. 5.8.

the approach described in Section 5.3.1. It has to be noted that an alternative way to obtain the numerical dispersion relation is to calculate the eigensystem of the

amplification matrix for which the eigenvalues are related to the frequencies and the eigenvectors. This method was also implemented and identical results were obtained.

In case of evanescent waves, k can be found using the exponentially decaying behaviour of the fields. Evidently, $E_0 exp(jkx) exp(-j\omega t)$ is a solution to the wave equation. If k is a purely imaginary number, so then it can be replaced by $j\beta$, where β is a real number. Accordingly, the expression $E_0 exp(jkx) exp(-j\omega t)$ becomes $E_0 exp(-\beta x) exp(-j\omega t)$. This no longer oscillates as a function of position- it exponentially decays, but it is still oscillates as a function of time. Thus on a logarithmic scale the solution mentioned above has the form $log(E) = log(E_0 exp(-j\omega t)) - \beta x$, from which β can be obtained by making a linear fit. For example, Fig. 5.10 shows a sample of the behaviour of the electric field in the case of evanescent waves. For this specific case of the homogeneous collisionless plasma the following parameters are chosen: $n_e = n_{HD} = 10^{19}$ $(1/m^3)$. The background magnetic field is equal to 3 T. The source frequency ω is $1.07 \cdot 10^{10}$ rad/sec. The space lattice increment Δr is 0.000102 m. For convenience, Fig. 5.10 is presented on a logarithmic scale. Clearly there is some range in which the data is linear, and some other ranges where the amplitude is too low and is noise-dominated. Nevertheless, the points in between which the plot is sufficiently linear are picked by hand. The slope of the chosen line relates to the decay length. Fig. 5.8 and Fig. 5.9 show a good agreement with the theory.

5.3.3 Magnetized plasma case. Inhomogeneous magnetic field

Here, in Fig. 5.12 the simulation results in magnetized 2-ion plasma in case of an inhomogeneous magnetic field are compared with the analytical results [10]. The initial parameters are $n_e = 3{\cdot}10^{19}$ $(1/m^3)$, $n_{HD} = 0.2{\cdot}10^{19}$ $(1/m^3)$, $n_{DE} = 0.8{\cdot}10^{19}$ $(1/m^3)$. The plasma frequency of the species is $\omega_{pe} = 3.08 \cdot 10^{11}$ (rad/sec), $\omega_{pHD} = 1.86 \cdot 10^9$ (rad/sec), $\omega_{pDE} = 2.63 \cdot 10^9$ (rad/sec). The background magnetic field decreases as $9/r$ and its behaviour is shown in Fig. 5.11. In Fig. 5.12 the FDTD simulation results are seen to be in a very good agreement with the analytical results.

The set of numerical examples provided in Section 5.3 shows that the developed algorithm based on the hybrid FDTD method performs properly and that the dispersive behavior is predicted correctly.

5.4 Impact of the cylindrical geomentry

★ ★ ★

In this Section the impact of the curvature geometry on the behaviour of the electromagnetic wave is shown.

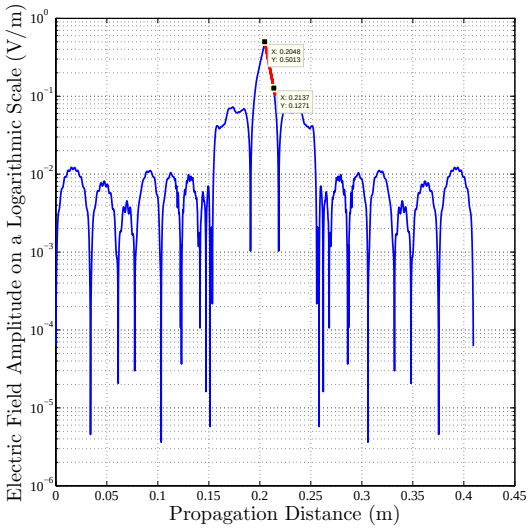

Figure 5.10: Calculation of the wavelength in case of evanescent waves. The initial simulation parameters are: $n_e = n_{HD} = 10^{19}\ (1/m^3)$. The background magnetic field is equal to 3 T. The source frequency ω is $1.07 \cdot 10^{10}\ rad/sec$. The space lattice increment Δr is 0.000102 m.

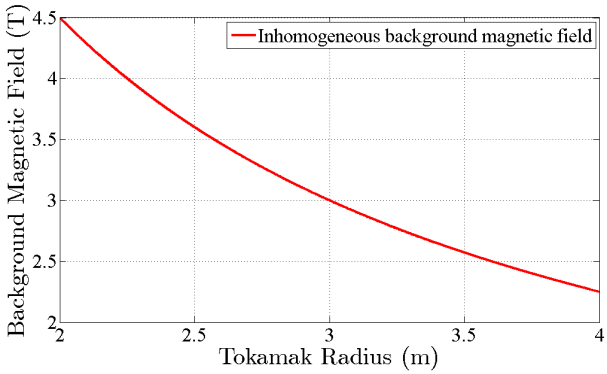

Figure 5.11: Behaviour of the inhomogeneous background magnetic field. The background magnetic field decreases as $9/r$.

The typical geometry of the JET tokamak and its plasma parameters will be used to carry out some of the numerical tests. The RF antenna is located at $r_a = 4$ (m). The diameter of the plasma column is 2 m therefore $r_b = 2$ (m). In order to simplify the numerical tests we assume that the magnetic field is uniform and it is

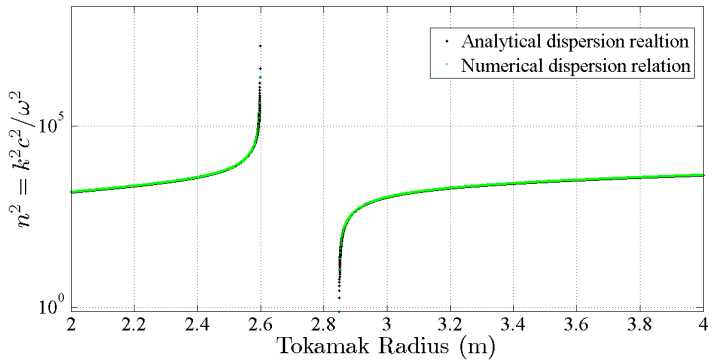

Figure 5.12: Dispersion relation of the fast wave in a magnetized plasma with an inhomogeneous background magnetic field. The initial parameters are $n_e = 3{\cdot}10^{19}$ $(1/m^3)$, $n_{HD} = 0.2 \cdot 10^{19}$ $(1/m^3)$, $n_{DE} = 0.8 \cdot 10^{19}$ $(1/m^3)$. The plasma frequency of the species is $\omega_{pe} = 3.08 \cdot 10^{11}$ (rad/sec), $\omega_{pHD} = 1.86 \cdot 10^9$ (rad/sec), $\omega_{pDE} = 2.63 \cdot 10^9$ (rad/sec). The background magnetic field decreases as $9/r$ (see Fig. 5.11).

equal to 3 (T). The antenna launches the fast wave (FW) with a source frequency f that is equal to 45.7 (MHz). The corresponding angular frequency ω is $2.87{\cdot}10^8$ (rad/sec). The ion- and electron density in the plasma is $3 \cdot 10^{19}$ (m^{-3}).

Fig. 5.13 shows the comparison of the field structures in the Cartesian (red dotted solid line) and the cylindrical (black dotted solid line) coordinate systems. The figures show the steady state distribution of the wave fields. The amplitude of the wave field is constant in a plasma column in the Cartesian coordinate system. Using the definition of the energy flux density, i.e. Poynting vector $\mathbf{S} = [\mathbf{E} \times \mathbf{B}]$, the growth of the amplitude in the cylindrical coordinate system may be estimated. For example, we propose to compare the magnitude of the time-averaged Poytning flux at two different positions: at $r_a = 4$ (m) and at $r_b = 2$ (m), which gives us

$$S_1 r_a = S_2 r_b \tag{5.3}$$

that leads to $S_2 = \frac{r_a}{r_b} S_1$. Since for sinusoidal electromagnetic plane waves the time-averaged Poyting flux S is equal to E_0^2 (E_0 is the amplitude of the electric field), the amplitude of the electromagnetic wave grows in $\sqrt{\frac{r_a}{r_b}}$ times, which means that in our case it grows in $\sqrt{2}$ times and as it can be seen on a Fig. 5.13, the numerical results are in good agreement with theoretical predictions.

5.5 Mode conversion simulations

★ ★ ★

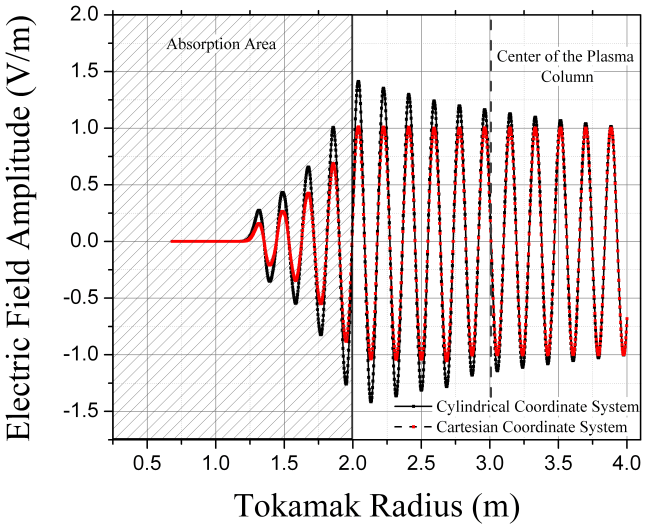

Figure 5.13: Curvature effects.

This Section presents the results of the numerical simulations including toroidal and poloidal components of the background magnetic field.

To start Fig. (5.14) and Fig. (5.15) show a space-dependent dispersion relation (real and imaginary components of k_r, respectively) obtained using the discrete dispersion relation obtained in A. It has to be noted that Fig. (5.14) is an approximation which gives us only the approximate wavelength that are expected but not the exact ones. In Fig. (5.14) it can be seen that the blue line that correspond to the fast wave that propagates with the long wavelength and therefore smaller k_r at some point sharply transforms into the ion-cyclotron wave with the shorter wavelength and thus bigger k_r. Therefore the mode conversion can be expected in this particular region when the fast wave suddenly converts to the ion-cyclotron wave. Also the imaginary part of the k_r can help to predict where the mode conversion occurs. (see Fig. (5.15)). To construct the dispersion relation the plasma model is taken from [11] and [12] and has the following parameters: the components of the background magnetic field are $B_r = 0.15B(r)\cos(\pi/4)$, $B_\varphi = B(r)$, $B_z = 0.15B(r)\sin(\pi/4)$, where $B(r)$ decreases like $1/r$ from 6.5 T at high field side (HFS) to 5.5 T and low field side (LFS) and has the form $B_r = a/(r+b)$ where

$$a = B_{LFS}(r_{LFS} + \frac{B_{LFS}r_{LFS} - B_{HFS}r_{HFS}}{B_{HFS} - B_{LFS}}) \tag{5.4}$$

and

$$b = \frac{B_{LFS}r_{LFS} - B_{HFS}r_{HFS}}{B_{HFS} - B_{LFS}} \tag{5.5}$$

The 3-ion specie plasma has the following density: $n_e = 2 \cdot 10^{20}\ 1/m^3$, $n_{HD} = 0.33n_e$, $n_{DT} = 0.44n_e$, $n_{He} = 0.115n_e$. The frequency of the antenna used to construct the dispersion relation is $5.057 \cdot 10^8\ rad/sec$. The simulation has PEC boundary conditions and $k_\varphi = 14.5\ 1/m$. To perform the numerical simulations $\Delta_r = 0.176mm$ has been chosen which is 1/100 of the shortest wavelength that we expect to see based on the dispersion relation. The Gaussian pulse (5.6) that is used as a source to perform the numerical simulations has a form

$$G = exp(-10^{16}\pi^2(t\Delta t - 3 \cdot 10^{-8})^2)cos(610^8\pi(t\Delta t - 3 \cdot 10^{-8})cos(\Delta\varphi \cdot j \cdot k_\varphi)) \tag{5.6}$$

The techniques developed in chapter related to the steady state criteria could be conceivably used to reach a state which is dominated by a single mode that is desired to be investigated, but that would require absorbing boundary conditions. As in [11] and [12] PEC boundary conditions are used, instead a wide-band source will be used and the desired mode will be isolated by means of the Fourier transform. Also, since the PEC is chosen as a boundary condition, the use of the Gaussian pulse makes sure that only a limited amount of energy in injected into the cavity, and therefore the fields will remain bounded while a nearly single-frequency source ($sin(\omega t)Heaviside(t)$) would keep adding energy to the system and never converge. This can be justified by the fact that gaussian pulse is a square-integrable function while $sin(\omega t)Heaviside(t)$ is a non-square-integrable.

In order to avoid the influence of the reflection from the boundaries the collision damping frequency term ($\vartheta_s = \omega/100$) has been added at the end of the simulation region to damp the propagation of the electromagnetic wave.

Since Gaussian pulse is used to excite the electromagnetic wave the fast fourier transform (FFT) algorithm has to be used to extract the desired mode. Fig. 5.16 shows the behaviour of the electric field amplitude at the aforementioned frequency $\omega = 5.075 \cdot 10^8\ rad/s$ in space. It can be seen that the wavelength of the wave on the left side of the graph is slighly longer than on the right hand side as expected from the dispersion relation (see Fig. 5.14).

In order to show that the mode conversion occurs in the predicted area the double FFT (Fast Fourier Transform) procedure, first in time, than in space, has been applied to get the k- spectrum. Fig. 5.17 shows two forward modes, one with a shorter wavelength than the other, clearly showing that mode conversion occurs.

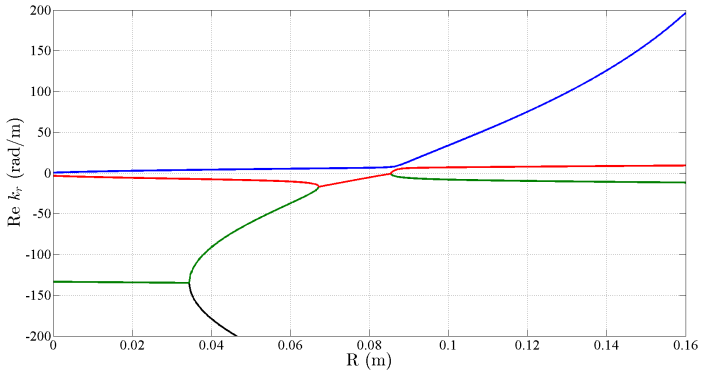

Figure 5.14: Numerical dispersion relation of the real values of k_r in space.

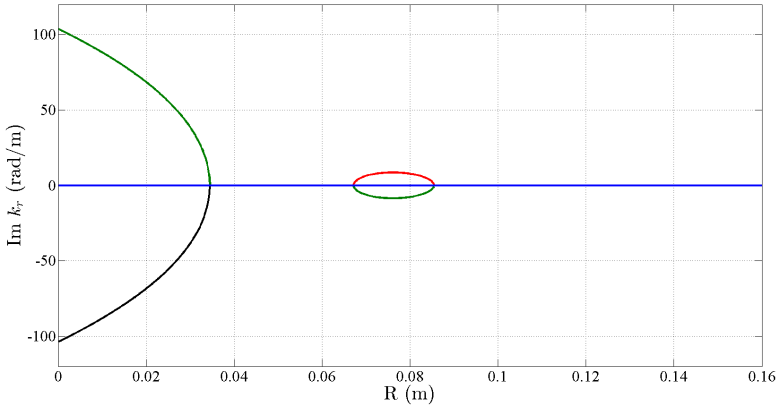

Figure 5.15: Numerical dispersion relation of the imaginary values of k_r in space.

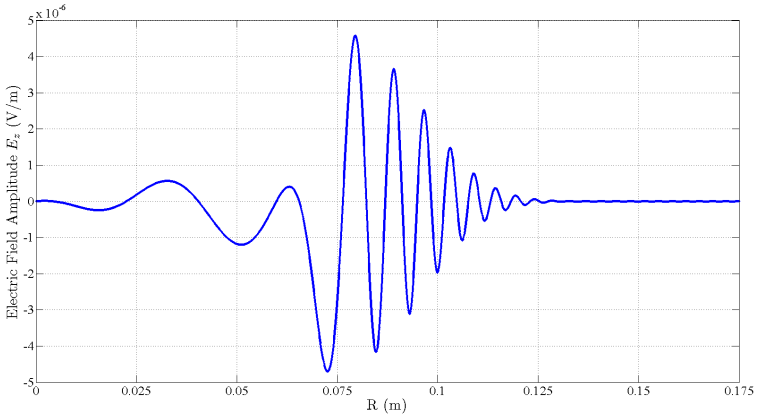

Figure 5.16: The behaviour of the radial electric field component in space.

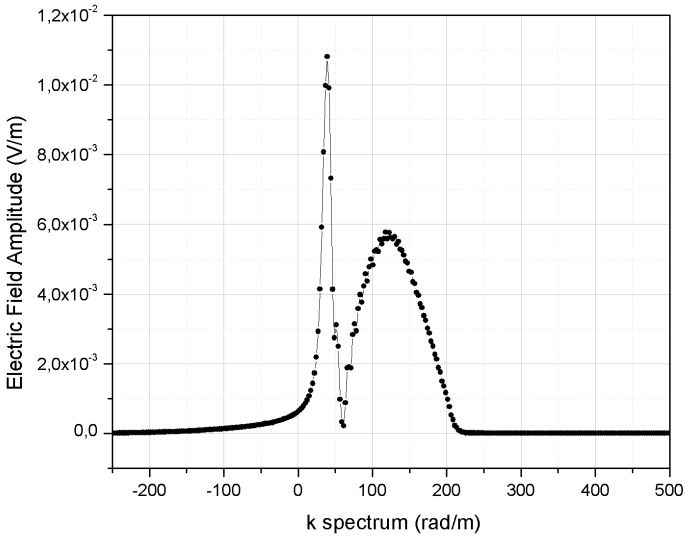

Figure 5.17: k -spectrum.

References

[1] K. Moore, *An examination of stability criteria for ierative numerical schemes used in solving differential equations*, Royal Aircraft Establishment, Jul. 1981.

[2] S. A. Cummer, "An analysis of new and existing fdtd methods for isotropic cold plasma and a method for improving their accuracy", *IEEE Trans. Antennas Propag.*, vol. 45, no. 3, pp. 392 –400, Mar. 1997.

[3] P. G. Petropoulos, "Stability and phase error analysis of fd-td in dispersive dielectrics", *IEEE Trans. Antennas Propag.*, vol. 42, no. 1, pp. 62 –69, Jan. 1994.

[4] J. Young, A. Kittichartphayak, Y. Kwok, and D. Sullivan, "On the dispersion errors related to fdtd type schemes", *IEEE Trans. Microw. Theory Tech.*, vol. 43, no. 8, pp. 1902 –1909, Aug. 1995.

[5] J.-H. Lee and D. K. Kalluri, "Three-dimensional fdtd simulation of electromagnetic wave transformation in a dynamic inhomogeneous magnetized plasma", *IEEE Trans. Antennas Propag.*, vol. 47, no. 7, pp. 1146 –1151, Jul. 1999.

[6] M. Brambilla, *Kinetic Theory of Plasma problems: Homogeneous Plasma*. Clarendon Press, 1998, vol. 1.

[7] M. D. A. P. A. O. G. I. O. Pavlenko I. V., "Precision of a fdtd method to simulate cold magnetized plasmas", vol. 20, no. 6, pp. 37–40, 2014.

[8] A. Taflove and S. C. Hagness, *Computational Electrodynamics*. Artech House, 2005.

[9] D. M. Sullivan, *Electromagnetic simulation using the FDTD method*. John Wiley & Sons, 2013.

[10] T. H. Stix, *Waves in plasmas*. Springer, 1992.

[11] W. Tierens and D. De Zutter, "An unconditionally stable time-domain discretization on cartesian meshes for the simulation of nonuniform magnetized cold plasma", vol. 231, no. 15, pp. 5144 –5156, Jun. 2012.

[12] D. N. Smithe, "Finite-difference time-domain simulation of fusion plasmas at radiofrequency time scales", vol. 14, no. 5, pp. 056 104–056 1047–, Apr. 2007.

[13] F. Costen, J.-P. Berenger, and A. K. Brown, "Comparison of fdtd hard source with fdtd soft source and accuracy assessment in debye media", *IEEE Trans. Antennas Propag.*, vol. 57, no. 7, pp. 2014 –2022, May 2009.

6 Conclusions and future work

6.1 Conclusions

The aim of this dissertation is to develop a global FDTD model that includes the effects of the toroidal symmetrical configuration to account for physics introduced by the magnetized cold plamsa.

To generate this model, a cylindrical magnetized cold plasma algorithm based on the hybrid finite-difference time-domain principle is developed and validated first in Cartesian and then in the cylindrical coordinate systems. A full discrete dispersion relation is derived and compared to the existing analytical solutions. The accuracy and stability analysis are performed, in particular, the analytical proof of stability in case of nonmagnetized plasma is established. It is demonstrated that in case of nonmagnetized cold plasma the maximum stable Courant number of the hybrid method coincides with the vacuum Courant condition. In case of magnetized plasma the stability of the applied numerical scheme is investigated numerically using von Neumann method. The developed numerical algorithm has been validated by calculating the numerical dispersion relations of electromagnetic waves in vacuum, nonmagnetized and magnetized plasma cases. Additional numerical studies if EM wave propagation are also demonstrated. The conducted analysis show that the developed numerical algorithm is trustworthy and accurate.

Next, in order to compare computational results with theoretical predictions, focusing on wave dynamics rather than wave interference, an effective absorbing layer that acts like as an accurate and computationally efficient damping condition has been constructed. The advantage of this boundary condition lies in its flexibility. The collision frequency term that acts like a damping condition can

be switch on/off when it is necessary. Besides, the collision frequency term can perform as a 'bridge' between two branches of the dispersion curve. The inclusion of the collision frequency term provides an additional power dissipation near the evanescent layer, i.e. near the range between the resonance and the cut-off.

Also in this work, a special numerical technique to terminate a simulation the moment steady state is reached is developed and validated both in the Cartesian and in the cylindarical coordinate systems. The physics of Poynting flux has been taken as the basis to develop this particular stopping criteria.

The results of the numerical simulations including the toroidal and poloidal components of the background magnetic field are performed and the results of the mode conversion simulations are presented in this thesis.

6.2 Future work

Ongoing work includes the implementation of the other mode conversion scenarios and further extensive tests with the code. Moreover, the extension to the full 3D scenarios can be performed. Besides, future work could be dedicated to the modification of the numerical code in such a way that it will be suitable for parallelization.

Appendix

A

Derivation of the time-discrete space-continuous dispersion relation of the explicit/implicit FDTD method to model magnetized toroidal plasma using the amplification matrix

A.1 Basic Equations

Including the equation of motion, Maxwell's equations in the three-dimensional case describing cold two-specie (ion and electron) plasma in time-domain are:

$$\frac{\partial \mathbf{H}}{\partial t} = -\frac{1}{\mu_0}\nabla \times \mathbf{E}; \tag{A.1}$$

$$\epsilon_0 \frac{\partial \mathbf{E}}{\partial t} = -\sum_{s=1,2} \mathbf{J}_s + \nabla \times \mathbf{H}; \tag{A.2}$$

$$\frac{\partial \mathbf{J}_s}{\partial t} = \epsilon_0 \omega_{ps}^2 \mathbf{E} - \boldsymbol{\Omega}_s \times \mathbf{J}_s. \tag{A.3}$$

Here, $\mathbf{E}$ is the electric field vector V/m, $\mathbf{H}$ is the magnetic field vector A/m, $\mathbf{J}_s$ is the current density vector of a particular specie A/m^2. The vacuum permeability

$\mu_0\ H/m$ and vacuum permittivity $\epsilon_0\ F/m$ are independent of the frequency. The plasma frequency $\omega_{ps}\ 1/sec$ is defined as

$$\omega_{ps} = \sqrt{\frac{n_s q_s^2}{m_s \epsilon_0}} \tag{A.4}$$

where n_s is the density, q_s is the charge and m_s is the effective mass of a given specie. The cyclotron frequency is:

$$\Omega_s = \frac{q_s B_0}{m_s}, \tag{A.5}$$

where B_0 is the background magnetic field oriented along the z-axis, denoted as $\mathbf{B}_0 = B_0\mathbf{z}$.

A.2 Derivation of the Discrete Dispersion Relation

A.2.1 One-Dimensional Case

Continuous Dispersion Relation

To start we restrict ourselves to a one-dimensional situation, i.e. a case in which the fields only depend on x, but remain independent of y and z. We are looking for an eigensolution proportional to $e^{ikx}e^{i\omega t}$ with ω the circular frequency and k the wave-number. The dispersion relation of interest is $k(\omega)$. For the continuous case the dispersion relation is found to be:

$$n^2 = \frac{(k(\omega))^2 c^2}{\omega^2} = \frac{RL}{S}, \tag{A.6}$$

with

$$R = 1 - \frac{\omega_{pe}^2}{\omega(\omega + \Omega_{ce})} - \frac{\omega_{pi}^2}{\omega(\omega + \Omega_{ci})}; \tag{A.7}$$

$$L = 1 - \frac{\omega_{pe}^2}{\omega(\omega - \Omega_{ce})} - \frac{\omega_{pi}^2}{\omega(\omega - \Omega_{ci})}; \tag{A.8}$$

$$S = \frac{1}{2}(R+L), \tag{A.9}$$

where ω_{pe}, ω_{pi} are defined as species plasma frequency, and where Ω_{ce} and Ω_{ci} are the electron and ion cyclotron frequency.

Discrete Dispersion Relation

We choose the mode where the electric field **E** is perpendicular to the background magnetic field. In this one-dimensional case only the E_x, E_z and H_y components play a role, together with the currents J_{xs} and J_{zs} ($s = 1, 2$) of the two particle species. Time-domain discretization of (A.1)-(A.3) with the method of [1] yields

$$\frac{1}{\Delta t}\begin{pmatrix} H_y(t+\Delta t) - H_y(t) \\ E_x(t+1/2\Delta t) - E_x(t-1/2\Delta t) \\ E_z(t+1/2\Delta t) - E_z(t-1/2\Delta t) \\ J_{1x}(t+1/2\Delta t) - J_{1x}(t-1/2\Delta t) \\ J_{1z}(t+1/2\Delta t) - J_{1z}(t-1/2\Delta t) \\ J_{2x}(t+1/2\Delta t) - J_{2x}(t-1/2\Delta t) \\ J_{2z}(t+1/2\Delta t) - J_{2z}(t-1/2\Delta t) \end{pmatrix} = [M]^T \begin{pmatrix} H_y(t) \\ E_x(t-1/2\Delta t) \\ E_z(t-1/2\Delta t) \\ J_{1x}(t-1/2\Delta t) \\ J_{1z}(t-1/2\Delta t) \\ J_{2x}(t-1/2\Delta t) \\ J_{2z}(t-1/2\Delta t) \\ H_y(t+\Delta t) \\ E_x(t+1/2\Delta t) \\ E_z(t+1/2\Delta t) \\ J_{1x}(t+1/2\Delta t) \\ J_{1z}(t+1/2\Delta t) \\ J_{2x}(t+1/2\Delta t) \\ J_{2z}(t+1/2\Delta t) \end{pmatrix} \tag{A.10}$$

with Δt the time step and with the matrix M given by

$$[M]^T = \begin{pmatrix}
0 & 0 & \frac{i}{\epsilon_0}\frac{d}{dx} & 0 & 0 & 0 & 0 \\
0 & 0 & 0 & \frac{\epsilon_0\omega_{pe}^2}{2} & 0 & \frac{\epsilon_0\omega_{pi}^2}{2} & 0 \\
0 & 0 & 0 & 0 & \frac{\epsilon_0\omega_{pe}^2}{2} & 0 & \frac{\epsilon_0\omega_{pi}^2}{2} \\
0 & -\frac{1}{2\epsilon_0} & 0 & 0 & -\frac{\Omega_{ce}}{2} & 0 & 0 \\
0 & 0 & -\frac{1}{2\epsilon_0} & \frac{\Omega_{ce}}{2} & 0 & 0 & 0 \\
0 & -\frac{1}{2\epsilon_0} & 0 & 0 & 0 & 0 & -\frac{\Omega_{ci}}{2} \\
0 & 0 & -\frac{1}{2\epsilon_0} & 0 & 0 & \frac{\Omega_{ci}}{2} & 0 \\
0 & 0 & 0 & 0 & 0 & 0 & 0 \\
0 & 0 & 0 & \frac{\epsilon_0\omega_{pe}^2}{2} & 0 & \frac{\epsilon_0\omega_{pi}^2}{2} & 0 \\
\frac{i}{\mu_0}\frac{d}{dx} & 0 & 0 & 0 & \frac{\epsilon_0\omega_{pe}^2}{2} & 0 & \frac{\epsilon_0\omega_{pi}^2}{2} \\
0 & -\frac{1}{2\epsilon_0} & 0 & 0 & -\frac{\Omega_{ce}}{2} & 0 & 0 \\
0 & 0 & -\frac{1}{2\epsilon_0} & \frac{\Omega_{ce}}{2} & 0 & 0 & 0 \\
0 & -\frac{1}{2\epsilon_0} & 0 & 0 & 0 & 0 & -\frac{\Omega_{ci}}{2} \\
0 & 0 & -\frac{1}{2\epsilon_0} & 0 & 0 & \frac{\Omega_{ci}}{2} & 0
\end{pmatrix} \tag{A.11}$$

Expressing the $e^{i\omega t}$ dependence in A.10 allows to relate $E_x\left(t+\frac{1}{2}\Delta t\right)$ to $E_x\left(t-\frac{1}{2}\Delta t\right)$, i.e. $E_x\left(t+\frac{1}{2}\Delta t\right) = e^{i\omega\Delta t}E_x\left(t-\frac{1}{2}\Delta t\right)$ (and similarly for the other field components). The e^{ikx}-dependence allows to replace $\frac{d}{dx}$ in (A.11) by

ik. Hence, (A.10) becomes

$$\frac{1}{\Delta t}\begin{pmatrix} H_y(t)(e^{i\omega\Delta t}-1) \\ E_x(t-1/2\Delta t)(e^{i\omega\Delta t}-1) \\ E_z(t-1/2\Delta t)(e^{i\omega\Delta t}-1) \\ J_{1x}(t-1/2\Delta t)(e^{i\omega\Delta t}-1) \\ J_{1z}(t-1/2\Delta t)(e^{i\omega\Delta t}-1) \\ J_{2x}(t-1/2\Delta t)(e^{i\omega\Delta t}-1) \\ J_{2z}(t-1/2\Delta t)(e^{i\omega\Delta t}-1) \end{pmatrix} = \begin{pmatrix} \frac{ik}{\mu_0}E_z(t-1/2\Delta t)e^{i\omega\Delta t} \\ -\frac{1}{2\epsilon_0}J_{1x}(t-1/2\Delta t)(e^{i\omega\Delta t}+1)-\frac{1}{2\epsilon_0}J_{2x}(t-1/2\Delta t)(e^{i\omega\Delta t}+1) \\ \frac{ik}{\epsilon_0}H_y(t)-\frac{1}{2\epsilon_0}J_{1z}(t-1/2\Delta t)(e^{i\omega\Delta t}+1)-\frac{1}{2\epsilon_0}J_{2z}(t-1/2\Delta t)(e^{i\omega\Delta t}+1) \\ \frac{\epsilon_0\omega_{pe}^2}{2}E_x(t-1/2\Delta t)(e^{i\omega\Delta t}+1)+\frac{\Omega_{ce}}{2}J_{1z}(t-1/2\Delta t)(e^{i\omega\Delta t}+1) \\ \frac{\epsilon_0\omega_{pe}^2}{2}E_z(t-1/2\Delta t)(e^{i\omega\Delta t}+1)-\frac{\Omega_{ce}}{2}J_{1x}(t-1/2\Delta t)(e^{i\omega\Delta t}+1) \\ \frac{\epsilon_0\omega_{pi}^2}{2}E_x(t-1/2\Delta t)(e^{i\omega\Delta t}+1)+\frac{\Omega_{ci}}{2}J_{2z}(t-1/2\Delta t)(e^{i\omega\Delta t}+1) \\ \frac{\epsilon_0\omega_{pi}^2}{2}E_z(t-1/2\Delta t)(e^{i\omega\Delta t}+1)-\frac{\Omega_{ci}}{2}J_{2x}(t-1/2\Delta t)(e^{i\omega\Delta t}+1) \end{pmatrix} \tag{A.12}$$

The system matrix M_d of seven linear equation is:

$$M_d = \begin{pmatrix} i\tilde{\omega} & 0 & -\frac{i\tilde{k}}{\mu_0} & 0 & 0 & 0 & 0 \\ 0 & i\tilde{\omega} & 0 & \frac{1}{\epsilon_0} & 0 & \frac{1}{\epsilon_0} & 0 \\ -\frac{i\tilde{k}}{\epsilon_0} & 0 & i\tilde{\omega} & 0 & \frac{1}{\epsilon_0} & 0 & \frac{1}{\epsilon_0} \\ 0 & -\epsilon_0\omega_{pe}^2 & 0 & i\tilde{\omega} & 0 & 0 & \\ 0 & 0 & -\epsilon_0\omega_{pe}^2 & \Omega_{ce} & i\tilde{\omega} & 0 & 0 \\ 0 & -\epsilon_0\omega_{pi}^2 & 0 & 0 & 0 & i\tilde{\omega} & -\Omega_{ci} \\ 0 & 0 & -\epsilon_0\omega_{pi}^2 & 0 & 0 & \Omega_{ci} & i\tilde{\omega} \end{pmatrix} \tag{A.13}$$

where $\tilde{k}$ is equal to $k\sec(\omega\frac{\Delta t}{2})$ and $\tilde{\omega}$ stands for $\frac{2tg(\omega\frac{\Delta t}{2})}{\Delta t}$.

The set of equations A.12 is homogeneous. A non-trivial solution only exists if the determinant of (A.13) becomes zero. This turns to be the case provided

$$\tilde{n}^2 = \frac{\tilde{R}\tilde{L}}{\tilde{S}}, \tag{A.14}$$

where $\tilde{n}^2 = \frac{\tilde{k}^2 c^2}{\tilde{\omega}^2}$. The quantities $\tilde{R}, \tilde{L}, \tilde{S}$ are equal to their counterparts in (A.7)-(A.9) with ω replaced by $\tilde{\omega}$ and k by $\tilde{k}$. Equation A.14 shows that if Δt is sufficiently small the discrete dispersion relation tends towards the continuous case. Moreover, for small Δt the error will be of the order of $(\omega \Delta t)^2$.

A.2.2 Three-Dimensional Case

The discrete dispersion relation in the three-dimensional case can be obtained in complete analogy to the previous one-dimensional case. The eigensolution is now proportional to: $e^{ikr} e^{i\omega t} = e^{ik_x x} e^{ik_y y} e^{ik_z z} e^{i\omega t}$.

In the general three-dimensional case the system matrix takes the form:

$$M_s = \begin{pmatrix}
i\tilde{\omega} & 0 & 0 & 0 & -\frac{ik_z}{\mu_0}\tilde{f} & \frac{ik_y}{\mu_0}\tilde{f} & 0 & 0 & 0 & 0 & 0 & 0 \\
0 & i\tilde{\omega} & 0 & \frac{ik_z}{\mu_0}\tilde{f} & 0 & -\frac{ik_x}{\mu_0}\tilde{f} & 0 & 0 & 0 & 0 & 0 & 0 \\
0 & 0 & i\tilde{\omega} & -\frac{ik_y}{\mu_0}\tilde{f} & -\frac{ik_x}{\mu_0}\tilde{f} & 0 & 0 & 0 & 0 & 0 & 0 & 0 \\
0 & \frac{ik_z}{\epsilon_0}\tilde{f} & -\frac{ik_y}{\epsilon_0}\tilde{f} & i\tilde{\omega} & 0 & 0 & \frac{1}{\epsilon_0} & 0 & 0 & \frac{1}{\epsilon_0} & 0 & 0 \\
-\frac{ik_z}{\epsilon_0}\tilde{f} & 0 & -\frac{ik_x}{\epsilon_0}\tilde{f} & 0 & i\tilde{\omega} & 0 & 0 & \frac{1}{\epsilon_0} & 0 & 0 & \frac{1}{\epsilon_0} & 0 \\
\frac{ik_y}{\epsilon_0}\tilde{f} & -\frac{ik_x}{\epsilon_0}\tilde{f} & 0 & 0 & 0 & i\tilde{\omega} & 0 & 0 & \frac{1}{\epsilon_0} & 0 & 0 & \frac{1}{\epsilon_0} \\
0 & 0 & 0 & -\epsilon_0\omega_{pe}^2 & 0 & 0 & i\tilde{\omega} & 0 & -\Omega_{ce} & 0 & 0 & 0 \\
0 & 0 & 0 & 0 & -\epsilon_0\omega_{pe}^2 & 0 & 0 & i\tilde{\omega} & 0 & 0 & 0 & 0 \\
0 & 0 & 0 & 0 & 0 & -\epsilon_0\omega_{pe}^2 & \Omega_{ce} & 0 & i\tilde{\omega} & 0 & 0 & 0 \\
0 & 0 & 0 & -\epsilon_0\omega_{pi}^2 & 0 & 0 & 0 & 0 & 0 & i\tilde{\omega} & 0 & -\Omega_{ci} \\
0 & 0 & 0 & 0 & -\epsilon_0\omega_{pi}^2 & 0 & 0 & 0 & 0 & 0 & i\tilde{\omega} & 0 \\
0 & 0 & 0 & 0 & 0 & -\epsilon_0\omega_{pi}^2 & 0 & 0 & 0 & \Omega_{ci} & 0 & i\tilde{\omega}
\end{pmatrix} \tag{A.15}$$

where $\tilde{\omega}$ remains $\frac{2tg(\omega\frac{\Delta t}{2})}{\Delta t}$, $\tilde{f}$ is equal to $sec(\omega\frac{\Delta t}{2})$ and k_x, k_y, k_z are the $x-$, $y-$, $z-$ components of the propagation vector $\mathbf{k}$ respectively. We again see that the discrete case will tend to the continuous one for small Δt.

Moreover, remark that all the components of the propagation vector $\mathbf{k}$ are multiplied by the *same* factor. Hence, the discretization does not introduce unwanted anisotropy.

References

[1] D. N. Smithe, “Finite-difference time-domain simulation of fusion plasmas at radiofrequency time scales”, vol. 14, no. 5, pp. 056 104–056 1047–, Apr. 2007.